THE UNIVERSITY OF
SYDNEY

ADVANCED CONTROL AND OPTIMIZATION FOR FUTURE GRID WITH ENERGY STORAGE DEVICES

By

Liyan Zhang

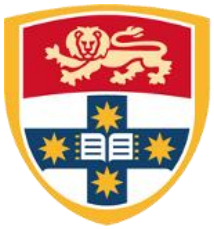

THE UNIVERSITY OF SYDNEY

A thesis submitted in fulfilment of the

Requirements for the degree of Master of Philosophy

Centre of Excellence in Future Energy Networks

School of Electrical and Information Engineering,

The University of Sydney

December 2015

Statement of Originality

The work and the results produced in this thesis have been carried out by the author whose name appears below. The work was carried out under the supervision of Prof. David Hill.

I declare that the material in this thesis has never been previously submitted to any institution for any other degree. The work is entirely original except where duly referenced.

Author: Liyan Zhang

Date: December 2015

Acknowledgement

The author would like to thank all who have provided help and assistance during the course of the thesis.

I would like to express my deepest appreciation and gratitude to my supervisor, Professor David Hill, who has rigorous scientific attitude and wide perspective: he continually provided me with priceless guidance and encouragement. His generous support and knowledge enabled a much better insight and understanding for this topic and research.

I would like to thank our Head of School, Professor Joe Dong, who inspired me and provided me with valuable opportunities to access to numerous workshops, seminars and discussions held by world-class researchers. Without his kind assistance and persistent help the completion of this research project would not have been possible.

In addition, I would like to thank my co-supervisor Dr. Guo Chen for his guidance and his help to introduce his friend Dr. Jueyou Li to make great suggestions and contribution to my research.

Then, I want to thank all my colleagues, especially Ben and Arthur in Lab 329 and the Centre for Future Energy Networks for your help, support and advice. I really enjoy working with you my dear friends and wish you all have a brighter future after graduation.

Publications

The author of this thesis published the following articles during the process of the Masters Degree:

1. **Liyan Zhang, Guo Chen, Zhaoyang Dong, David Hill, K. P. Wong.** "Enhanced Optimal Distributed Consensus Control of Scattered Devices Given Security and Economic Operation Constraints", prepare to submit to *IEEE Trans. on Smart Grid*.

2. **Liyan Zhang, Guo Chen, Zhuoyang Wang, Zhaoyang Dong, David Hill.** "Robust H_∞ Load Frequency Control of Future Power Grid with Energy Storage Considering Parametric Uncertainty and Time Delay", published in *IEEE PES General Meeting*, 2014, Washington DC, USA, pp. 1-5. (Best Paper Prize)

3. **Liyan Zhang, Cuo Zhang, Jueyou Li, Guo Chen, David Hill.** "Modified Accelerated Consensus Optimization for Future Distribution Network", accepted by 9th *IFAC Symposium on Control of Power and Energy Systems* (*CPES*) 2015, New Delhi, India.

4. **Zhuoyang Wang, Liyan Zhang, Guo Chen, David Hill.** "Communication Network Topology Analysis on Distributed Optimization Performance in PV-ES Combined System", published in *IEEE PES General Meeting*, 2015, Denver, USA.

5. **Zhuoyang Wang, Guo Chen, Liyan Zhang, David Hill, Zhaoyang Dong.** "Vulnerability Analysis for Power Grid Given Renewable Energy Integration", published in *AORC-CIGRE Technical Meeting*, 2014, Tokyo, Japan, pp. 1-5.

6. **Zhuoyang Wang, Wang Zhang, Liyan Zhang, Guo Chen, Zhaoyang Dong, Tingwen Huang.** "Impact of High Penetration of Renewable Energy and Demand Side Management on the Australian Future Grid", published in *First Workshop on Smart Grid and Renewable Energy* (*SGRE*) 2015, Doha, Qatar.

Abstract

In the future grid environment, more sustainable resources, such as wind power (WP) and photovoltaic (PV) generation will be increasing steadily. Along with the soaring renewable penetration level also comes concerns over reliable, stable and economical operation of the power grid, because their inherent unpredictable and intermittent characteristics will inevitably cause adverse impacts on the system static, dynamic and economic performance simultaneously: such as jeopardising the voltage and frequency stability or deteriorating the power flow distribution, etc.

In this context, energy storage (ES) devices have been receiving growing attention because of their significant falling prices. It is anticipated in the future that energy storage facilities will be installed in most houses. Therefore, how to utilize these ES to help alleviate the problem of renewable energy (RE) sources integration has become more and more attractive. In my thesis, I will try to resolve some of the related problems from several perspectives.

First of all, a comprehensive Future Australian transmission network simulation platform is constructed in the software DIgSILENT Power Factory. Based on the analysis of different scenarios, basic conclusions can be drawn on how different levels of renewable resources would influence the static power flow distribution and system dynamic stability (including frequency, voltage and rotor angle). Then in-depth research has been done on the aspect of frequency controller design. Based on rigorous mathematical reasoning, an advanced robust H_∞ Load Frequency Controller (LFC) is developed, which can be used to assist the power system to maintain a stable frequency when accommodating more renewables with the help of energy storage. Afterwards, I focus on the voltage and line power over-limit issues in a future

distribution network. I develop a power system sensitivity analysis based-Enhanced Optimal Distributed Consensus Algorithm (EODCA) that combines the theory of power systems and the concept of multi-agents together. The facilities can update their individual information during the iteration process based on a control law through the communication and data exchange with their adjacent neighbours so as to eventually reach a final consensus optimal value. In the following study, a Modified Consensus Alternating Direction Method of Multipliers (MC-ADMM) is proposed, with this approach it can be verified that the convergence speed is notably accelerated even for complex large dimensional systems. Furthermore, the impact of the communication network topology on algorithm dynamic performance is also studied in terms of graph theory so that guidance on how to design a relatively more optimal communication network is given as well.

Overall, in the Master thesis, I successfully provide several novel and practical solutions, algorithms and methodologies in regards to tackling both the frequency, voltage and the power flow issues in a future grid with the assistance of energy storage devices. The scientific control and optimal dispatch of these facilities could provide us with a promising approach to mitigate the potential threats that the intermittent renewables posed on the power system in the following decades.

Table of Contents

1. Introduction 10
1.1 Motivation 10
1.2 Background & Literature Review 11
1.2.1 The Impacts of the Renewables on Future Grid 11
1.2.2 Energy Storage and its Application in Frequency Control 13
1.2.3 Distributed Consensus Optimization for Distributed Energy Resources 14
1.3 Contributions of the Thesis 18
1.4 Organization of the Thesis 19
2. Future Grid Simulations in South Eastern Australia and the Impacts Analysis of High Renewable Penetration 22
2.1 The Future Grid Modelling of South Eastern Australia in DIgSILENT 22
2.1.1 The Simplified 14-Generator Model of the South-Eastern Australia Power System 23
2.1.2 The Enhanced Analysis Model with Renewables in Future Grid Scenarios 30
2.1.3 Demand Side Management Model with Energy Storage Integrated 34
2.2 Steady-State Calculation and Analysis 36
2.2.1 Renewable Thriving 36
2.2.2 Rise of Prosumers and Energy Storage Devices 38
2.2.3 Impact of Location of the Distribution RE and ES 40
2.3 Dynamic Simulation and Analysis 42
2.3.1 Voltage Stability with RE integration 43
2.3.2 Rotor Angle Stability with RE integration 44
2.3.3 Frequency Stability with RE integration 45
3. Robust H_∞ Load Frequency Control (LFC) of Future Power Grid with Energy Storage Devices 48
3.1 Dynamic Modelling of the Grid-Connected Battery Energy Storage 48
3.2 Traditional PI Controller and its Limitations 51
3.3 Closed Loop Diagram of the LFC System with ES 53

3.3.1 Block Diagram of the System with Energy Storage 53
3.3.2 Analysis of Parametric Uncertainty and Time Delay 55
3.3.3 The State-Space Formulation of the Proposed System with Parametric Uncertainty and Time Delay 57
3.4 Controller Design based on LMI Theory 61
3.4.1 Summary of the LMI Methods 61
3.4.2 LMI Based Design of the Robust Controller 64
3.5 Case Studies 68
3.5.1 System Description 68
3.5.2 Comparison of Control Methods 71
3.5.3 Effects of Duration and Forms of Time Delay on System Dynamic Characteristics 72
3.5.4 Effects of Parametric Uncertainty on System Dynamic Characteristics 73
3.5.5 Effects of Energy Storage on System Accommodation of Intermittent RE 74
4. The Enhanced Optimal Distributed Consensus Control of Scattered Devices Considering Security and Economic Operation Issues 77
4.1 Mechanism Analysis of Energy Storage Installation 77
4.2 Problem Description and Mathematical Modelling 80
4.2.1 Three Control Schemes in Distribution Network 80
4.2.2 Problem Description 83
4.2.3 Mathematical Modelling 83
4.3 Prototype of Sub-Gradient based Distributed Consensus Algorithm 87
4.4 Linearized Enhancement based on Power System Sensitivity Analysis 89
4.4.1 The Limitations of the Existing Methodology 89
4.4.2 The Power System Sensitivity Analysis based Piecewise Linearization Modification and Enhancement 90
4.5 Case Studies 94
4.5.1 System Description 94
4.5.2 The Consensus Behaviour of the Agents during Iteration Process 98
4.5.3 The Objective Function (Net Profit of the Company) in three Different Scenarios 100
4.5.4 The Comparison of Line Flows in three Scenarios 102
4.5.5 The Comparison of the Voltage Profiles in three Scenarios 104

5. Modified Consensus Direction Method of Multipliers (MC-ADMM) and Communication Network Topology Analysis on Performance 107
5.1 Modified Consensus Alternating Direction Method of Multipliers (MC-ADMM) 107
5.2. Case Studies & Algorithm Analysis 109
5.2.1 System Description 109
5.2.2 Comparison between Algorithms 110
5.2.3 Comparison between Different Communication Network Topologies 115
5.2.4 The Parametric Sensitivity Analysis of MC-ADMM 118
5.3 Topology Types of the Communication Network 119
5.4 Influence of the Different Communication Network Topology on Calculation Performance 123
6. Conclusions 128
References 132

1. Introduction

1.1 Motivation

As concerns about anthropogenic climate change grow in Australia, the reduced consumption of fossil energy such as coal, petroleum and oil has become one of the most important and pivotal problems waiting to be solved in modern society. In this context, the penetration level of renewable energy, such as wind power and photovoltaic generation into the future power grid has been steadily increasing in recent years in Australia [1].

In the future, a promising pattern of renewable integration in Australia appears to be unfolding. Clearly, integration of solar PV into the distribution networks due to the vast amounts of solar energy available will continue to increase. Shortages of water will render high use of hydro technologies inapplicable [2]. Actually, the geographically distributed generators (DG) like household rooftop PV in Queensland and South Australia has become quite prevalent so far. Further, in Canberra and South Australia, wind farms are being integrated into the transmission grid as well.

Although the advantages of integrating renewables seem to be quite obvious, especially from an environmental perspective, the concern over reliable, stable and economical operation of the power grid also arises. Due to the inherent unpredictable fluctuating characteristics of RE, they will inevitably cause adverse impacts [3] on system static/dynamic performance indexes and deteriorate the economic performance without the appropriate dispatching and control approaches. Therefore, it is extremely important to identify their influences on the future power network structure, and set up an effective mechanism to help to alleviate the adverse impacts as well as enhance the efficiency and economic operation of the system simultaneously.

To solve this dilemma, Energy Storage devices have been received growing attention because the price has decreased significantly. Storage can be used as an effective "buffer" to alleviate the problem brought by renewable integration if appropriate control and optimization methods are implemented. Actually, there are many different kinds of energy storages that can be utilized [4] in power system operation, ranging from high transmission level to low distribution level. Therefore, it is of high theoretical and practical value to do research on how to control and dispatch these promising devices in the future grid to assist the system to perform in a more reliable and economical way. This is the motivation for me to do research on this topic: "ADVANCED CONTROL AND OPTIMIZATION FOR FUTURE GRID WITH ENERGY STORAGE DEVICES".

1.2 Background & Literature Review

1.2.1 The Impacts of the Renewables on Future Grid

As renewables thrive, the influences of integrating them into the grid should be further studied. There have been some research works relating to this issue from different perspectives, the following literatures are some of the significant ones:

Reference [5] is an important summary showing the impacts of the renewable resources on power delivery systems. As is known to all, conventional power distribution system is designed assuming that the substation is the only source of energy and short-circuits capacity. This may not be true in the future grid scenarios with high renewables. In this context, the author discusses some important system issues when considering the DG:

- The voltage issues: the changes of node voltages when consider DG, interaction of DG and capacitor/voltage regulator.

- Protection issues: fuse coordination, feeding faults after utility protection opens, impact of DG on interrupting rating of devices, faults on adjacent feeders, fault detection, ground source impacts, single phase interruption on three phase line, recloser coordination and conductor burn down.
- Loss of power grid issues;
- Vulnerability and overvoltage issues due to islanding and coordination with reclosing.
- System restoration and network issues.

The conclusion is that, if not carefully designed, DG penetration can potentially have very significant adverse system effects, including exposing system and customer equipment to potential damage, deteriorate the power quality, decrease in reliability, extended time to restoration after outage, and potential risks to public and worker safety as well.

Apart from the systematic issues mentioned in the previous paper, there are also some interesting discussions with regards to some other aspects in engineering practice. Paper [6] studies the voltage profile changes of the load nodes when considering PV power station. In accordance with the relevant provisions, the impact factor depends primarily on a variety of different characters, including the number, location, size, and type of grid-connected PV power plants. From the paper we can draw a conclusion that we should install some reactive power support devices to help to alleviate the adverse influences that the PV exerts in voltage profile. In the paper [7], the author simulated a hypothetical network, assuming a large number of fuel cells and micro-turbines as dispersed units in low-voltage distribution network. In the study, the author simulates four categories of stability, i.e. frequency stability, oscillatory stability, transient stability and voltage stability. Based on the results and discussions, it can be concluded that DG

can improve the stability of power systems if suitable types and appropriate locations are designed. Ref. [8] proposes a multi-objective performance index for evaluating the DG impacts. Distributed generation is extensively located and sized within the IEEE-34 test feeder, wherein the multi-objective performance index is computed for each configuration. The advantage of the proposed relevance factors is its flexibility since electric utilities have different concerns about losses, voltages, protection schemes, etc. However, it is also quite obvious that some of the important indexes are neglected and not taken into account, such as the static line power transfer limitations.

Through the above mentioned literature and their references, we could obtain an overview of the impacts that the renewable generation could impose on the future electricity networks.

1.2.2 Energy Storage and its Application in Frequency Control

Use of energy storage devices has become a hot research topic recently especially considering their potential abilities in helping to maintain the stability of the system voltage and frequency. Unlike the voltage issue, which is a local power issue that has a close relationship with the reactive power injection or absorption, the frequency of a certain area implies a global performance of the active power balance between the total generation and demand. The unpredictable nature and highly intermittent outputs of the RE sources require a much higher frequency adjusting ability of the future power system to accommodate them, so it is a challenge for the traditional frequency regulation approaches. In frequency control area, to use ES is quite promising.

Some of the previous works have discussed the grid-connected energy storage and their impacts on power system frequency. Reference [9] proposes a new supplementary LFC method by using both battery energy storage and the additional cluster of mobile electric vehicles along with heat pump water heaters as controllable loads. The effectiveness has been tested by numerical simulation in the system with wind power and PV. In [10], the authors employ integrated energy storage to smooth the power output of the double fed induction generator (DFIG). The result tends to be limited because only one wind turbine and one embedded storage device are considered. In [11], the impact of the integration of battery energy storage systems on a short-term frequency control in autonomous micro grids is studied. However, as the author points out himself, it should consider "an adaptive control that optimally tunes the frequency controller parameters according to the changes occurring in the MG dynamics." It is essentially the robustness of the system against parametric uncertainties.

In the existing literature, there are two important factors that are often disregarded. One is the parametric uncertainty due to the difficulties of precision measurement, and time-drifting character. The other is the time delay that ubiquitously exists in control channels. Both of them should be considered in practice because these inevitable phenomena could significantly degrade the system dynamic performance, especially in a relatively complex future grid environment. Although some of the literatures have discussed the time delay problem (e.g. [12]) in LFC application, the parametric uncertainties of the energy storage has not yet been addressed and analysed simultaneously in the designing process.

1.2.3 Distributed Consensus Optimization for Distributed Energy Resources

Having realized the potential adverse impacts that these renewables will pose on electricity grid especially distribution network, some researchers have proposed some possible

solutions to better manage and control these devices. Compared with the traditional centralized control in transmission networks, it is more challenging to utilize large numbers of these small distributed energy resources (DER) safely, effectively and economically in low voltage distribution networks compared with high-voltage transmission grid. In distribution networks, the grid tends to be more vulnerable without the support of synchronous generators and all the stabilizers and facilities in transmission network.

In the existing control patterns, DERs would need to be centrally controlled by the system operator to maximize the total profit. However, in practice, for geographically dispersed DER, the centralized dispatch mode will inevitably lead to the difficulty of transferring all individual DER information (including operating status, cost, and revenue) to the dispatch centre, huge investment cost for high-bandwidth communication channels between the centre and each DER. Besides, the ubiquitous time delay in the information transmission channel also makes it easy to get false/bad data, introducing the potential failure in control process. Thus, although the centralized approach is an easier way to obtain globally optimal solution, it is obviously impractical. On the other hand, the decentralized dispatch without communications can only achieve optimal decision results for each DER, but not a global optimum for the entire system. In order to implement a practical, flexible, and scalable multi-agent dispatch that require lower communication investment, a distributed dispatch scheme should be suitable for this practical problem. By coordinating individual decision-making of agents who control several DER, the optimal dispatch strategies can be achieved by only exchanging information between neighbouring DER, rather than sharing global information.

The mathematical theory of multi-agent and distributed consensus algorithm could be adopted to tackle this problem. Actually, the utilization of the distributed consensus algorithm

has been studied intensively by control theorists and the progress can be identified as follows. In [13], the author proposes a general framework for parallel and distributed computation over a set of processors. A wide range of references includes [14] tackling continuous-time consensus, [15]- [16] investigating discrete-time versions, and [17] where asynchronous implementation of consensus algorithms is discussed. The papers [18]-[20] treat randomized consensus via gossip communication, achieving consensus through quantized information, consensus over random graphs and average consensus through memory- less erasure broadcast channels, respectively. In [21], the authors solve a multi-agent unconstrained convex optimization problem through a novel combination of average consensus algorithms with sub-gradient methods. More recently, the paper [22] further takes local constraint sets into account.

Although distributed algorithms are relatively developed in theory, the application into industrial problem is still preliminary so far. Here are some applications of these distributed algorithms into power system analysis and their advantages and limitations: Reference [23] uses optimal power flow to compare the two methods and shows that intelligent distributed voltage and reactive power control of the DG gives similar results to those obtained by centralized management in terms of the potential for connecting increased capacities within existing networks. Therefore, if suitable incentive mechanism is designed, the distributed approach would be promising instead of using centralized one. Papers [24-25] propose a robust approach to coordinate customers' resources and manage voltage rise in residential LV networks. The suggested coordination approach in this paper includes both localized control strategy, based on local measurement, and distributed control strategy based on consensus algorithm. The approach can completely avoid maximum permissible voltage limit violation. However, the drawback is that the author neglects the other constraints such as the power flow limit and the economic

objectives. The focus of paper [26] is to develop a distributed control algorithm of PVs in a distribution network. To this end, the cooperative control methodology from network control theory is used to make a group of PV generators converge and operate at certain (or the same) ratio of available power, which is determined by the status of the distribution network and the PV generators. The proposed control only requires asynchronous information intermittently from neighbouring PV generators. It is shown that the analysis and design methodology has the advantages that the corresponding communication networks are local, their topology can be time varying, and their bandwidth may be limited. The utilization of energy storage is neglected in this paper, which could be improved in future study. The paper [27] illustrates the feasibility of implementing the multi-agent system scheme in the control/optimization problem. The prototype problem considered is the dispatching of distributed generators on a distribution feeder to provide voltage support. The popular Control Net Protocol (CNP) for Multi-Agent System (MAS) has been adopted to facilitate distributed control. This paper illustrates that characterization of the optimal solution is necessary in order to develop a protocol for the MAS to implement. It also shows that MAS facilitates a model-free control procedure, as it can monitor the local sensitivities. Test results show that the MAS-based control scheme is effective in obtaining the solution for the prototype problem. Nonetheless, the MAS-based method needs fast communication among the DGs in order to assure fast response during emergency conditions. Ref. [28] analyses an extended multi-agent convex optimization problem in which the agents are to collectively minimize a global objective function subject to a global inequality constraint, a global equality constraint, and a global constraint set. The objective function is defined by a sum of local objective functions, while the global constraint set is produced by the intersection of local constraint sets. Specifically, the author studies two scenarios: one is with the absence of the

equality constraint, and the other one is that the local constraint sets are identical. Then he devises two distributed primal-dual sub-gradient algorithms. These algorithms can allow the agents to asymptotically agree on optimal solutions and optimal values of the optimization problem under the Slater's condition. This approach is quite new and it seems that can be implemented into the power system scenarios as well. However, the strict requirement of the linear constraint in the definition limits its scope of application.

Drawing on these papers, it can be seen that the research on the application of distributed optimization algorithms on future grid with DER and ES is still preliminary so far. Hence continued research may further explore the development of the existing approaches and the combination with future power systems.

1.3 Contributions of the Thesis

The main contributions of this thesis are:

1. A comprehensive simulation platform for Australian future grid with a high penetration level RE scenario is built in DIgSILENT, which includes both steady state power flow scanning and dynamic stability analysis considering different RES penetration as well as DSM uptakes. Simulation experiments are performed to demonstrate the impacts of renewables on future power transmission system in several typical scenarios.

2. A novel control block diagram of the closed-loop LFC system with ES and wind power module has been proposed. Two important factors that exist in future power network, i.e. parametric uncertainty as well as ubiquitous time delay in control channel, are considered simultaneously.

3. The unpredictable nature and highly intermittent outputs of the RE sources require a much higher frequency adjusting ability of the future power system to accommodate them, so it is a challenge for the traditional frequency regulation approaches. The problem of how to maintain the frequency stability under a much more complicated environment should be studied. Based on mathematical LMI theory, a Robust H∞ controller is designed to deal with the problem. The effectiveness of the controller is tested in Matlab Simulink software package.

4. A sensitivity analysis based-Enhanced Optimal Distributed Consensus Algorithm (EODCA) that combines the theory of power systems and the concept of multi-agents is proposed. The effectiveness of the proposed algorithm is verified: it can help the power distribution company to maximize its net profits with very limited information channel built among devices instead of setting up a control centre. Furthermore, the optimal solutions can also guarantee the safety operation of the distribution network at the same time.

5. Based on the traditional ADMM theory in mathematics, I propose a Modified Consensus Alternating Direction Method of Multipliers (MC-ADMM) to solve the practical control problem in future power distribution networks. Compared with a latest version of the distributed optimization algorithm called DLPDS, we can see that MC-ADMM performs much better in terms of the speed, the accuracy and the ability to handle larger systems with more devices.

6. The influence of the communication network topology on the calculation performance is studied. Laplacian eigenvalue plays a crucial role and a conclusion is made that an optimum topology for communication network connections exists.

1.4 Organization of the Thesis

The thesis is structured in three parts that all relate to the future scenarios of renewable integration and energy storage utilization. Each part focuses on an aspect of this problem, namely: **Impacts on Power System with RE and ES (Chapter 2)**; **Frequency Control with RE and ES (Chapter 3)**; **Optimal Dispatch with RE and ES (Chapter 4-5)**. Following are the details of each chapter:

Part 1- Impacts on Power System with RE and ES (Chapter 2)

Chapter 2-constructs a comprehensive platform in the software DIgSILENT, based on which various scenarios of Australian future grid can be tested. Some typical situations including both static power flow scanning calculation and short circuit dynamic simulations (frequency, voltage and rotor angle behaviour) with/without ES are performed to identify the influence on the Australian transmission network under different levels of RE/ES sources penetration and different levels of DSM uptakes with multiple levels of granularity.

Part 2-Frequency Control with RE and ES (Chapter 3)

Chapter 3- develops the dynamic model of the grid-connected ES and the closed-loop frequency-domain block diagram. Then a novel controller is proposed based on rigorous linear matrix inequalities (LMI) theory to ensure the robustness and stability of the system, when taking into account the parametric uncertainty and random time delay in control channels in the complex environment. Comprehensive case studies are performed to demonstrate the effectiveness of the proposed Controller.

Part 3-Optimal Dispatch with RE and ES (Chapter 4-5)

Chapter 4- proposes a novel Enhanced Optimal Distributed Control Algorithm (EODCA) based on power system sensitivity analysis to regulate the scattered energy storage devices while the overall economic performance and network security constraints are considered. The comprehensive case study also demonstrates the effectiveness of the proposed method.

Chapter 5- proposes a Modified Consensus Alternating Direction Method of Multipliers (MC-ADMM) to demonstrate the effectiveness of accelerating the convergence speed. Afterwards, some guidance is given on how to design a better communication network by innovatively analysing the performance of network topology.

Chapter 6- Concludes the whole thesis and discusses the future work.

2. Future Grid Simulations in South Eastern Australia and the Impacts Analysis of High Renewable Penetration

Large thermal power plants have traditionally underpinned the whole operation of conventional power systems. The traditional planning and control models will be challenged by all new features of the future grid: renewable energy (RE) sources, distributed generation (DG), energy storage devices (ES) and new type of loads, etc. Meanwhile, other changes, such as new control mechanisms, will be applied to the demand side as well. In all the changes above, the role of modelling and analysis related to security for large numbers of scenarios remains of central importance. In this context, it inspired us to analyse the various scenarios under the future grid infrastructure based on the 14-Generator model for National Electricity Market (NEM) in Australia. In this Chapter, I firstly construct a platform in the software DIgSILENT Power factory, based on which various scenarios of Australian future grid network security can be simulated, then I choose some typical situations including both static power flow calculation without ES and short circuit dynamic simulations (frequency, voltage and rotor angle behaviour) to identify the influence on the Australian transmission network under different levels of RE sources penetration and different levels of DSM uptakes with multiple levels of granularity.

2.1 The Future Grid Modelling of South Eastern Australia in DIgSILENT

The starting point of my studies is the observation that to the best of my knowledge, no international research so far has developed/provided a standardized comprehensive modelling framework and platform for the Australian future grid close to what we have been accustomed to for the existing systems. We need to develop a comprehensive tool and platform that can reflect the real situation in the future that can also deal with the potential problems in future power system: e.g. power flow calculation, stability analysis, economic dispatch, security and reliability

simulation, etc. We use the analysis software DIgSILENT as providing us a satisfactory approach in modelling and tackling renewable energy generations.

2.1.1 The Simplified 14-Generator Model of the South-Eastern Australia Power System

The simplified 14-Generator, 50 Hz system model for the South-Eastern (SE) Australian grid is used as the base model here. For convenience, it has been divided into 5 areas which stand for different states and regions in Australia [29]:

- Area 1: Snowy Mountains
- Area 2: New South Wales
- Area 3: Victoria
- Area 4: Queensland
- Area 5: South Australia

Areas 1 and 2 are more closely coupled. Thus, there are in essence 4 main areas and hence 3 inter-area modes, as well as 10 local-area modes. Australian Electricity Market Operator (AEMO) has proposed this network to 16 zones for the NEM as shown in the Fig. 1.

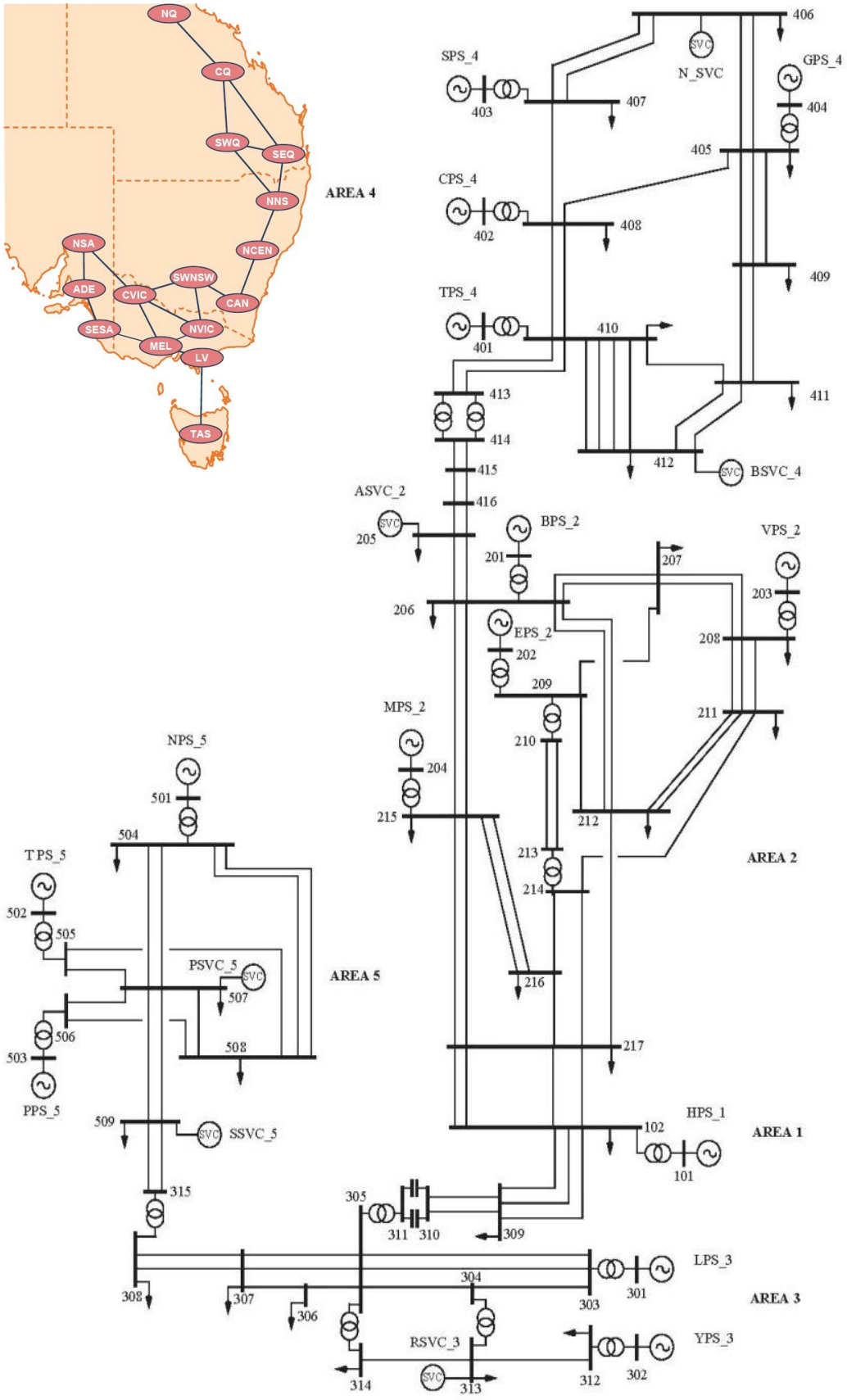
NQ
CQ
SWQ
SEQ
NNS
NCEN
NSA
ADE
CVIC
SWNSW
CAN
SESA
NVIC
MEL
LV
TAS
AREA 4
SPS_4
403
407
SVC
N_SVC
406
GPS_4
404
405
CPS_4
402
408
409
TPS_4
401
410
411
413
414
415
412
SVC
BSVC_4
ASVC_2
416
205
SVC
BPS_2
201
207
VPS_2
203
206
EPS_2
202
208
209
MPS_2
211
210
204
215
212
213
214
AREA 2
216
217
NPS_5
501
504
TPS_5
502
505
PSVC_5
SVC
507
AREA 5
506
503
508
PPS_5
509
SVC
SSVC_5
HPS_1
102
101
AREA 1
315
305
311
310
309
LPS_3
304
308
307
303
301
AREA 3
306
RSVC_3
YPS_3
314
SVC
313
312
302

Fig. 1 The Simplified 14-Generator Model of the SE Australia Power System

The more detailed parameter settings of the platform are given in the following tables.

The transmission line parameters are listed in the following table 1:

Table 1 Transmission Line Parameters: Values per Circuit

From bus/to bus	**Line No.**	**Line *r+jx*; *b* (*p.u.* on 100MVA)**		
102 217	1,2	0.0084	0.0667	0.817
102 217	3,4	0.0078	0.0620	0.760
102 309	1,2	0.0045	0.0356	0.437
102 309	3	0.0109	0.0868	0.760
205 206	1,2	0.0096	0.0760	0.931
205 416	1,2	0.0037	0.0460	0.730
206 207	1,2	0.0045	0.0356	0.437
206 212	1,2	0.0066	0.0527	0.646
206 215	1,2	0.0066	0.0527	0.646
207 208	1,2	0.0018	0.0140	0.171
207 209	1	0.0008	0.0062	0.076
208 211	1,2,3	0.0031	0.0248	0.304
209 212	1	0.0045	0.0356	0.437
210 213	1,2	0.0010	0.0145	1.540
211 212	1,2	0.0014	0.0108	0.133
211 214	1	0.0019	0.0155	0.190

212	217	1	0.0070	0.0558	0.684
214	216	1	0.0010	0.0077	0.095
214	217	1	0.0049	0.0388	0.475
215	216	1,2	0.0051	0.0403	0.494
215	217	1,2	0.0072	0.0574	0.703
216	217	1	0.0051	0.0403	0.494
303	304	1	0.0010	0.0140	1.480
303	305	1,2	0.0011	0.0160	1.700
304	305	1	0.0003	0.0040	0.424
305	306	1	0.0002	0.0030	0.320
305	307	1,2	0.0003	0.0045	0.447
306	307	1	0.0001	0.0012	0.127
307	308	1,2	0.0023	0.0325	3.445
309	310	1,2	0.0090	0.0713	0.874
310	311	1,2	0.0000	-0.0337	0.000
312	313	1	0.0020	0.0150	0.900
313	314	1	0.0005	0.0050	0.520
315	509	1,2	0.0070	0.0500	0.190
405	406	1,2	0.0039	0.0475	0.381
405	408	1	0.0054	0.0500	0.189
405	409	1,2,3	0.0180	0.1220	0.790
406	407	1,2	0.0006	0.0076	0.062
407	408	1	0.0042	0.0513	0.412

408	410	1,2	0.0110	0.1280	1.010
409	411	1,2	0.0103	0.0709	0.460
410	411	1	0.0043	0.0532	0.427
410	412	1 to 4	0.0043	0.0532	0.427
410	413	1,2	0.0040	0.0494	0.400
411	412	1,2	0.0012	0.0152	0.122
414	415	1,2	0.0020	0.0250	0.390
415	416	1,2	0.0037	0.0460	0.730
504	507	1,2	0.0230	0.1500	0.560
504	508	1,2	0.0260	0.0190	0.870
505	507	1	0.0008	0.0085	0.060
505	508	1	0.0025	0.0280	0.170
506	507	1	0.0008	0.0085	0.060
506	508	1	0.0030	0.0280	0.140
507	508	1	0.0020	0.0190	0.090
507	509	1,2	0.0300	0.2200	0.900

The transformer ratings and reactance are demonstrated in the following table 2:

Table 2 Transformer Ratings and Reactance

Buses		Number	Rating, each Unit (MVA)	Reactance per transformer	
From	To			% on	per unit

				Rating	on 100MVA
101	102	g	333.3	12.0	0.0360
201	206	g	666.7	16.0	0.0240
202	209	g	555.6	16.0	0.0288
203	208	g	555.6	17.0	0.0306
204	215	g	666.7	16.0	0.0240
209	210	4	625.0	17.0	0.0272
213	214	4	625.0	17.0	0.0272
301	303	g	666.7	16.0	0.0240
302	312	g	444.4	15.0	0.0338
304	313	2	500.0	16.0	0.0320
305	311	2	500.0	12.0	0.0240
305	314	2	700.0	17.0	0.0243
308	315	2	370.0	10.0	0.0270
401	410	g	444.4	15.0	0.0338
402	408	g	333.3	17.0	0.0510
403	407	g	444.4	15.0	0.0338
404	405	g	333.3	17.0	0.0510
413	414	3	750.0	6.0	0.0080
501	504	g	333.3	17.0	0.0510
502	505	g	250.0	16.0	0.0640
503	506	g	166.7	16.7	0.1000

The parameters of the 14 generators are listed in Table 3.

Table 3 Generator Parameters

Generator	HPS_1	BPS_2	EPS_2	MPS_2	VPS_2	LPS_3	YPS_3
Bus	101	201	202	204	203	301	302
Order	5	6	6	6	6	6	5
Rating/ MVA	333.3	666.7	555.6	666.7	555.6	666.7	444.4
No. of Units	12	6	5	6	4	8	4
H MWs/MVA	3.60	3.20	2.80	3.20	2.60	2.80	3.50
Xa/pu	0.14	0.20	0.17	0.20	0.20	0.20	0.15
Xd/pu	1.10	1.80	2.20	1.80	2.30	2.70	2.00
Xq/pu	0.65	1.75	2.10	1.75	1.70	1.50	1.80
Xd'/pu	0.25	0.30	0.30	0.30	0.30	0.30	0.25
Tdo'/s	8.5	8.50	4.50	8.50	5.00	7.50	7.50
Td"/pu	0.25	0.21	0.20	0.21	0.25	0.25	0.20
Tdo"/s	0.05	0.04	0.04	0.04	0.03	0.04	0.04
Xq'/pu	-	0.70	0.50	0.70	0.40	0.85	-
Tqo'/s	-	0.30	1.50	0.30	2.00	0.85	-
Xq"/pu	0.25	0.21	0.21	0.21	0.25	0.25	0.20
Tqo"/s	0.20	0.08	0.06	0.08	0.25	0.12	0.25

Generator	CPS_4	GPS_4	SPS_4	TPS_4	NPS_5	TPS_5	PPS_5
Bus	402	404	403	401	501	502	503
Order	6	6	6	6	6	6	6
Rating/ MVA	333.3	333.3	444.4	444.4	333.3	250.0	166.7
No. of Units	3	6	4	4	2	4	6
H MWs/MVA	3.00	4.00	2.60	2.60	3.50	4.00	7.50
Xa/pu	0.20	0.18	0.20	0.20	0.15	0.20	0.15
Xd/pu	1.90	2.20	2.30	2.30	2.20	2.00	2.30
Xq/pu	1.80	1.40	1.70	1.70	1.70	1.50	2.00
Xd'/pu	0.30	0.32	0.30	0.30	0.30	0.30	0.25
Tdo'/s	6.50	9.00	5.00	5.00	7.50	7.50	5.00
Td"/pu	0.26	0.24	0.25	0.25	0.24	0.22	0.17
Tdo"/s	0.035	0.04	0.03	0.03	0.025	0.04	0.022
Xq'/pu	0.55	0.75	0.40	0.40	0.80	0.80	0.35
Tqo'/s	1.40	1.40	2.00	2.00	1.50	3.00	1.00
Xq"/pu	0.26	0.24	0.25	0.25	0.24	0.22	0.17
Tqo"/s	0.04	0.13	0.25	0.25	0.10	0.20	0.035

With the given parameter settings of the electrical components, we can perform simulations with the platform to test different scenarios and cases in future grid environment.

2.1.2 The Enhanced Analysis Model with Renewables in Future Grid Scenarios

To make a model which can serve the purpose of the future study [30], the base 14-Generator Model was rebuilt in DIgSILENT environment with the following enhancements:

- The capability to add a solar thermal, PV or wind farm at all buses of the grid, including possible grid extensions;
- The traditional generator models have also been enhanced to allow a wider range of dynamic studies than just small-disturbance stability;
- The capability to include the demand-side representation of load, storage and demand-response at city level.

The modelling framework aims to be very flexible for considering scenarios of RE placement, randomly or from specific proposals, and optimizing which ones will provide the best overall performance. In this chapter, we illustrate this flexibility with additional RE at nodes in the four main areas. The traditional generators are replaced by RE sources with different percentages of their capacity to see their influence on system performance.

According to the practical data in Australia, we can select the following nodes to accommodate the renewable energy sources.

SA: Node 501; NPS_5; Wind Farm Lake Bonney

VIC: Node 301; LPS_3; Wind Farm Waubra

NSW: Node 204; MPS_2; Wind Farm Capital

QLD: Node 401; TPS_4; Photovoltaic Power Station

The geographic positions of the four power stations are denoted in the Fig.2:

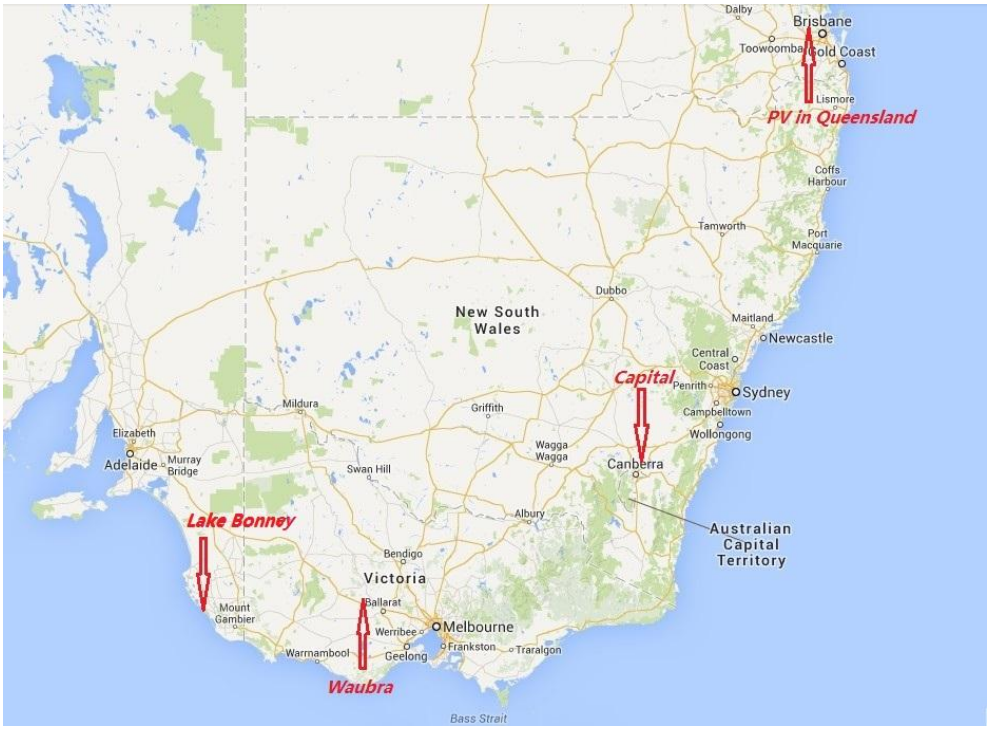

Fig. 2 Locations of the 4 Renewable Energy Resources in SE Australia

The scenarios are divided into two categories, i.e. 1) Power flow calculation under steady operation conditions and the 2) Transient analysis under short circuit conditions. Both of the two categories are performed within different penetration levels of sustainable energy sources.

Firstly, we divide daily load curve into three different levels, i.e. light load level(0 am-8 am, 22 pm-0 pm), medium load level (9 am-17 pm) and heavy load level (18 pm-21 pm) respectively. In each scenario, the penetration of the wind farm and photovoltaic varies from 0% to 40%. In different time points in a day, the power outputs of the wind farms and PV stations are drawn from the real-time data of AEMO online reports. From the practical power output data, we can convert the corresponding capacity factor of the different types of generators throughout the day. The following Figs. 3-4 is the practical real-time PV power output data and the corresponding capacity factor in a day. We can use the PV power output capacity factor (the

hourly PV power output data divided by the corresponding total capacity of the PV station) to show the PV power generation ability within a day at different time points, as illustrated in Fig. 3

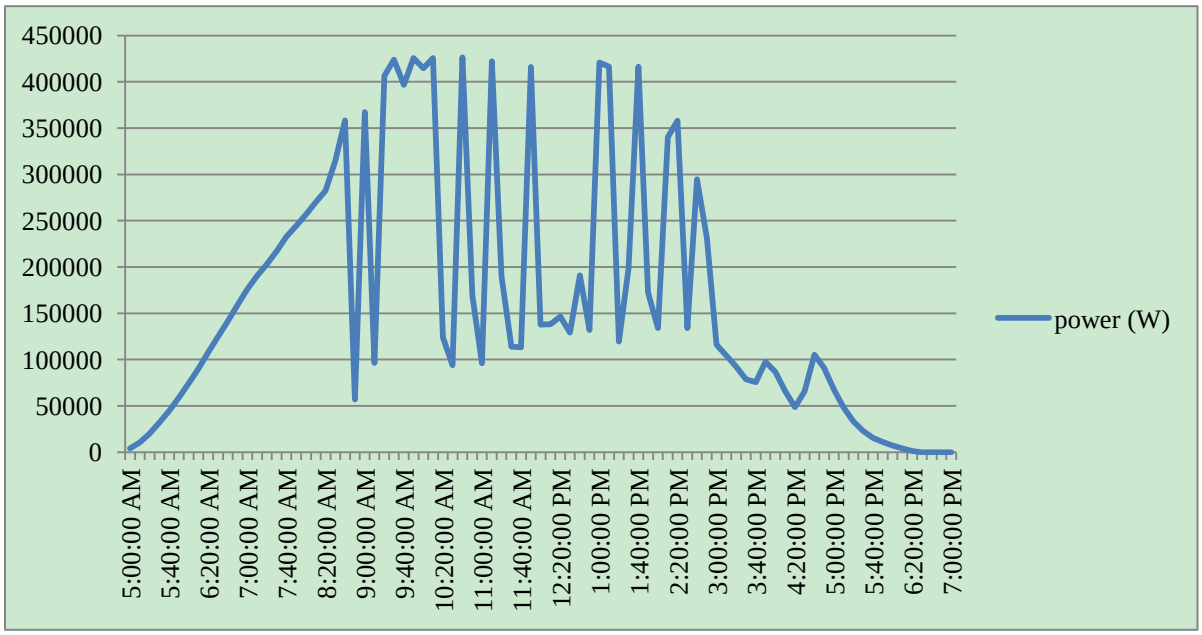

Fig. 3 The Real-time PV Power Output within a Day

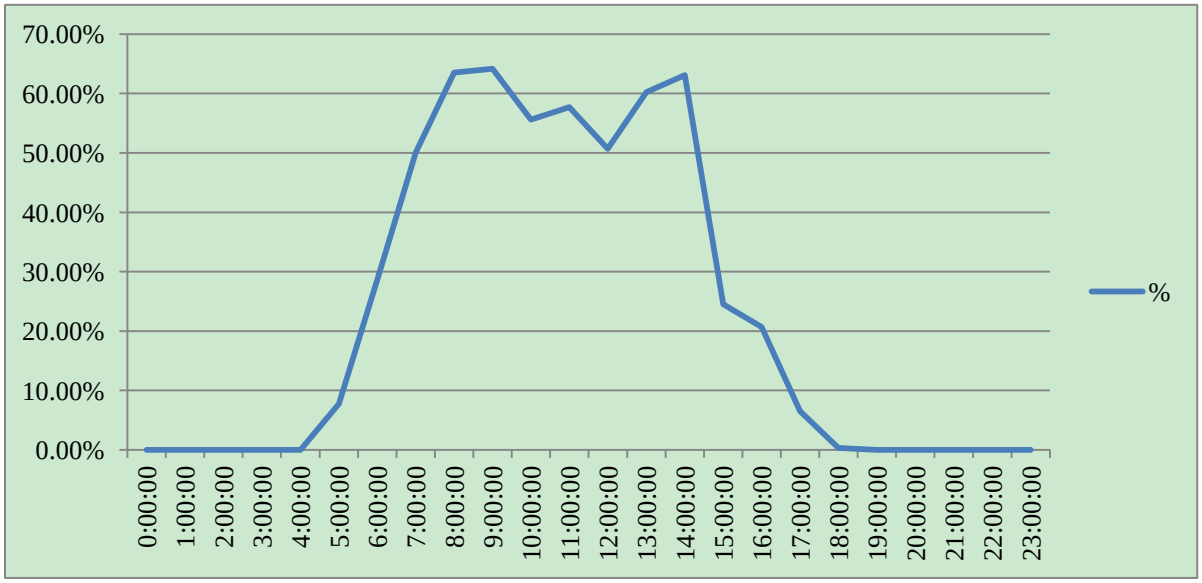

Fig. 4 The PV Power Output Capacity Factor within a Day

In each penetration level, we calculate the power flow in a day (24 time points) of the system with real-time varying load level and wind/PV power outputs to test whether the transmitted power are out of limit in transmission lines.

To simply represent the change of actual load within a day's period, The daily load curve are divided into three different levels, i.e. light load level(0 am-8 am, 22 pm-0 pm), medium load level (9 am-17 pm) and heavy load level (18 pm-21 pm) respectively. In each scenario, the wind and photovoltaic farms replace traditional generators in 10%, 20%, 30% and 40% of their capacity at each specified nodes, namely Node 501, Node 301, Node 204 and Node 401. By calculation, the penetration levels are 3.23%, 6.46%, 9.68% and 12.92% accordingly in terms of the energy generated.

In different time points of a day, the power outputs of wind/PV farms are drawn from the real-time data of online reports [31] (Wind Farm Performance and University of Queensland Solar Photovoltaic Data) and scaled to different scenarios. From the practical power output data, the corresponding capacity factors of different generators have been converted throughout the day.

2.1.3 Demand Side Management Model with Energy Storage Integrated

The demand side management model is also analysed in this study under future grid scenario. In order to do that, firstly, the market simulation is done by PLEXOS, which is a well-known market simulation software. The scenario is based on the dispatch process from AEMO. The model is designed based the residential level then granulated into city levels of the NEM future grid model according to the requirement for different study purposes. Specifically

speaking, the model that we designed in a decision making optimization programming where the decision can be computed at each household in order to achieve the objective of minimizing electricity bills. Mathematically, the model can be described as an optimization problem where the objective function and constraints can be described as follows,

$$\min \ C_i = \sum_{k=1}^{K} \lambda(k)(A_i^k + E_i^k - P_{pv,i}^k) \tag{1}$$

$$s.t. \ A_i^k \in [m_i^k, M_i^k] \tag{2}$$

$$E_i^k = SOC(k+1) - SOC(k) \tag{3}$$

$$Q_i^- \le E_i^k \le Q_i^+ \tag{4}$$

$$P_{pv,i}^k \ge 0 \tag{5}$$

Where C_i denotes the electricity bill of the user i for the studies time period, normally a day and K=24. Here is the list of denotation:

$\lambda(k)$: the rate of purchasing electricity from/selling electricity to the grid at time slot t;

A_i^k :the electricity consumption of all appliances of user i within time slot k;

$P_{pv,i}^k$: the photovoltaic system generation of user i within time slot k;

The constraint $A_i^k \in [m_i^k, M_i^k]$ shows that the total consumption of household i in time slot k should between the minimum and maximum consumption value; $E_i^k = SOC(k+1) - SOC(k)$ and $Q_i^- \le E_i^k \le Q_i^+$ represent that constraints on the state of charge

SOC(*k*) and maximum charge/discharge rate Q_i^- and Q_i^+ respectively. The term $A_i^k + E_i^k - P_{pv,i}^k$ actually equals to the amount of electricity that is exchanged with the grid from user *i* in time slot *k*, denoted by $P_{g,i}^k$. Therefore it indicates that the user *i* is purchasing the electricity from the grid at time slot *k* when $P_{g,i}^k > 0$; and the user *i* is sending back the electricity to the grid when $P_{g,i}^k < 0$. The price is assumed to be *Time of Use* (*ToU*) and the consumers are only considered as the price taker at this stage.

Later this demand side model is granulated into the city level in order to analyse the scenarios when the demand side management is considered in the future grid stability study.

2.2 Steady-State Calculation and Analysis

The primary analysis tool for steady-state operation is power flow analysis, where the voltages (magnitude and phase), line power flows and losses in the system are determined. This analysis is widely used for both operation and planning studies throughout the system i.e. both transmission and distribution systems.

2.2.1 Renewable Thriving

It is well known that Australia has an abundance of renewable energy resources, such as wind, solar, geothermal etc. The CSIRO Australia has formulated several scenarios for the Australian grid in 2050 [32]. Among these one called “Renewables Thrive” represents the increasing to high usage of renewable energy sources. The purpose of this study that is to reveal with the integration of the DG and ES (and residential sized), how could the impact of ‘renewable thriving’ under different penetration level of RE.

Therefore, the scenarios are formulated at the same location under different level of renewable penetration and then compared to find out whether the power flow of the system is converged or not.

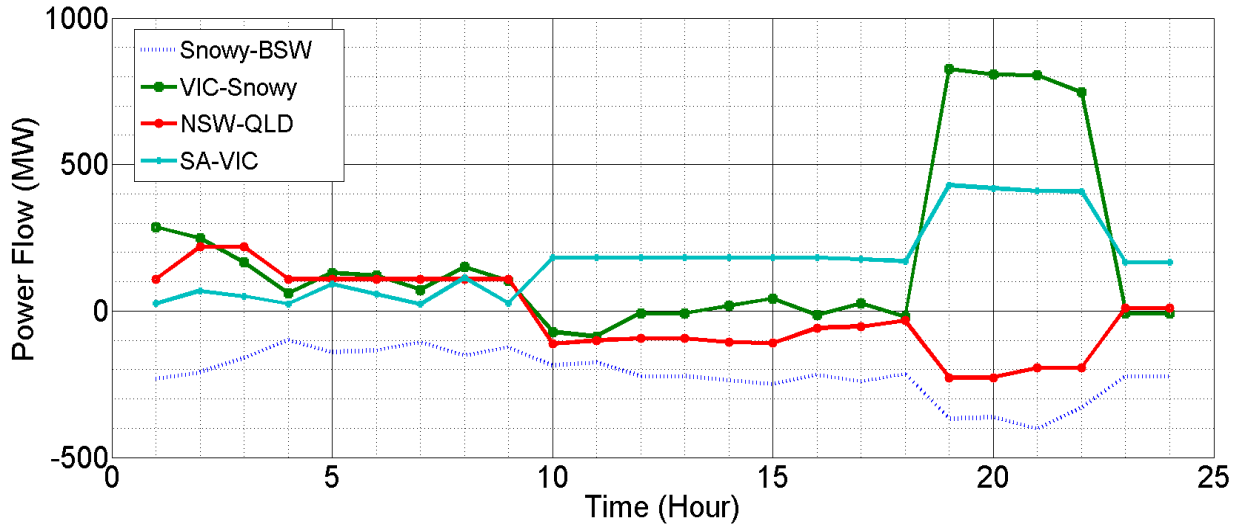

Fig. 5 The Power Flow Distribution under 6.46% Renewables without Energy Storage

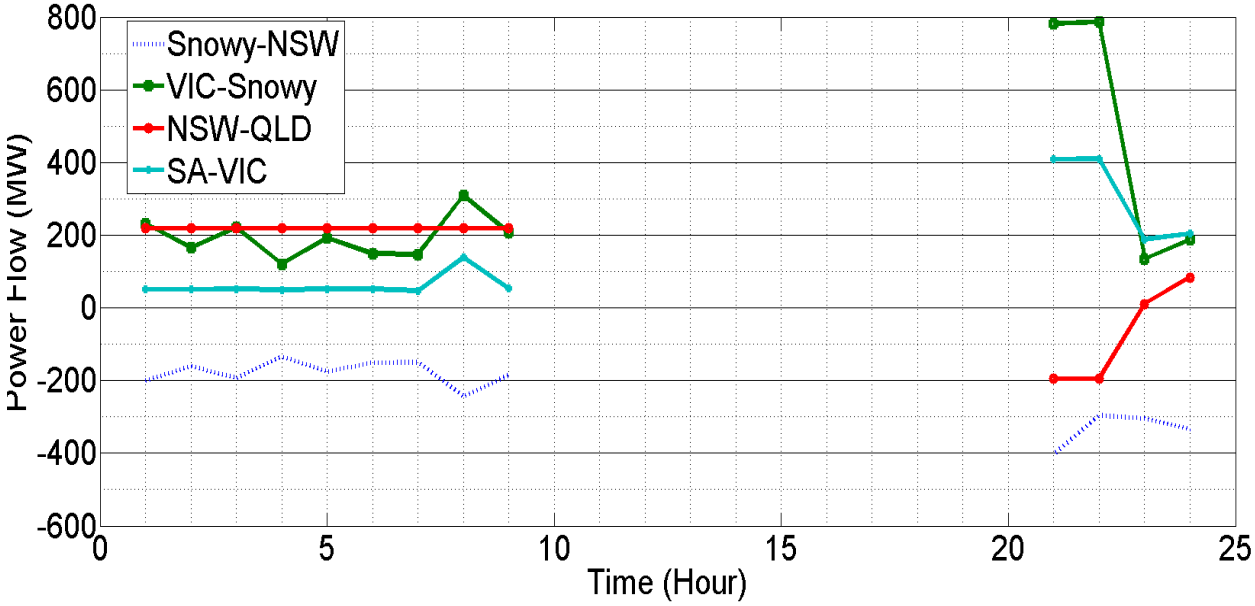

Fig. 6 The Power Flow Distribution under 12.92% Renewables without Energy Storage

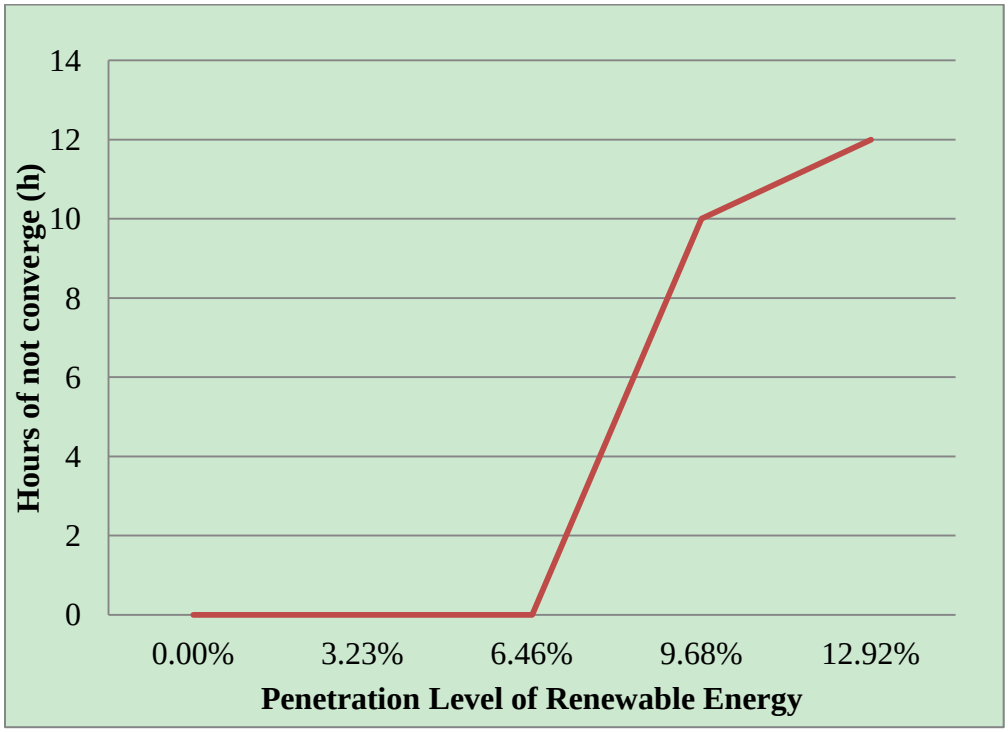

Fig. 7 The Hours of Power Flow not converging with the Increase of Penetration Level

The Fig. 5-6 shows the power flow on inter-connected transmission line under the RE penetration level of 6.46% and 12.92% without ES respectively and Fig. 7 demonstrates the none-convergence period becomes longer with the penetration level increases. It can be seen that under higher penetration level of renewables without energy storage integrated, the power flow cannot converge in certain periods, i.e. 11:00-21:00. It is because the intermittent characteristic of these renewables may incur imbalance between active power generation and consumption.

2.2.2 Rise of Prosumers and Energy Storage Devices

A second scenario in [32] is called “Rise of Prosumers”. Prosumers are the residential customers who also supply their own electricity. The sustained high retail prices of electricity, falling costs of solar roof-top panels and increasingly innovative financing and product packaging from energy services companies leads to large increases in the scale of on-site generations. In this study the demand-side model has been aggregated into city level. Parameters in this model can capture the percentages of uptake for the technologies involved.

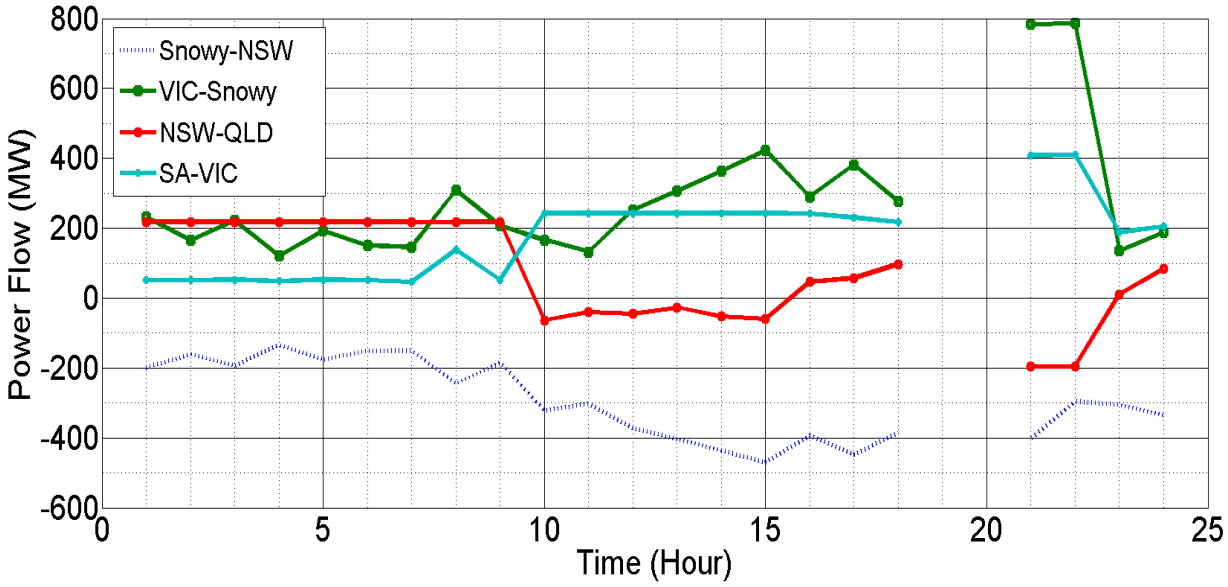

Fig. 8 The Power Flow Distribution under 12.92% Renewables with 40% Energy Storage

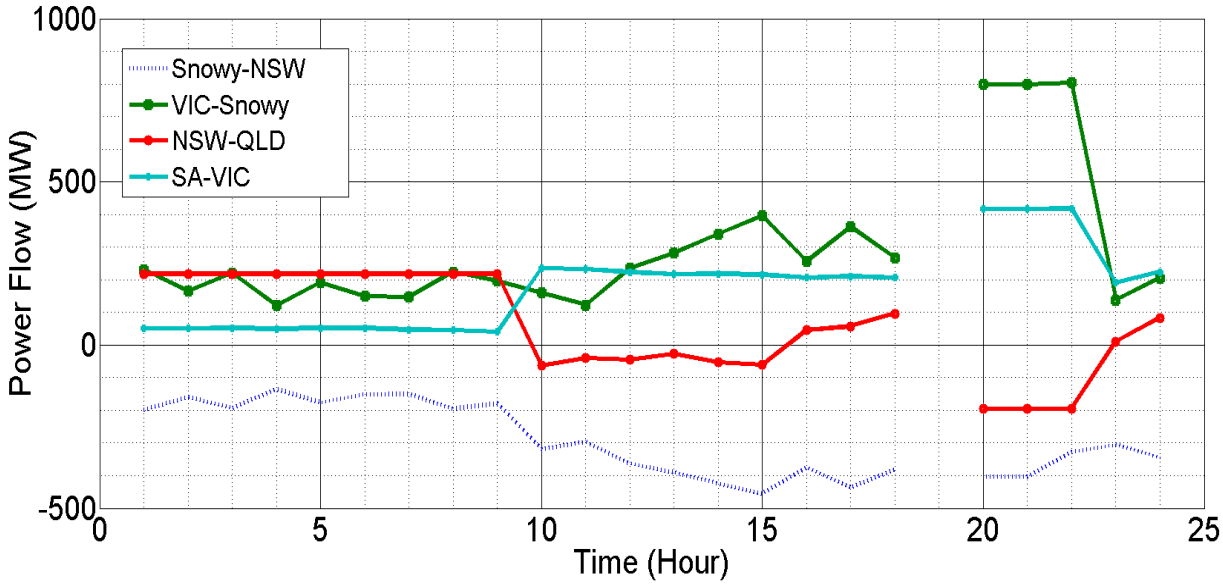

Fig. 9 The Power Flow Distribution under 12.92% Renewables with 80% Energy Storage

The Fig. 8-9 shows when there is accumulated energy storage integrated into some critical nodes (such as Sydney city), the none-convergence problem of power flow could be dramatically alleviated, which can be seen from Fig. 6 and Fig. 8 that the power flow none-converge period time is reduced significantly. Also with the penetration level of energy storage increases (From Fig. 8 to Fig. 9), the supporting function also strengthens, making the none-converge time shorter (from 2 hours to 1 hour). Therefore, the optimal dispatch of energy storage can indeed help the system survive from the harsh situations in the future with high penetration level of intermittent renewable resources.

2.2.3 Impact of Location of the Distribution RE and ES

The simulation also concludes that with the same energy storage modelling, same renewable energy generation penetration level and the same energy storage level, the impact of the energy storage to the grid could vary according to the location of the load.

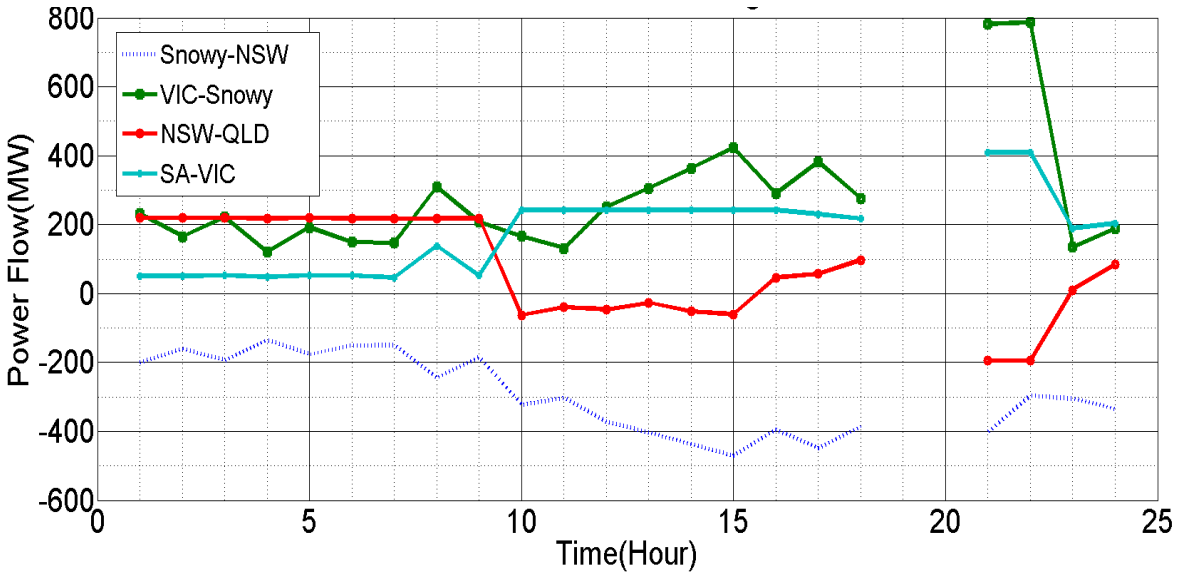

Fig. 10 The Power Flow Distribution under 12.92% Renewables with 80% ES at Node 212

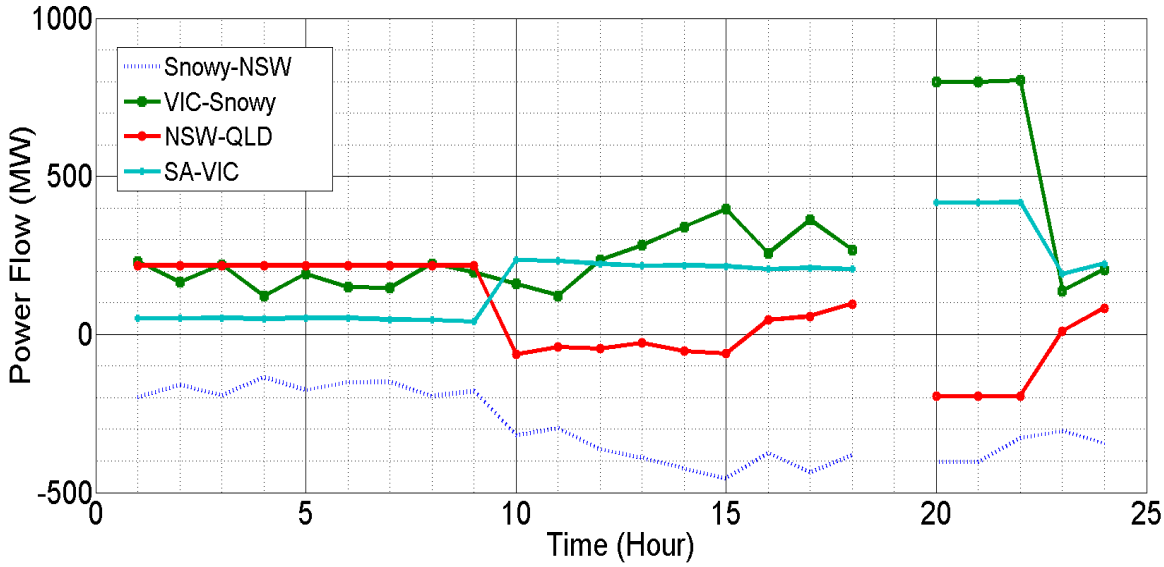

Fig. 11 The Power Flow Distribution under 12.92% Renewables with 80% ES at Node 509

It can be seen that when energy storage devices are integrated in node 509 (remote load), power flows in 8 pm converge. On the other hand, as shown in Fig. 10, when the energy storages are placed in node 212 (load centre), the power flows are not converged at 8 pm. This could indicate with same level of renewable energy penetration and ES uptake, the stability diverse for different locations.

2.3 Dynamic Simulation and Analysis

A fault such as a common short circuit event in a power system leads to a dynamic condition. Such an incident can start a variety of different dynamic phenomena in the system such as instability and/or oscillations. Hence studies with various dynamic models in future grid are essential as well. Specifically, power system dynamic analysis deals with the power system response to small and large disturbances. This usually relates to dynamics of the system around some equilibrium point (possibly quasi-static). The steady-state analysis of these dynamic equilibrium using dynamic power flow models and associated indices can demonstrate the dynamic behaviour of the grid a lot. Thus, the security scanning tools and framework are based on steady-state and dynamic analysis. For each scenario considered, the framework can be used to make comprehensive security assessment through diverse scanning tools and finally, the assessment report can be generated.

Power system dynamic analysis aims to analyse the ability of an electric power system to regain a state of operating equilibrium after a physical disturbance for a given initial operating condition [34]. The basic security requirement after balancing (energy, power and ramping) is

maintaining adequate stability margins (angle, voltage, frequency) for specified contingencies. Power system stability for classical grids can be divided into three types [34], i.e. voltage stability, rotor angle stability and frequency stability.

In this section, the preliminary results of the RE integration on system stability are presented. The dynamic analysis is done under different RE penetration levels without considering ES in this chapter whilst the control and dispatch methodologies of ES will be discussed in the following chapters from the frequency, voltage and power flow perspectives. As mentioned above, different stabilities have been simulated and assessed in DIgSILENT.

2.3.1 Voltage Stability with RE integration

Voltage stability [34] analysis can be classified as large disturbance voltage stability and small disturbance voltage stability. Large disturbance voltage stability refers to the system's ability to maintain steady voltages following large disturbances such as system faults, loss of generation, or circuit contingencies. Determination of large-disturbance voltage stability requires the examination of the nonlinear response of the power system over a period of time sufficient to capture the performance. Small disturbance voltage stability refers to the system's ability to maintain steady voltages when subjected to small perturbations such as incremental changes in system load. This form of stability is influenced by the characteristics of loads, continuous controls, and discrete controls at a given instant of time.

In my research, voltage stability analysis is studied with both large disturbance and small disturbance, where a short circuit is selected for the large disturbance and a reduction on the system load is used for the small disturbance analysis.

It can be seen from Fig. 12 that generally speaking, as the penetration level of RE increases, the voltage dynamic performance deteriorates significantly. The reason is that most of the REs are inverter-based and running in the condition of constant power factor. When the penetration level increases, i.e. the active power injected soars, the compensation reactive power derived from the power electronic circuits are insufficient to support the voltage stability. Therefore, the voltage tends to be more vulnerable and susceptible to disturbances when more REs are connected to the power system.

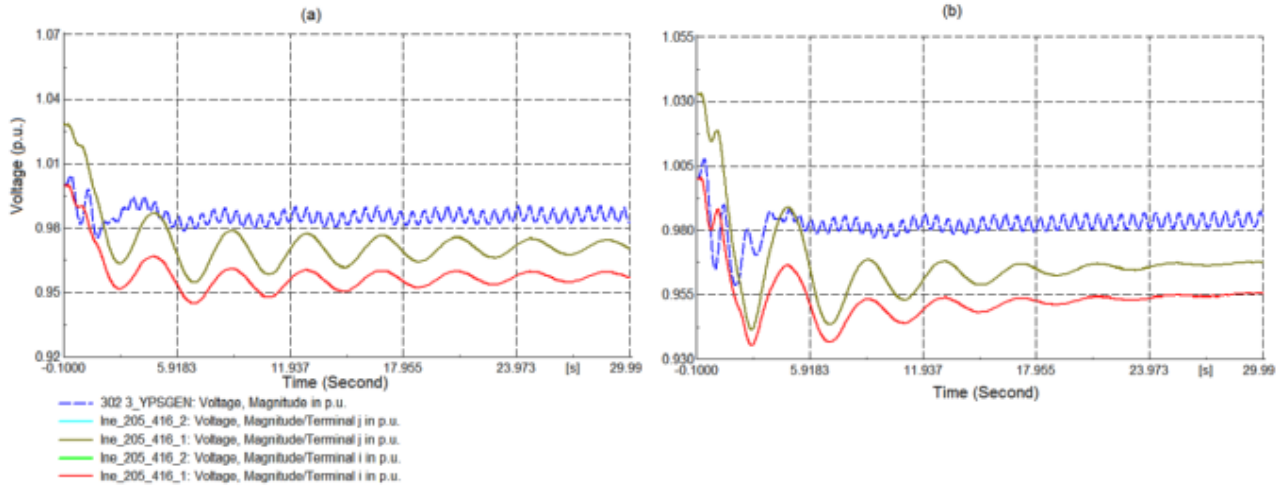

Fig. 12 Voltage Stability with Different RE Penetration under Small Disturbance

(*a*) 6.46% RE Penetration (*b*)12.92% RE Penetration

2.3.2 Rotor Angle Stability with RE integration

Rotor angle stability [34] refers to the ability of the synchronous machines of an interconnected power system to remain in synchronism after being subjected to a disturbance. It

depends on the ability to maintain/restore equilibrium between electromagnetic torque and mechanical torque of each synchronous machine in the system.

Compared with voltage stability, the RE does not in this case show much impact on rotor angle stability. Even though there are some wings after the disturbance, they are still acceptable value and the system can achieve to a new stable situation. We can see the dynamic behaviour is insensitive with regard to the increasing penetration level of RE, but further studies would be needed.

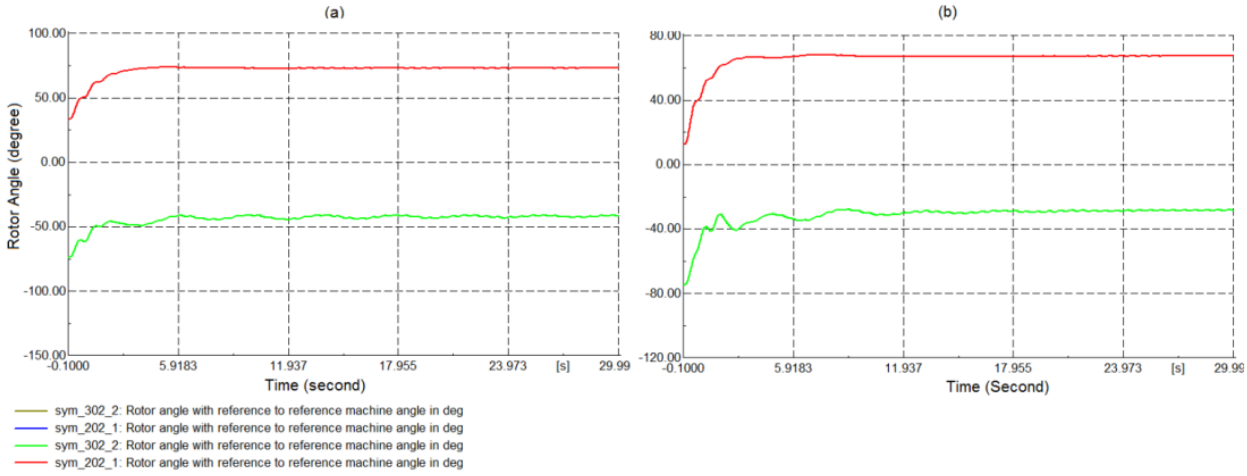

Fig. 13 Rotor Angle Stability with Different RE Penetration under Small Disturbance

(*a*) 6.46% RES Penetration (*b*)12.92% RES Penetration

2.3.3 Frequency Stability with RE integration

According to the standard definition [34], frequency stability refers to the capability of an inter-connected power system to maintain steady frequency around the rated value after a significant active power imbalance between generation and load. It depends on the ability to

maintain/restore equilibrium between system generation and load, with minimum unintentional loss of load. Instability occurs in the form of sustained frequency swings leading to the tripping of generating units and/or loads.

Therefore, in the dynamic study, we test the system frequency behaviour after a disturbance caused by load step change. The Fig. 14 shows the result.

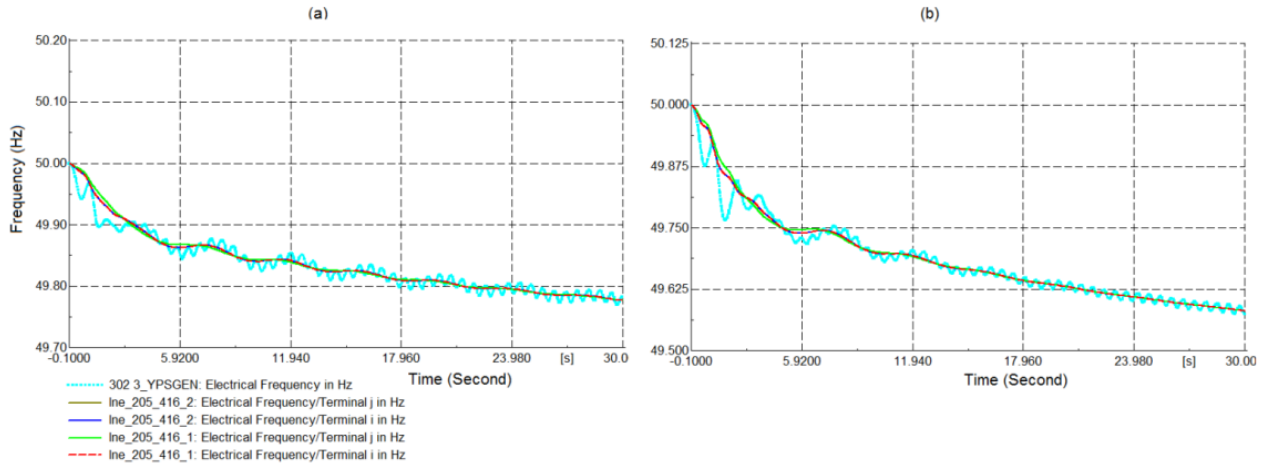

Fig. 14 Frequency Stability with Different RE Penetration Level under Small Disturbance

(*a*) 6.46% RE Penetration (*b*)12.92% RE Penetration

It can be seen that the frequency stability of the system decreases with the RE penetration level increases under disturbance and the final value of frequency is also worse.

However, another interesting and noteworthy phenomenon is that under higher RE penetration level, the decreasing speed (dynamic process) becomes faster compared with lower level situation. This is caused by the inverter-based RE reducing the rotation inertia of the system compared with conventional rotating generators so that the active power balancing process is accelerated. Since the energy storages are also connected to the system with power

electronic based equipment, it inspires us to design an appropriate controller to utilize this characteristic to assist the traditional AGC units to maintain the frequency stable in future grid scenarios with high penetration level of intermittent RE to balance the active power. This is also the central discussion topic in Chapter 3.

3. Robust H_∞ Load Frequency Control (LFC) of Future Power Grid with Energy Storage Devices

As illustrated in chapter 2, the integration of RE will inevitably cause adverse impacts on both system static power flow distribution and dynamic performance such as jeopardizing the frequency and voltage stability [35]. In this chapter, I will focus on the frequency perspective. Unlike the voltage quality which is a local power issue that has a close relationship with the reactive power injection or absorption, the frequency of a certain area implies a global performance of the active power equilibrium between the total generation and consumption. The unpredictable nature and highly intermittent outputs of the RE sources require a much higher frequency adjusting ability of the future power system to accommodate them, so it is a challenge for the traditional frequency regulation approaches. Meanwhile, the utilization of energy storage (ES) can play a positive and noteworthy role in dealing with the above problems. Firstly, the dynamic model of the grid-connected ES and the closed-loop frequency-domain block diagram is developed. Then a novel controller is proposed based on linear matrix inequalities (LMI) theory to ensure the robustness and stability of the system, when taking into account parametric uncertainty and random time delay in control channels in the complex environment. The system can utilize ES to participate in Load Frequency Control (LFC) process so as to assist conventional thermal units. Finally, comprehensive case studies are performed to demonstrate the effectiveness of the proposed methods.

3.1 Dynamic Modelling of the Grid-Connected Battery Energy Storage

There are many different kinds of ES that can be utilized in power system operation. In the literature [3], the merits and limitations of available choices of storage devices are studied.

We can conclude that for high power grid-connected storage level (sec/min), the Lithium-ion battery energy storage (BES) remains the best compromise between performance and cost.

In practice, the ESA (Energy Storage Association) of USA has given the guidance of using energy storage in frequency regulation. It points out that in the group of "ancillary services" provide in the open market management of the grid, frequency regulation has the highest value, which typically takes minutes and battery electricity storage has the capacity for doing this job in milliseconds, making it an ideal and competitive choice. The practical examples are various, such as the AES Energy Storage Angamous Battery Energy Storage System (BESS) in North Chile; the AES Energy Storage Laurel Mountain Battery Energy Storage in Belington; the AES Los Andes Battery Energy Storage System (BESS) in Atacama; the Kaheawa Windfarm Dynamic Power Resource (DPR) Energy Storage on the island of Maui, etc. These are all successful examples of using grid-connected energy storage devices to help the power system to operate more reliable and economical.

The following battery photo Fig.15 is an example: it shows the 12MW A123 lithium battery at AES Gener's Los Andes substation in the Atacama Desert in Chile used for frequency regulation [36].

Fig. 15 The Lithium Battery Storage in Chile

The equivalent circuit of the battery ES can be represented by a DC/AC converter connecting an equivalent battery, which is composed of a set of batteries in parallel/series connection as shown in Fig. 16[37].

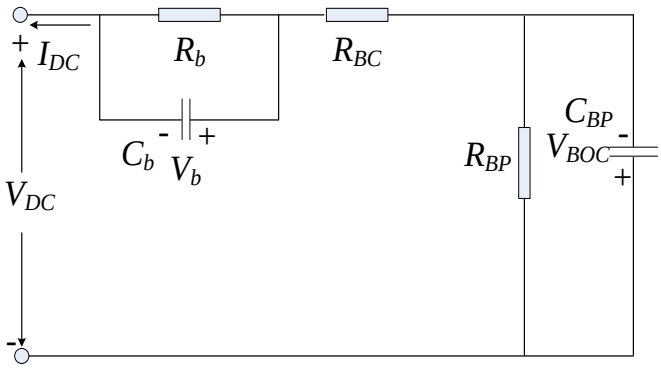

Fig. 16 Equivalent Circuit of Battery Energy Storage

The battery can provide both active power and reactive power as the power system requires. In order to enable the battery energy storage being easily used in the stability analysis and controller design, the model should be transformed into the frequency domain, which has been derived in the previous work [37]. The active power increment ΔP_{ES} transferred through the converter is controlled relying on the system measured frequency deviation, which can be expressed as:

$$\Delta P_{ES} = \frac{K_b}{1+sT_{ES}} \Delta f \tag{6}$$

3.2 Traditional PI Controller and its Limitations

The system cannot work at all without appropriate controllers. The conventional PI control scheme shown in Fig. 17 is one of the most widely used approaches to regulate the frequency in practical interconnected power systems.

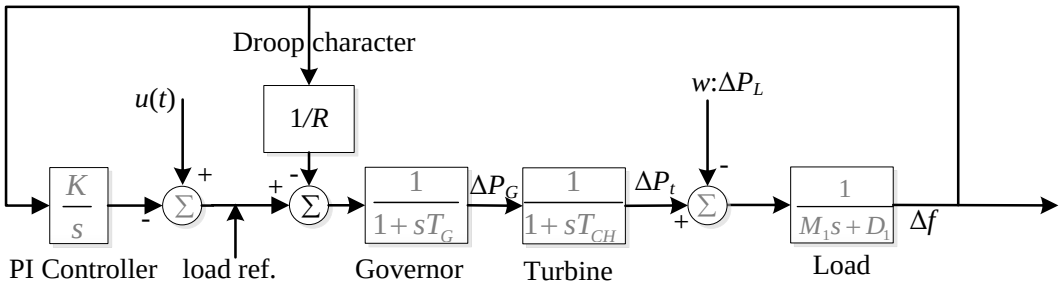

Fig. 17 Conventional PI LFC Controller

However, the traditional PI controller has quite a few limitations: most importantly, it cannot tackle these two important factors in future grid scenarios:

- One is the parametric uncertainty due to the difficulties of precision measurement, time-varying characters under different working conditions and the lack of sufficient knowledge to describe some certain system parameters in an accurate value;
- The other factor is the ubiquitous time delay that exists not only in the control channels but also in the data propagation, switching, accessing and queuing process.

Both of them should be considered in practice because these inevitable phenomena could significantly degrade the system dynamic performance. Besides, with one set of PI coefficients, the system would lose the stability when time delay accumulates to a certain level or system parameter variation occurs. Therefore, the robustness of the power grid cannot be guaranteed in the complex environment in the future when we consider the cyber-physical power system. Although some of the references have discussed the time delay problem (e.g. [12]) in LFC application, the parametric uncertainties of the energy storage has not yet been addressed and analysed simultaneously in the design process.

In the following sections, a novel H_∞ Controller is designed based on Linear Matrix Inequalities (LMI) Theory to help to solve this problem.

The reason to choose H_∞ control is that it is readily applicable to problems involving multivariate systems with cross-coupling between channels, and H_∞ techniques can also be used to minimize the closed loop impact of a perturbation, which is quite suitable for tackling the problem discussed in the thesis. Besides, the H_∞ controller has the rigorous mathematical foundation to guarantee its effectiveness theoretically, and the commercial software is also available to support H_∞ controller synthesis, making it an ideal and promising approach in the future.

3.3 Closed Loop Diagram of the LFC System with ES

3.3.1 Block Diagram of the System with Energy Storage

A two-area system is considered here, as shown in Fig. 18 where the topology of the New England 39-bus power system has been augmented with energy storage integrated.

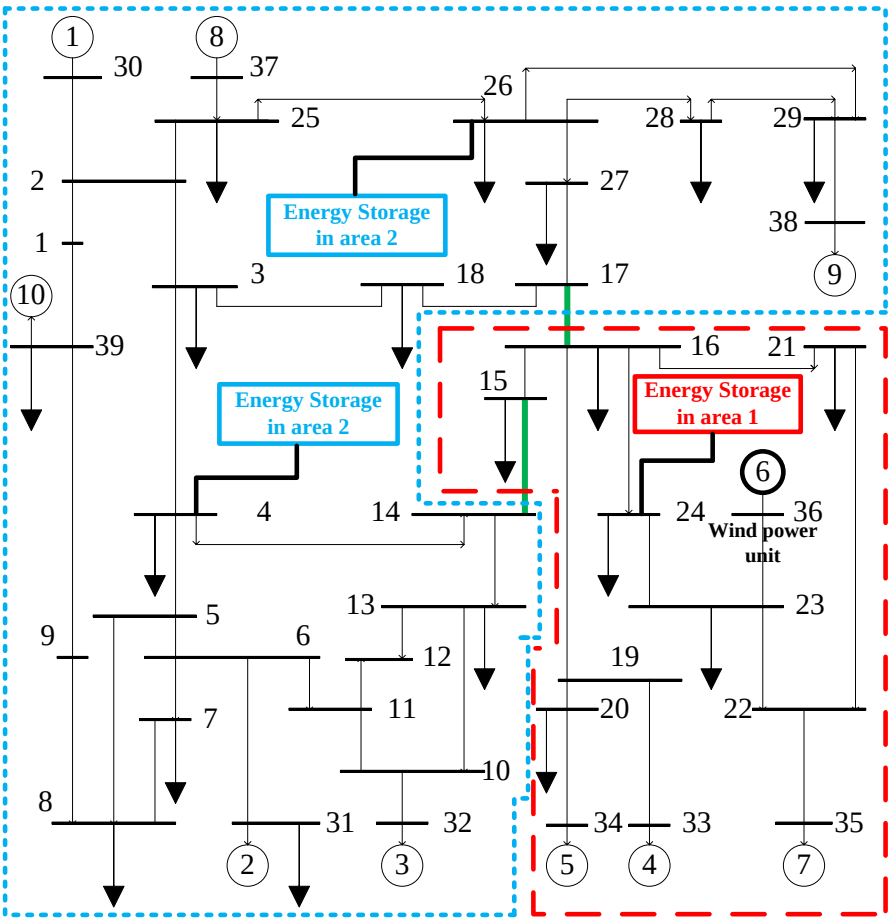

Fig. 18 The Topology Structure of the IEEE 10-Unit 39-Bus Two-Area Test System (with BES and WP)

For the purpose of committing LFC, a comprehensive model has to be built. The grid-connected battery ES station together with conventional AGC units are controlled together to change their injection power so as to follow the load disturbances. Without loss of generality, the block diagram for above mentioned two-area system is abstracted from Fig. 18 to Fig. 19:

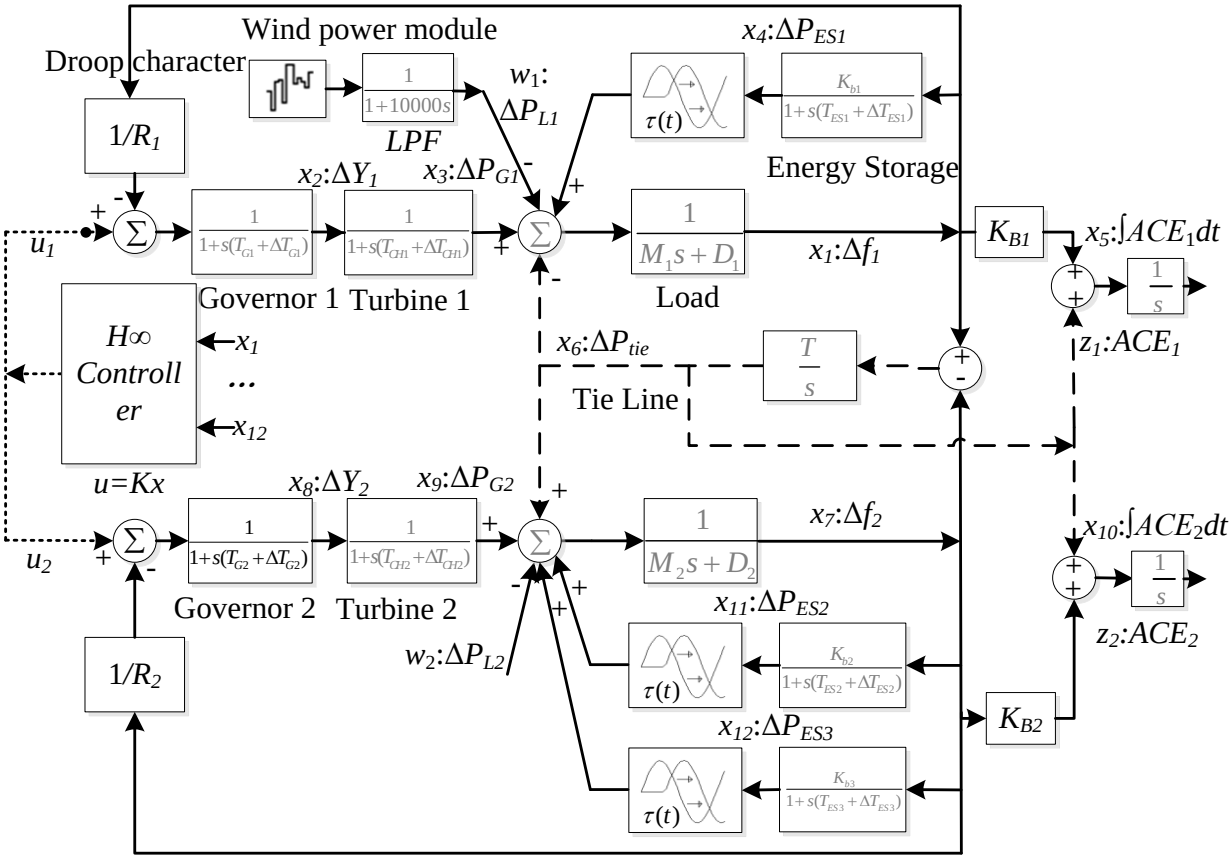

Fig. 19 The Block Diagram of the LFC System with Battery Energy Storage, Wind power Module and Time Delay

Here, the AGC units are lumped as a single equivalent generating component separately for the purpose of analysis. We assume that there is one battery ES in area 1 and two in area 2. The method proposed below is also applicable if more energy storage devices are integrated. The

active power unbalance could either come from load change, or from the fluctuation of REs such as wind turbine output. Note that the network induced time delay $\tau(t)$ exists in some parts of the communication channels and the parametric uncertainty is also considered here, which will be discussed in mathematical modelling later.

3.3.2 Analysis of Parametric Uncertainty and Time Delay

In order to make an effective design, the differences between the simplified model and the real objects are called the model uncertainties. In addition to the uncertainties that emerge when simplifying the model, because of the lack of sufficient knowledge, difficulties on precision measurement would also introduce model uncertainties [38]. For example, the uncertainty of some parameters, such as the time constants of generators and ES, are very difficult to be described in a precise value. Furthermore, most likely these parameters are time-varying according to different conditions in the process of operation. Then, the actual system model should be described with a linear model plus a time-varying uncertainty part. The linear part is called the nominal model of the system, while the time-varying part reflects the reality of the system in practical situation. Generally, the parameters vary in a specific bounded area.

Another important factor that affects the system dynamic performance is the ubiquitous time delay that is scattered in the control network. In particularly in future smart grid environment, the widely usage of general-purpose communication network (e.g. the Internet or Ethernet) would make the network-induced delay non-negligible. Thus it can significantly degrade the system performance.

The main reasons for the network-induced delay are as follows:

1) Data queue waiting time. When the network is busy or the collision of the packet happens, the data has to wait for sending until the network is idle again.

2) Information generation. At transmitting end, the information has to wait for packaging to enter the network.

3) Transmission. The transmission time for the data in the medium depends on the packet size, the bandwidth and transmission delay.

Table 4 lists some of the typical access control modes and their corresponding delay characteristics and parameters.

Table 4 Control Networks and Delay Characteristics

Network	Ethernet	CAN Bus	TP Bus
Access Mode	Random Access	Random Access	Token Passing
Network Protocol	IEEE 802.3 CSMA/CD	CSMA/AMP	IEEE 802.4
Data Packet	Maximum 1500	Maximum 8	Maximum 504
Delay Characteristics	Random; Unbounded	Random; Bounded	Random; Bounded; Periodic

As is shown in Table 4, the delay characteristics are different in different forms of control networks. The following research is for Ethernet, but the methodology and framework also apply to other control networks. Although Ethernet has its advantages of high data transfer rates, low power consumption, easy installation and compatibility, the disadvantages, however, are also

quite obvious. When the serious heavy load condition happens, the time delay is random and unbounded, which puts a relatively higher requirements for maintaining the stability and robustness of the control method and system.

Without loss of generality and for the purpose of analysis, we simplify the distributed network-induced delays as a single delay module that exists in parts of the control channels, which can be used for simulating the impacts on the system frequency dynamic performance.

3.3.3 The State-Space Formulation of the Proposed System with Parametric Uncertainty and Time Delay

Based on the closed-loop diagram and the above analysis, the state-space equations with parametric uncertainty and time delay can be mathematically derived as follows through linearization near the steady operating point of the system for small disturbance stability analysis:

$$\begin{cases} \dot{\boldsymbol{x}}(t) = (\boldsymbol{A} + \Delta\boldsymbol{A}(t))\boldsymbol{x}(t) + (\boldsymbol{A}_{\boldsymbol{d}} + \Delta\boldsymbol{A}_{\boldsymbol{d}}(t))\boldsymbol{x}(t - \tau(t)) + (\boldsymbol{B}_{\boldsymbol{2}} + \Delta\boldsymbol{B}_{\boldsymbol{2}}(t))\boldsymbol{u}(t) + \boldsymbol{B}_{\boldsymbol{1}}\boldsymbol{w}(t) \\ \boldsymbol{z}(t) = \boldsymbol{C}\boldsymbol{x}(t) + \boldsymbol{D}_{\boldsymbol{11}}\boldsymbol{w}(t) + \boldsymbol{D}_{\boldsymbol{12}}\boldsymbol{u}(t) \end{cases} \quad (7)$$

$$\boldsymbol{A}=\begin{bmatrix}
-\frac{D_1}{M_1} & 0 & -\frac{1}{M_1} & 0 & 0 & -\frac{1}{M_1} & 0 & 0 & 0 & 0 & 0 & 0 \\
-\frac{1}{R_1T_{G1}} & -\frac{1}{T_{G1}} & 0 & 0 & 0 & 0 & 0 & 0 & 0 & 0 & 0 & 0 \\
0 & \frac{1}{T_{CH1}} & -\frac{1}{T_{CH1}} & 0 & 0 & 0 & 0 & 0 & 0 & 0 & 0 & 0 \\
\frac{K_{b1}}{T_{ES1}} & 0 & 0 & -\frac{1}{T_{ES1}} & 0 & 0 & 0 & 0 & 0 & 0 & 0 & 0 \\
b_1 & 0 & 0 & 0 & 0 & 1 & 0 & 0 & 0 & 0 & 0 & 0 \\
T & 0 & 0 & 0 & 0 & 0 & -T & 0 & 0 & 0 & 0 & 0 \\
0 & 0 & 0 & 0 & 0 & \frac{1}{M_2} & -\frac{D_2}{M_2} & 0 & \frac{1}{M_2} & 0 & 0 & 0 \\
0 & 0 & 0 & 0 & 0 & 0 & -\frac{1}{R_2T_{G2}} & -\frac{1}{T_{G2}} & 0 & 0 & 0 & 0 \\
0 & 0 & 0 & 0 & 0 & 0 & 0 & \frac{1}{T_{CH2}} & -\frac{1}{T_{CH2}} & 0 & 0 & 0 \\
0 & 0 & 0 & 0 & 0 & 1 & b_2 & 0 & 0 & 0 & 0 & 0 \\
0 & 0 & 0 & 0 & 0 & 0 & \frac{K_{b2}}{T_{ES2}} & 0 & 0 & 0 & -\frac{1}{T_{ES2}} & 0 \\
0 & 0 & 0 & 0 & 0 & 0 & \frac{K_{b3}}{T_{ES3}} & 0 & 0 & 0 & 0 & -\frac{1}{T_{ES3}}
\end{bmatrix}$$

$$\boldsymbol{A_d}=\begin{bmatrix}
0 & 0 & 0 & \frac{1}{M_1} & 0 & 0 & 0 & 0 & 0 & 0 & 0 & 0 \\
0 & 0 & 0 & 0 & 0 & 0 & 0 & 0 & 0 & 0 & 0 & 0 \\
0 & 0 & 0 & 0 & 0 & 0 & 0 & 0 & 0 & 0 & 0 & 0 \\
0 & 0 & 0 & 0 & 0 & 0 & 0 & 0 & 0 & 0 & 0 & 0 \\
0 & 0 & 0 & 0 & 0 & 0 & 0 & 0 & 0 & 0 & 0 & 0 \\
0 & 0 & 0 & 0 & 0 & 0 & 0 & 0 & 0 & 0 & 0 & 0 \\
0 & 0 & 0 & 0 & 0 & 0 & 0 & 0 & 0 & 0 & \frac{1}{M_2} & \frac{1}{M_2} \\
0 & 0 & 0 & 0 & 0 & 0 & 0 & 0 & 0 & 0 & 0 & 0 \\
0 & 0 & 0 & 0 & 0 & 0 & 0 & 0 & 0 & 0 & 0 & 0 \\
0 & 0 & 0 & 0 & 0 & 0 & 0 & 0 & 0 & 0 & 0 & 0 \\
0 & 0 & 0 & 0 & 0 & 0 & 0 & 0 & 0 & 0 & 0 & 0
\end{bmatrix}$$

$$\boldsymbol{B_2}=\begin{bmatrix}
0 & 0 \\
\frac{1}{T_{G1}} & 0 \\
0 & 0 \\
0 & 0 \\
0 & 0 \\
0 & 0 \\
0 & 0 \\
0 & \frac{1}{T_{G2}} \\
0 & 0 \\
0 & 0 \\
0 & 0
\end{bmatrix}$$

$$\boldsymbol{B_1}=\begin{bmatrix}
-\frac{1}{M_1} & 0 \\
0 & 0 \\
0 & 0 \\
0 & 0 \\
0 & 0 \\
0 & 0 \\
0 & -\frac{1}{M_2} \\
0 & 0 \\
0 & 0 \\
0 & 0 \\
0 & 0
\end{bmatrix}$$

$$\boldsymbol{C}=\begin{bmatrix} b_1 & 0 & 0 & 0 & 0 & 1 & 0 & 0 & 0 & 0 & 0 & 0 \\ 0 & 0 & 0 & 0 & 0 & 1 & b_2 & 0 & 0 & 0 & 0 & 0 \end{bmatrix}; \boldsymbol{D_{11}}=\boldsymbol{D_{12}}=\begin{bmatrix} 0 & 0 \\ 0 & 0 \end{bmatrix}$$

Here,

the system state variables $\boldsymbol{X}=[x_1,\ldots, x_{12}]^T=[\Delta f_1,\ \Delta Y_1,\ \Delta P_{G1},\ \Delta P_{ES1},\ \int ACE_1 dt,\ \Delta P_{tie},\ \Delta f_2,\ \Delta Y_2,\ \Delta P_{G2},\ \int ACE_2 dt,\ \Delta P_{ES2},\ \Delta P_{ES3}]^T$.

Where Δf_i (i=1,2) is the frequency;

ΔY_i (i=1,2) is the valve opening variation of AGC units;

ΔP_{Gi} (i=1,2) is the active power variation of traditional AGC units;

ΔP_{ESi} (i=1,2,3) is the power variation of ES;

$\int ACE_i dt$ (i=1,2) is the integral of *ACE* signals as this ensures zero steady-state error to step-change load disturbances;

ΔP_{tie} is the power variation of the tie line that connects two areas.

The disturbance variables $\boldsymbol{w}(t)=[w_1, w_2]^T=[\Delta P_{L1},\ \Delta P_{L2}]^T \in L_2[0, \infty)$, i.e. square-integrable;

Control variables $\boldsymbol{u}(t)=[u_1\ u_2]^T$;

Control output variables $\boldsymbol{z}(t)=[z_1, z_2]^T=[ACE_1, ACE_2]^T$.

The system matrix $\boldsymbol{A}$, $\boldsymbol{A_d}$, $\boldsymbol{B_2}$, $\boldsymbol{B_1}$, $\boldsymbol{C}$, $\boldsymbol{D_{11}}$, $\boldsymbol{D_{12}}$ are real-valued constant matrices of appropriate dimensions that describe the nominal system, $\boldsymbol{\Delta A}(t)$, $\boldsymbol{\Delta A_d}(t)$, $\boldsymbol{\Delta B_2}(t)$ are real time-varying matrix functions representing parametric uncertainty. D_i (i=1,2) is the load frequency characteristic coefficient; M_i、R_i、T_{Gi} and T_{Chi} (i=1,2) are the inertia time constant of the AGC

units, the speed regulation due to governor action, the governor time constant, and the turbine time constant respectively; K_{bi} and T_{ESi} (i=1,2,3) are frequency response coefficients of ES and equivalent time constant of the batteries respectively; T is the tie line synchronization coefficient; $\tau(t)$ is the equivalent time delay that satisfying:

$$0 \le \tau(t) < \infty, \dot{\tau}(t) \le \rho < 1 \tag{8}$$

With regard to the parametric uncertainty, it is assumed that they can be modelled as:

$$[\Delta \boldsymbol{A}(t)\ \Delta \boldsymbol{A_d}(t)\ \Delta \boldsymbol{B_2}(t)] = \boldsymbol{HF}(t)[\boldsymbol{E_1}\ \boldsymbol{E_2}\ \boldsymbol{E_3}] \tag{9}$$

Where $\boldsymbol{H}$, $\boldsymbol{E_1}$, $\boldsymbol{E_2}$, $\boldsymbol{E_3}$ are known as real constant matrices, and $\boldsymbol{F}(t)$ is an unknown time-varying uncertainty matrix function that satisfying

$$\left\| F(t) \right\| \le 1, \forall t \in [0, +\infty) \tag{10}$$

The matrixes $\boldsymbol{H}$, $\boldsymbol{E_1}$, $\boldsymbol{E_2}$, $\boldsymbol{E_3}$ specify how the uncertain parameters in $\boldsymbol{F}(t)$ affects the nominal matrix of system (7), which implies that they essentially reflect the structure of the system. In this study, we assume that the variation ranges of the following parameters are:

$$\begin{cases} \dfrac{1}{T_{Gi}} \in \left[\dfrac{1}{\overline{T}_{Gi}} \pm \Delta_{Gi} \right], i = 1,2 \\ \dfrac{1}{T_{CHj}} \in \left[\dfrac{1}{\overline{T}_{CHj}} \pm \Delta_{CHj} \right], j = 1,2 \\ \dfrac{1}{T_{ESk}} \in \left[\dfrac{1}{\overline{T}_{ESk}} \pm \Delta_{ESk} \right], k = 1,2,3 \end{cases} \tag{11}$$

Through the matrix decomposition, we can acquire:

$$\boldsymbol{H}=\begin{bmatrix}0 & \Delta_{G1} & 0 & 0 & 0 & 0 & 0 & 0 & 0 & 0 & 0 & 0\\ 0 & 0 & \Delta_{CH1} & 0 & 0 & 0 & 0 & 0 & 0 & 0 & 0 & 0\\ 0 & 0 & 0 & \Delta_{ES1} & 0 & 0 & 0 & 0 & 0 & 0 & 0 & 0\\ 0 & 0 & 0 & 0 & 0 & 0 & 0 & \Delta_{G2} & 0 & 0 & 0 & 0\\ 0 & 0 & 0 & 0 & 0 & 0 & 0 & 0 & \Delta_{CH2} & 0 & 0 & 0\\ 0 & 0 & 0 & 0 & 0 & 0 & 0 & 0 & 0 & 0 & \Delta_{ES2} & 0\\ 0 & 0 & 0 & 0 & 0 & 0 & 0 & 0 & 0 & 0 & 0 & \Delta_{ES3}\end{bmatrix}^{T}$$

$$\boldsymbol{E_1}=\begin{bmatrix}-1/R_1 & -1 & 0 & 0 & 0 & 0 & 0 & 0 & 0 & 0 & 0 & 0\\ 0 & -1 & 1 & 0 & 0 & 0 & 0 & 0 & 0 & 0 & 0 & 0\\ K_{b1} & 0 & 0 & -1 & 0 & 0 & 0 & 0 & 0 & 0 & 0 & 0\\ 0 & 0 & 0 & 0 & 0 & 0 & -1/R_2 & -1 & 0 & 0 & 0 & 0\\ 0 & 0 & 0 & 0 & 0 & 0 & 0 & 0 & -1 & 0 & 0 & 0\\ 0 & 0 & 0 & 0 & 0 & 0 & K_{b2} & 0 & 0 & 0 & -1 & 0\\ 0 & 0 & 0 & 0 & 0 & 0 & K_{b3} & 0 & 0 & 0 & 0 & -1\end{bmatrix}$$

$$\boldsymbol{E_2}(i,j)=0;(i\in[1,2,...,5],\ j\in[1,2,\ldots 12])$$

$$\boldsymbol{E_3}=\begin{bmatrix}1 & 0 & 0 & 0 & 0 & 0 & 0\\ 0 & 0 & 0 & 1 & 0 & 0 & 0\end{bmatrix}^{T}$$

3.4 Controller Design based on LMI Theory

3.4.1 Summary of the LMI Methods

The system cannot work at all without a suitable controller. Since Zames first proposed H_∞ robust control method in 1981, this problem has aroused tremendous attention and developed rapidly. Not only does the H_∞ robust control have a rigorous mathematical foundation, but also the controller has been proved to be a great success in industry application.

A control system can be abstracted as the generalized object $G(s)$ that will be controlled by $K(s)$ as shown in Fig. 20.

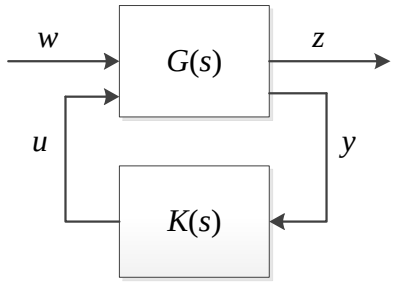

Fig. 20 The Block Diagram of H_∞ Robust Control

The goal of the H_∞ robust control is to design a real regular function controller $K(s)$ to ensure internal stability of the generalized object. In other words, $K(s)$ has to internal stabilize the whole system first, then inhibit the input disturbance $w(t)$ optimally. Here, "internal stability" is a term in robust control theory, which guarantees all the signals are bounded in the system given the fact that the input signals are bounded wherever they connected into the system. Under this constraint, the controller has to minimize the input disturbance, i.e. guarantees the transfer function (from the disturbance input $w(t)$ to control output $z(t)$) $G_{wz}(s)$'s H_∞ norm would not exceed a pre-given small positive constant γ, which means $\|z(t)\|_2<\gamma\|w(t)\|_2$, $\forall w\in L_2[0,+\infty)$ under the zero initial condition $x(t)=0$ ($t\in[-d,0]$). Here, $x(t)$ is the system state; d is the delay time; $\|z(t)\|_2$ is the signal's L_2 norm, which essentially represents the energy of the signal and can be mathematically defined as $\|z(t)\|_2=\|Z(j\omega)\|_2=\sqrt{\frac{1}{2\pi}\int_{-\infty}^{+\infty} tr(\hat{Z}^*(j\omega)\hat{Z}(j\omega))d\omega}$. $L_2[0,+\infty)$ denotes a set of the time-domain signals that are L_2 norm bounded. The controller obtained at this time is called a suboptimal robust H_∞ controller, with γ expresses the capability of the whole system to suppress the external input interference $w(t)$ and is called "interference suppression degree". The smaller γ is, the better robust performance and stability of the system will have. If we solve the

optimization problem to minimize γ so as to get the smallest value of the interference suppression degree, then the controller obtained at this time is called optimal robust H_∞ controller.

In this LFC problem, the H_∞ control method has to be used for time delayed system after concerning the parametric uncertainties. The traditional robust control often deals with this problem by solving algebraic Ricatti equation or solving the simplified Lyapunov equation. However, this approach is difficult to calculate, especially the second Ricatti equation is difficult to converge when solving two simultaneous Ricatti equations, which limits the application scope of this method greatly.

In recent years, with the development of the linear matrix inequality (LMI) theory, especially after the propose of interior point method and MATLAB-LMI Tool Box, LMI-based controller design has drawn more and more attention from control engineers, and it has been successfully applied in the practical systems.

The delay-independent and delay-dependent problems are two different issues and have to adopt different methods when analysing the stability character of the system. As mentioned above, this study is based on Ethernet so the controller design in the delay-independent situation is focused and deeply studied. In general, the stability conditions are more conservative under delay-independent situation, because the system can be stable with any large time delay as long as it satisfies delay-independent stability conditions, which nevertheless could be too strict for general small-delay system. With regards to the delay-dependent problem, it refers to the stability character of the system depends on the length or other characteristics of the delay, namely it depends on the length of time delay itself, thus is called delay-dependent design. For

some small-delay systems that the upper bound of the delay has been identified, the controller design could be simplified. However, there are quite a few merits for delay-independent controller; for example, it allows the delay to be uncertain, random and unknown, which means that the system can be stable without knowing the accurate information of the time delay, as well as guaranteeing the robustness of the system with any uncertain situations. As the future smart grid is wide-area distributed and the structure of the grid varies a lot geographically, it would be better to consider the more severe and extreme situation. Therefore, the following discussion mainly focuses on the controller design under delay-independent conditions, i.e. assumes that the time delay is random and unbounded.

3.4.2 LMI Based Design of the Robust Controller

It is better to design a full-state feedback controller, because the more states we can get, the better the dynamic performance of the system will be. The H_∞ part of the controller is depicted as Fig. 21:

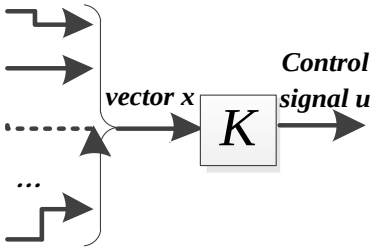

Fig. 21 The H_∞ Part of Full-State Feedback Control

In order to design the controller, a lemma should be introduced first:

Lemma 1[39]: For a system with time delay:

$$\begin{cases} \dot{\boldsymbol{x}}(t) = \boldsymbol{A}\boldsymbol{x}(t) + \boldsymbol{A}_d \boldsymbol{x}(t-\tau(t)) + \boldsymbol{B}\boldsymbol{w}(t) \\ \boldsymbol{z}(t) = \boldsymbol{C}\boldsymbol{x}(t) + \boldsymbol{D}\boldsymbol{w}(t) \end{cases} \tag{12}$$

And a pre-given constant γ, assuming the network delay $\tau(t)$ satisfies the condition (8), Then if there exist two positive definite matrixes P and S such that the following LMI holds (<0 indicates the matrix is negative definite):

$$\begin{bmatrix} \boldsymbol{A}^T\boldsymbol{P} + \boldsymbol{P}\boldsymbol{A} + \boldsymbol{S} & \boldsymbol{P}\boldsymbol{B} & \boldsymbol{C}^T & \boldsymbol{P}\boldsymbol{A}_d \\ \boldsymbol{B}^T\boldsymbol{P} & -\gamma\boldsymbol{I} & \boldsymbol{D}^T & 0 \\ \boldsymbol{C} & \boldsymbol{D} & -\gamma\boldsymbol{I} & 0 \\ \boldsymbol{A}_d^T\boldsymbol{P} & 0 & 0 & -(1-\rho)\boldsymbol{S} \end{bmatrix} < 0 \tag{13}$$

Then the system is robust stable, and the interference suppression degree character is γ. This lemma is used to determine whether the designed system has the H_∞ performance.

Lemma 2[40] Given the matrix $\boldsymbol{Y}$, $\boldsymbol{D}$, $\boldsymbol{E}$ with appropriate dimensions where $\boldsymbol{Y}$ is symmetrical, then

$$\boldsymbol{Y} + \boldsymbol{D}\boldsymbol{F}\boldsymbol{E} + \boldsymbol{E}^T\boldsymbol{F}^T\boldsymbol{D}^T < 0 \tag{14}$$

For all the matrix $\boldsymbol{F}$ that satisfies (10), if and only if there exists a constant ε>0, such that

$$\boldsymbol{Y} + \varepsilon\boldsymbol{D}\boldsymbol{D}^T + \varepsilon^{-1}\boldsymbol{E}^T\boldsymbol{E} < 0 \tag{15}$$

Lemma 3(Schur Theorem): Given the symmetric matrix $\boldsymbol{S}\in\boldsymbol{R}^{n\times n}$: $\boldsymbol{S} = \begin{bmatrix} \boldsymbol{S}_{11} & \boldsymbol{S}_{12} \\ \boldsymbol{S}_{21} & \boldsymbol{S}_{22} \end{bmatrix}$, in which the $\boldsymbol{S}_{11}\in\boldsymbol{R}^{r\times r}$, $\boldsymbol{S}_{12}\in\boldsymbol{R}^{r\times(n-r)}$, $\boldsymbol{S}_{21}\in\boldsymbol{R}^{(n-r)\times r}$, $\boldsymbol{S}_{22}\in\boldsymbol{R}^{(n-r)\times(n-r)}$, then the following three conditions are equivalent:

a) $\boldsymbol{S}$<0;

b) $\boldsymbol{S}_{11} < 0, \boldsymbol{S}_{22} - \boldsymbol{S}_{12}^T \boldsymbol{S}_{11}^{-1} \boldsymbol{S}_{12} < 0$;

c) $\boldsymbol{S}_{22} < 0, \boldsymbol{S}_{11} - \boldsymbol{S}_{12} \boldsymbol{S}_{22}^{-1} \boldsymbol{S}_{12}^T < 0$.

Here we propose a novel theorem that can be used to design the full-state feedback H_∞ controller based on the above mentioned three lemmas. With this approach, the γ robust performance can be guaranteed both with the parametric uncertainties bounded by (9)-(10) and time delay subjected to (8).

Theorem 1: consider a system (7) that the time delay satisfies (8), parametric uncertainties are bounded by (9)-(10) and $(\boldsymbol{A},\boldsymbol{B}_2,\boldsymbol{C}_2)$ is stabilized and can be detected. Then for a pre-given positive constant γ, we can design a memoryless full-state feedback controller $\boldsymbol{u}(t)=\boldsymbol{K}\boldsymbol{x}(t)$ if there exist a positive scalar ε, two positive definite matrixes $\boldsymbol{X}$, $\boldsymbol{Q}$ and a matrix $\boldsymbol{Y}$ such that the LMI (16) holds.

In particular, if $(\hat{\boldsymbol{X}},\hat{\boldsymbol{Y}},\hat{\boldsymbol{Q}})$ is a feasible solution of (16), $\boldsymbol{u}(t) = \hat{\boldsymbol{Y}}\hat{\boldsymbol{X}}^{-1}\boldsymbol{x}(t)$ is one of the γ-suboptimal full-state feedback controllers of the system. This problem can be solved using LMI Toolbox [41].

$$\begin{bmatrix} \boldsymbol{\Psi} & \boldsymbol{B}_1 & (\boldsymbol{C}\boldsymbol{X}+\boldsymbol{D}_{12}\boldsymbol{Y})^T & \boldsymbol{A}_d & (\boldsymbol{E}_1\boldsymbol{X}+\boldsymbol{E}_3\boldsymbol{Y})^T \\ \boldsymbol{B}_1^T & -\gamma\boldsymbol{I} & \boldsymbol{D}_{11} & 0 & 0 \\ \boldsymbol{C}\boldsymbol{X}+\boldsymbol{D}_{12}\boldsymbol{Y} & \boldsymbol{D}_{11}^T & -\gamma\boldsymbol{I} & 0 & 0 \\ \boldsymbol{A}_d^T & 0 & 0 & -(1-\rho)\boldsymbol{Q} & \boldsymbol{E}_2^T \\ \boldsymbol{E}_1\boldsymbol{X}+\boldsymbol{E}_3\boldsymbol{Y} & 0 & 0 & \boldsymbol{E}_2 & -\varepsilon\boldsymbol{I} \end{bmatrix} < 0 \qquad (16)$$

Where

$$\boldsymbol{\Psi} = \boldsymbol{A}\boldsymbol{X} + \boldsymbol{B}_2\boldsymbol{Y} + (\boldsymbol{A}\boldsymbol{X} + \boldsymbol{B}_2\boldsymbol{Y})^T + \boldsymbol{Q} + \varepsilon\boldsymbol{H}\boldsymbol{H}^T \qquad (17)$$

Proof: From (7) and $u(t)=Kx(t)$, we can get:

$$\begin{cases} \dot{\boldsymbol{x}}(t) = \bar{\boldsymbol{A}}\boldsymbol{x}(t) + \bar{\boldsymbol{A}}_{\boldsymbol{d}}\boldsymbol{x}(t-\tau(t)) + \bar{\boldsymbol{B}}\boldsymbol{w}(t) \\ \boldsymbol{z}(t) = \bar{\boldsymbol{C}}\boldsymbol{x}(t) + \bar{\boldsymbol{D}}\boldsymbol{w}(t) \end{cases} \tag{18}$$

Where, $\bar{\boldsymbol{A}} = (\boldsymbol{A} + \Delta\boldsymbol{A} + \boldsymbol{B}_2\boldsymbol{K} + \Delta\boldsymbol{B}_2\boldsymbol{K}); \bar{\boldsymbol{A}}_{\boldsymbol{d}} = (\boldsymbol{A}_{\boldsymbol{d}} + \Delta\boldsymbol{A}_{\boldsymbol{d}}); \bar{\boldsymbol{B}} = \boldsymbol{B}_1; \bar{\boldsymbol{C}} = \boldsymbol{C} + \boldsymbol{D}_{12}\boldsymbol{K}; \bar{\boldsymbol{D}} = \boldsymbol{D}_{11}$.

Apply the system (18) into the lemma 1, we can get the robust stable conditions of the system is that the following LMI holds:

$$\begin{bmatrix} \bar{\boldsymbol{A}}^T\boldsymbol{P} + \boldsymbol{P}\bar{\boldsymbol{A}} + \boldsymbol{S} & \boldsymbol{P}\bar{\boldsymbol{B}} & \bar{\boldsymbol{C}}^T & \boldsymbol{P}\bar{\boldsymbol{A}}_{\boldsymbol{d}} \\ \bar{\boldsymbol{B}}^T\boldsymbol{P} & -\gamma\boldsymbol{I} & \bar{\boldsymbol{D}}^T & 0 \\ \bar{\boldsymbol{C}} & \bar{\boldsymbol{D}} & -\gamma\boldsymbol{I} & 0 \\ \bar{\boldsymbol{A}}_{\boldsymbol{d}}^T\boldsymbol{P} & 0 & 0 & -(1-\rho)\boldsymbol{S} \end{bmatrix} < 0 \tag{19}$$

Replace the relevant parameters, we can get:

$$\boldsymbol{Y} + \boldsymbol{D}\boldsymbol{F}\boldsymbol{E} + \boldsymbol{E}^T\boldsymbol{F}^T\boldsymbol{D}^T < 0 \tag{20}$$

Where

$$\boldsymbol{Y} = \begin{bmatrix} (\boldsymbol{A} + \boldsymbol{B}_2\boldsymbol{K})^T\boldsymbol{P} + \boldsymbol{P}(\boldsymbol{A} + \boldsymbol{B}_2\boldsymbol{K}) + \boldsymbol{S} & \boldsymbol{P}\boldsymbol{B}_1 & (\boldsymbol{C} + \boldsymbol{D}_{12}\boldsymbol{K})^T & \boldsymbol{P}\boldsymbol{A}_{\boldsymbol{d}} \\ \boldsymbol{B}_1^T\boldsymbol{P} & -\gamma\boldsymbol{I} & \boldsymbol{D}_{11}^T & 0 \\ \boldsymbol{C} + \boldsymbol{D}_{12}\boldsymbol{K} & \boldsymbol{D}_{11} & -\gamma\boldsymbol{I} & 0 \\ \boldsymbol{A}_{\boldsymbol{d}}^T\boldsymbol{P} & 0 & 0 & -(1-\rho)\boldsymbol{S} \end{bmatrix};$$
$$\boldsymbol{D} = \begin{bmatrix} \boldsymbol{P}\boldsymbol{H} \\ 0 \\ 0 \\ 0 \end{bmatrix}; \boldsymbol{E} = \begin{bmatrix} (\boldsymbol{E}_1 + \boldsymbol{E}_3\boldsymbol{K})^T \\ 0 \\ 0 \\ \boldsymbol{E}_2^T \end{bmatrix}^T \tag{21}$$

According to lemma 2, there exists a constant $\varepsilon>0$, such that $\boldsymbol{Y} + \varepsilon\boldsymbol{D}\boldsymbol{D}^T + \varepsilon^{-1}\boldsymbol{E}^T\boldsymbol{E} < 0$, i.e.

$$\begin{bmatrix} \boldsymbol{\Xi} & \boldsymbol{PB_1} & (\boldsymbol{C}+\boldsymbol{D_{12}K})^T & \boldsymbol{PA_d}+\varepsilon^{-1}(\boldsymbol{E_1}+\boldsymbol{E_3K})^T\boldsymbol{E_2} \\ \boldsymbol{B_1^TP} & -\gamma\boldsymbol{I} & \boldsymbol{D_{11}^T} & 0 \\ \boldsymbol{C}+\boldsymbol{D_{12}K} & \boldsymbol{D_{11}^T} & -\gamma\boldsymbol{I} & 0 \\ \boldsymbol{A_d^TP}+\varepsilon^{-1}\boldsymbol{E_2^T}(\boldsymbol{E_1}+\boldsymbol{E_3K}) & 0 & 0 & -(1-\rho)\boldsymbol{S}\varepsilon^{-1}\boldsymbol{E_2^TE_2} \end{bmatrix} < 0 \qquad (22)$$

Where $\boldsymbol{\Xi} = (\boldsymbol{A}+\boldsymbol{B_2K})^T\boldsymbol{P}+\boldsymbol{P}(\boldsymbol{A}+\boldsymbol{B_2K})+\boldsymbol{S}+\varepsilon\boldsymbol{PHH^TP}+\varepsilon^{-1}(\boldsymbol{E_1}+\boldsymbol{E_3K})^T(\boldsymbol{E_1}+\boldsymbol{E_3K})$

With lemma 3, we can prove the (17) equals to:

$$\begin{bmatrix} (\boldsymbol{A}+\boldsymbol{B_2K})^T\boldsymbol{P}+\boldsymbol{P}(\boldsymbol{A}+\boldsymbol{B_2K})+\boldsymbol{S} & \boldsymbol{PB_1} & (\boldsymbol{C}+\boldsymbol{D_{12}K})^T & \boldsymbol{PA_d} & (\boldsymbol{E_1}+\boldsymbol{E_3K})^T \\ \boldsymbol{B_1^TP} & -\gamma\boldsymbol{I} & \boldsymbol{D_{11}^T} & 0 & 0 \\ \boldsymbol{C}+\boldsymbol{D_{12}K} & \boldsymbol{D_{11}^T} & -\gamma\boldsymbol{I} & 0 & 0 \\ \boldsymbol{A_d^TP} & 0 & 0 & -(1-\rho)\boldsymbol{S} & \boldsymbol{E_2^T} \\ \boldsymbol{E_1}+\boldsymbol{E_3K} & 0 & 0 & \boldsymbol{E_2} & -\varepsilon\boldsymbol{I} \end{bmatrix} < 0 \qquad (23)$$

Left multiply and right multiply the matrix

$$\begin{bmatrix} \boldsymbol{P}^{-1} & 0 & 0 & 0 & 0 \\ 0 & \boldsymbol{I} & 0 & 0 & 0 \\ 0 & 0 & \boldsymbol{I} & 0 & 0 \\ 0 & 0 & 0 & \boldsymbol{P}^{-1} & 0 \\ 0 & 0 & 0 & 0 & \boldsymbol{I} \end{bmatrix}$$

Then define $X=P^{-1}$, $Y=KP^{-1}$, $Q=P^{-1}SP^{-1}$, then Formula (23) can be changed as equation (16). We can complete the proof.

3.5 Case Studies

3.5.1 System Description

In order to verify the effectiveness of the proposed control method, the two-area LFC system derived from the New England 39-bus system in section 3.3.1 is studied. The parameters are shown in Table 5.

Table 5 Parameters of the Two-Area LFC System Case Studies

Parameters	Area1	Area2
Regional frequency deviation coefficient b_i (p.u.MW/Hz)	4.89	5.12
Speed regulation due to governor action R_i (Hz/p.u.MW)	0.12	0.08
Inertia time constant of the AGC units M_i(s)	6.23	5.77
Load frequency characteristic coefficient D_i (p.u.MW/Hz)	0.87	1.23
Frequency response coefficient of ES K_{bi} (p.u.MV/Hz)	3.00	2.00; 2.50
Governor time constant T_{Gi} (s)	0.23	0.27
Turbine time constant T_{CHi} (s)	0.56	0.45
Equivalent time constant of batteries T_{ESi} (s)	0.12	0.20; 0.15
Parametric uncertainty of Δ_{Gi} (s^{-1})	0.30	0.20
Parametric uncertainty of Δ_{CHi} (s^{-1})	0.10	0.12
Parametric uncertainty of Δ_{ESi} (s^{-1})	1.90	0.50; 0.48
Tie line synchronization coefficient T_i (p.u.MV/Hz)	2.00	
Time delay bound ρ	0.5	
Interference suppression degree γ	0.5	

The New England 39-bus test power system has 46 connection lines. Generator No.6 is a wind generator and there is one grid-connected battery energy storage station in area 1 and two ES in area 2. Bus 15 and 16 are low-voltage nodes, while the two lines that connects bus 14 and 15, 16 and 17 divide the whole system into two separate areas. The total capacity of the system is 627.5 MW. The required frequency regulation capacity is set to 8% of the total loads, namely 50.2 MW in which the conventional AGC plants and ES account for 80% (40.16MW) and 20% (10.02MW) respectively. Use the proposed approach, H_∞ controller is:

$$\boldsymbol{K}=\begin{bmatrix} -90.54 & -9.70 & -36.28 & 0.03 & -0.56 & -142.58 & 32.82 & -0.24 & -0.32 & 0.01 & 0.06 & 0.07 \\ 8.93 & 0.58 & 1.25 & -0.48 & 0.05 & -68.22 & -236.97 & -3.66 & -11.55 & -0.20 & -0.24 & -0.39 \end{bmatrix}$$

Set the step-test load fluctuation vector

$$w_1(t)\,\&\,w_2(t)=\begin{cases} 0 & ;0\le t\le 1 \\ 0.3\,\&\,0.1\,p.u. & ;1\le t\le 15 \\ 0.4\,\&\,-0.2\,p.u. & ;15\le t\le 30 \end{cases} \tag{24}$$

The power output variation of the traditional AGC units and the energy storages of the two-area system are shown in the Fig. 22.

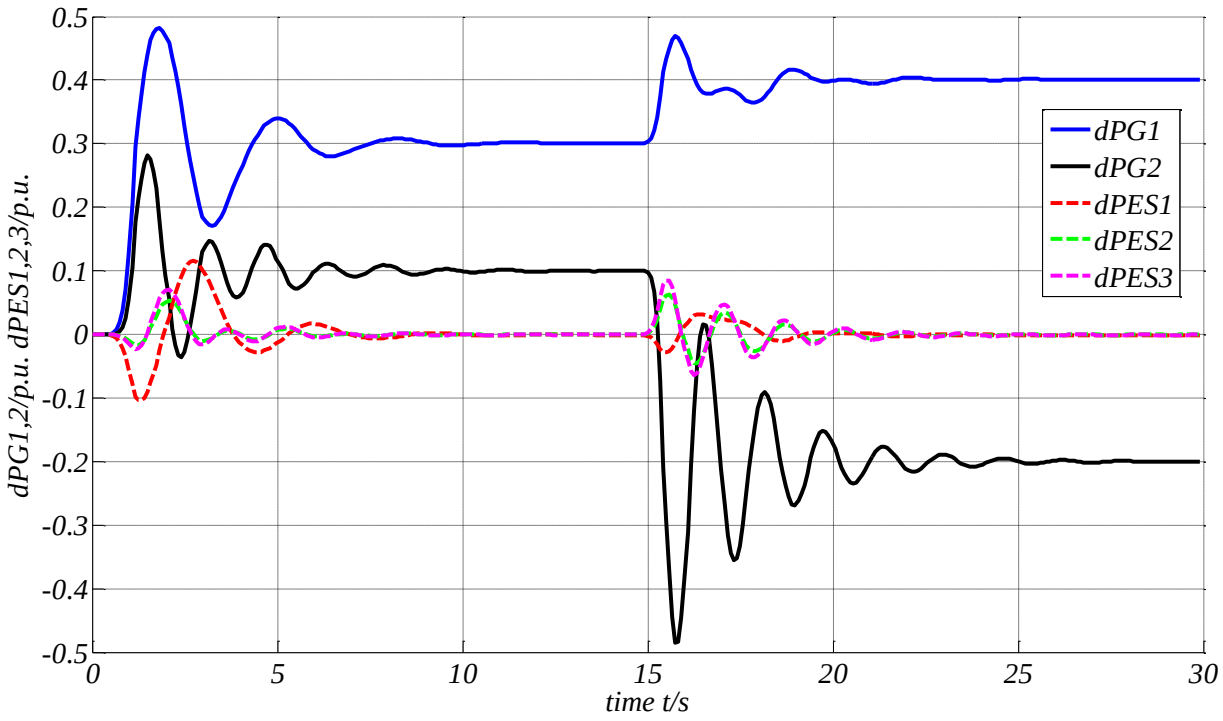

Fig. 22 The Power Output Variation of the Traditional AGC Units and the Energy Storages of the Two-Area System after Step Load Disturbance

From Fig. 22, we can conclude that the step load change is adjusted by both AGC units and ES at the first transient process while the final increment/decrement of the load is carried by generators. This is reasonable because the energy storage cannot supply or absorb power perpetually.

3.5.2 Comparison of Control Methods

First, the comparison of different control methods, namely the traditional PI controller and the proposed H_∞ controller is simulated. Fig. 23 shows the ACE_1 performance curve using different controllers under two different scenarios: one with no time delay while the other with 0.8s time delay.

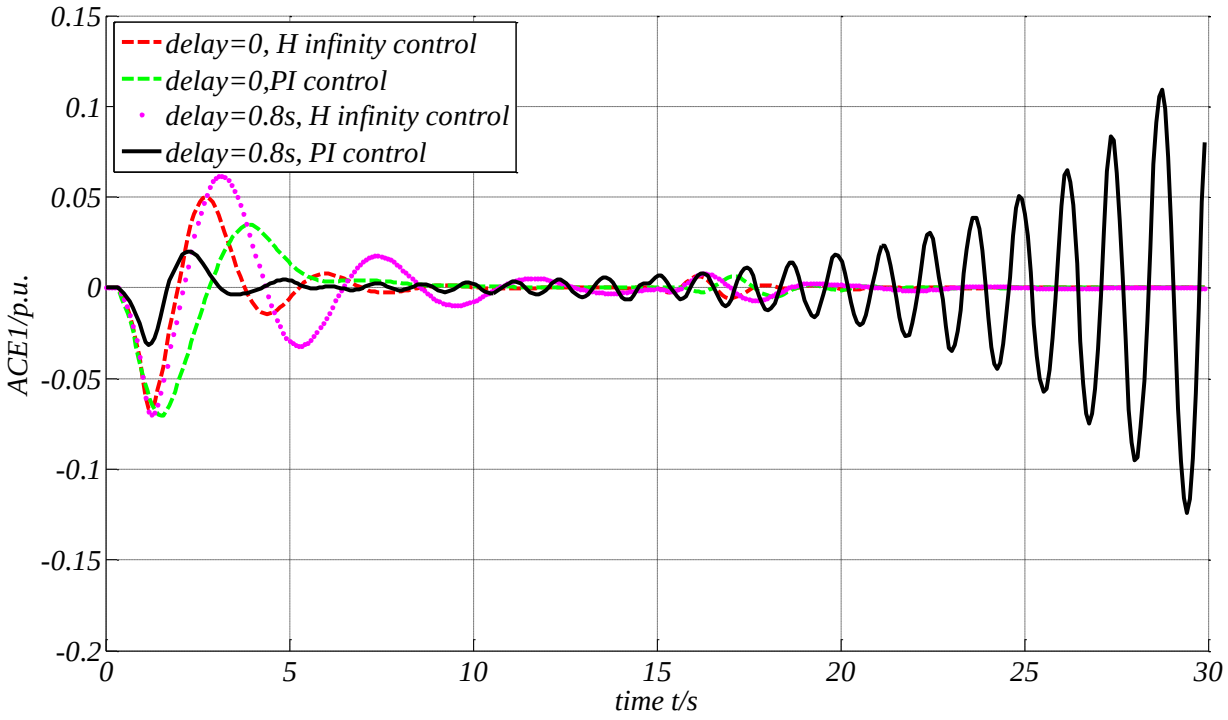

Fig. 23 ACE_1 Performance using Different Controllers under Different Time Delay Scenarios

It can be concluded from Fig. 23 that as the time delay increases to 0.8s, PI control losses its stability if we use the same coefficients all the time. This demonstrates that the robust performance of the system is quite poor. Due to the unpredictable and random character of the time delay, we cannot keep on adjusting the PI coefficients all the time in practical operation. By contrast, the proposed H_∞ controller can always help the system to be robustly stable without changing any parameters. This is a noteworthy advantage.

3.5.3 Effects of Duration and Forms of Time Delay on System Dynamic Characteristics

To test the controller further, different delay types are adopted. Fig. 24 shows the influence of different forms of time delay on ACE_1 performance using H_∞ controller.

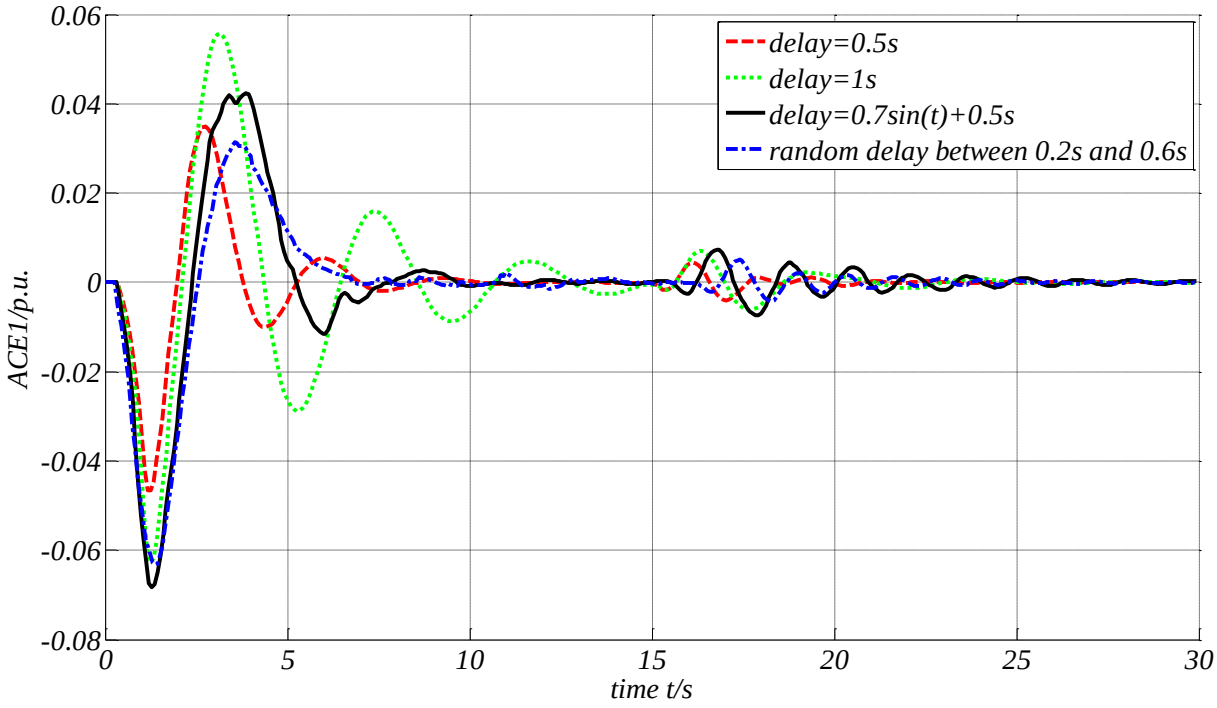

Fig. 24 The Influence of Different Forms of Time Delay on ACE_1 Performance using H_∞ Controller

It can be seen that for all the cases, the overall conclusion is that the proposed control method can ensure the stability of the system no matter what type of delay is experienced. To be specific, from the simulation result we can conclude that for the constant type of time delay, the system dynamic performance deteriorates when the delay increases (From 0.5s to 1s): we can see that overshoot and oscillation period both increases. For the sine-type time delay and the random time delay, the system dynamic performance behaves more unpredictably because the delay changes continuously. However, as long as the delay satisfy the restrictions and is bounded, the system will eventually come back to its normal status.

3.5.4 Effects of Parametric Uncertainty on System Dynamic Characteristics

In order to test the robustness of the designed controller against parametric uncertainty, two most hash scenarios are selected, i.e. according to (11), all of these parameters reach their upper limit simultaneously or, reach their lower limit simultaneously. The Fig. 25 shows the influence of parametric uncertainty on ACE_1 performance using H_∞ controller.

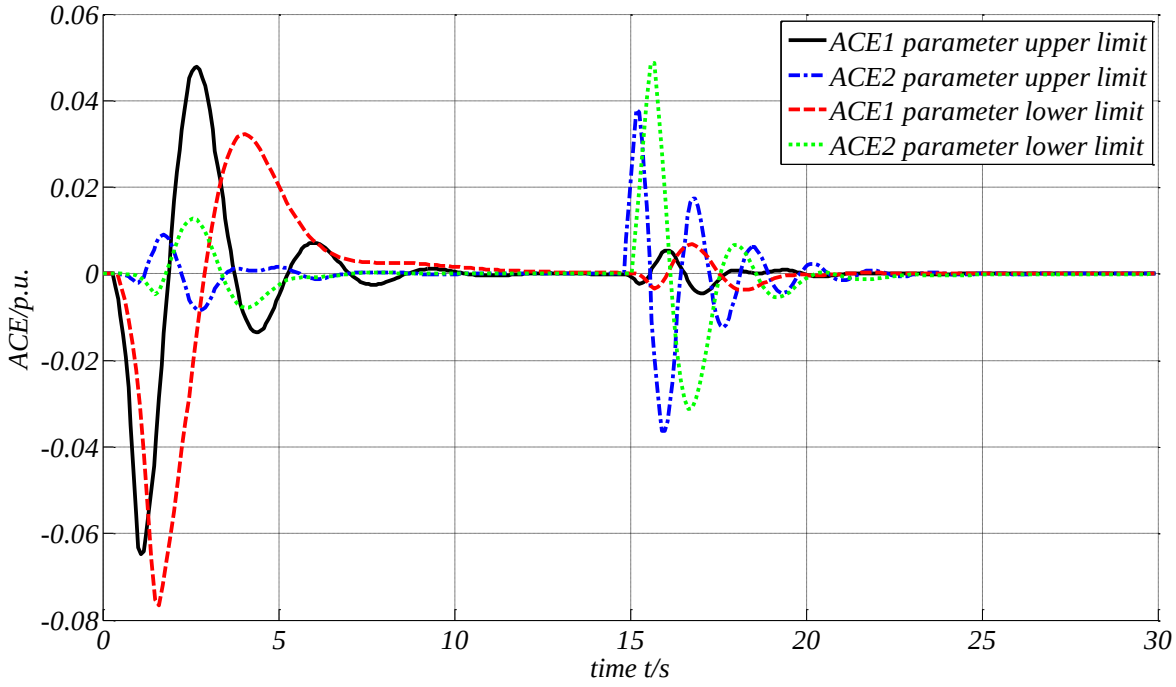

Fig. 25 The Influence of Parametric Uncertainty on ACE_1 Performance using H_∞ Controller

It can be seen that the system can maintain robustly stable no matter how the certain parameters of the model varies, as long as they do not exceed an pre-known boundary as (11) specifies.

3.5.5 Effects of Energy Storage on System Accommodation of Intermittent RE

The following study assumes that the active power unbalance comes from the fluctuation of wind power outputs. The variation of wind power output module is simulated with band-

limited white noise and a low-pass filter [42], as shown in Fig. 19. The Fig. 26 shows the ACE_1 performance under two scenarios: with or without the participation of energy storage.

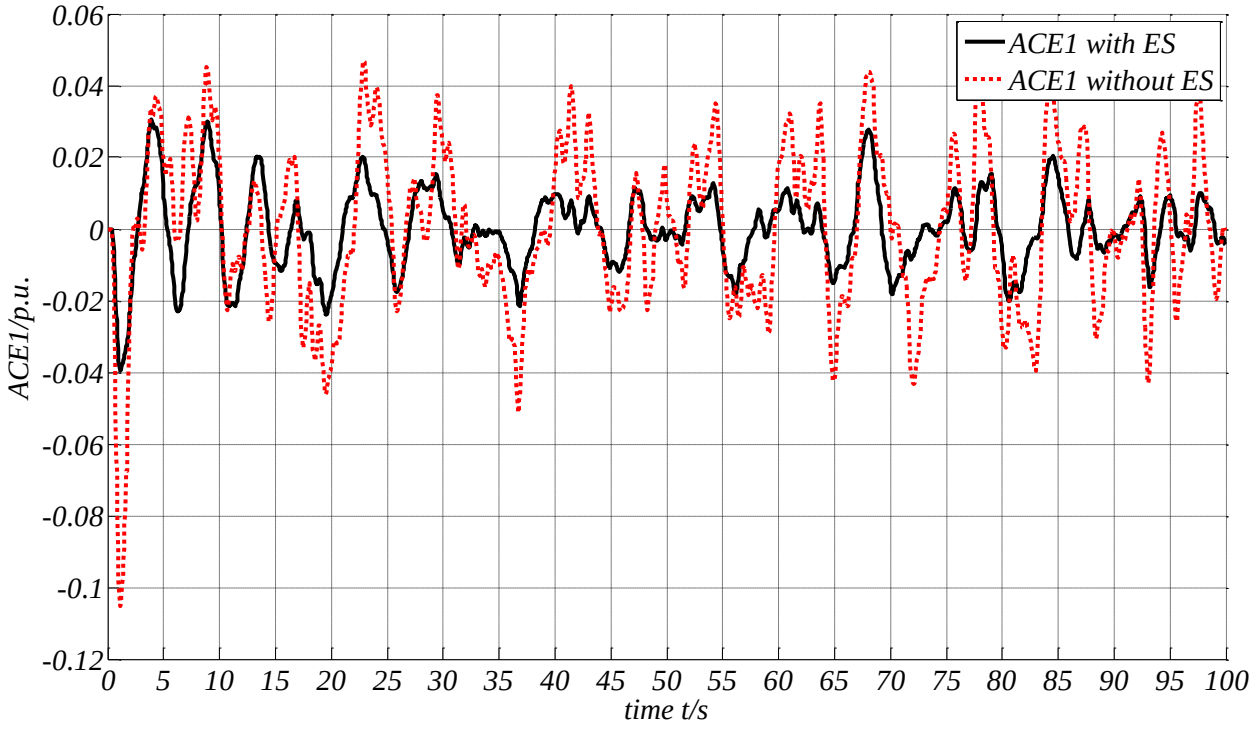

Fig. 26 The ACE_1 Performance under two Scenarios: with or without the Participation of ES

From Fig. 26, the ES has reduced the overall fluctuation interval by 55.8%. This demonstrates that with an appropriate controller, the ES could play a positive role in helping the system respond more accurately and rapidly towards the integration of unpredictable intermittent renewables.

In the next Chapter 4, we will focus on the voltage issues and power flow problem in future distribution network and a novel distributed consensus algorithm will be designed to resolve the problem.

4. The Enhanced Optimal Distributed Consensus Control of Scattered Devices Considering Security and Economic Operation Issues

As we can see from the above chapter 3, the intermittent characteristics of wind or PV power will have an adverse impact on system frequency stability. Actually, apart from the frequency aspect, the increasing penetration level of intermittent renewable generations will also inevitably cause adverse impact on other indexes such as power flow distribution, causing reverse power flow and node voltage/line power over-limit problems. Therefore, novel dispatching strategies are essential to be developed and studied. In this chapter, I propose a novel Enhanced Optimal Distributed Control Algorithm (EODCA) based on power system sensitivity analysis to regulate the scattered energy storage devices in order to alleviate these problems while the overall economic performance and network security constraints are considered. These scattered devices can be regarded as small "agents" who can update their individual information during the iteration process based on control law through the communication and data exchange with their adjacent neighbours so as to eventually reach a final consensus optimal value. The comprehensive case study also demonstrates the effectiveness of the proposed method: not only can it help to find the global economic optimal solutions in a distributed manner, but also it can guarantee the secure operation of the distribution network and enhance the robustness of the system as well.

4.1 Mechanism Analysis of Energy Storage Installation

In smart grid environment, increasing small-scale Distributed Generations (DG), such as Photovoltaic (PV) Panels or Combined Heat and Power (CHP) Generators are installed and connected into the distribution network. For example, the household rooftop PV in Queensland and South Australia has become quite prevalent. However, the conventional distribution system

is designed based on the assumption that the substation is the only source of energy. In the new situation, this system has to face new challenges. For example, reverse power flow, voltage and transmission power over-limit problems may frequently occur [5] [8]. Furthermore, the common radial structure of the distribution grid is more vulnerable to disturbances compared with the high-voltage transmission network that has more stabilizers, protections and controllers in it. Therefore, the security operation of the distribution system is an important issue given increasing DG integration.

On the other hand, the scattered Energy Storage (ES) devices have been received growing attention because of their falling price. They can be utilized as an effective "buffer" to help the system alleviate these problems if an appropriate control approach is adopted.

Generally speaking, there are two mechanisms of installing and manipulating of these DGs. These devices can be purchased and installed by the customers themselves, or, alternatively, set up by local companies, such as the "aggregator" in the future. The main merit of the former scheme is its flexibility and no extra costs/control processes for utilities. Users' electricity bills can be reduced through Demand Response (DR). Thus, plenty of recent literature (e.g. [43]) have discussed how to design a suitable incentive mechanism for motivating the households to perform better DR [44]. However, most of them use the simplified power balance constraints instead of precise power flow calculation. For a practical system, both the electrical topology and power flow distribution issues are crucial and should be considered properly. What is more, there are some drawbacks of this mechanism noteworthy as well:

- The cost of the ES device is so high that it is somehow unbearable for individuals to install in the foreseeable future;

- Most importantly, without a well-designed policy and highly developed mature market mechanism, the enormous individual profit-driven behaviours, even vicious competitions would put serious threat to power system security operation process (such as forming another peak load, etc.);

By contrast, the adoption of the concept "aggregator" provides a promising perspective. These aggregators are essentially some local distribution companies. They purchase energy from the grid and sell it to the local residents so as to gain profits; furthermore, it is their responsibility to maintain the security operation of the whole system. In this scheme, the devices are purchased, installed and manipulated by the aggregators, which can overcome the demerits of the former scheme. For example:

- ✓ The aggregators have the financial ability for installing expensive storage devices;
- ✓ They can optimize PV and ES size and location where needed, so that the waste of resources and the blind investment behaviours of individuals can be avoided;
- ✓ Comprehensive control strategy for these devices can guarantee the security operation of the whole system, avoiding serious safety hazards posed by the individuals;
- ✓ Last but not the least, for the customers, they do not have any extra burdens; on the contrary, through appropriate control strategy, the net profit of the aggregators can increase in spite of new investment. This trend indicates the decrease of the electricity price in turn in a long run. Undoubtedly, this win-win mechanism is promising.

The limitations are the suitable control method should be adopted to ensure the secure operation of the system; otherwise, it is neither practical nor reliable to control numerous devices. Besides, the net profit of the power distribution company should be guaranteed to motivate the facility construction and renewable integration.

Lately, the theory of multi-agent and distributed consensus algorithm has received much attention. However, the application of distributed algorithms in power system is still quite preliminary so far. The over simplification of the electrical system and power flow calculation in existing research may incur critical information loss and cannot reflect the real situations accurately[28][45]. In this context, this chapter includes the power system theory to enhance the distributed consensus algorithm. With a more accurate model of the system calculation, two key indexes in future grid scenarios, i.e. both the power flow and the voltage issues are considered simultaneously to make the whole optimization process more objective, detailed and practical.

The rest of the Chapter is organized as follows: three different forms of control schemes are analysed and then mathematical modelling of the practical problem is derived in Section 4.2. In Section 4.3, the prototype of a sub-gradient based distributed consensus algorithm is briefly introduced. In Section 4.4, we propose the linearization enhancement based on power system sensitivity analysis, which makes the algorithm applicable for dealing with the non-linear constraints and issues existing in this problem. Comprehensive case studies are presented in section 4.5 to test the performance of the proposed Enhanced Optimal Distributed Consensus Algorithm (EODCA), and verify its effectiveness compared with different scenarios (e.g. the random behaviour or centralized dispatch).

4.2 Problem Description and Mathematical Modelling

4.2.1 Three Control Schemes in Distribution Network

There are three different control structures shown in Fig. 27. We can also analyse the drawbacks and merits of each configuration:

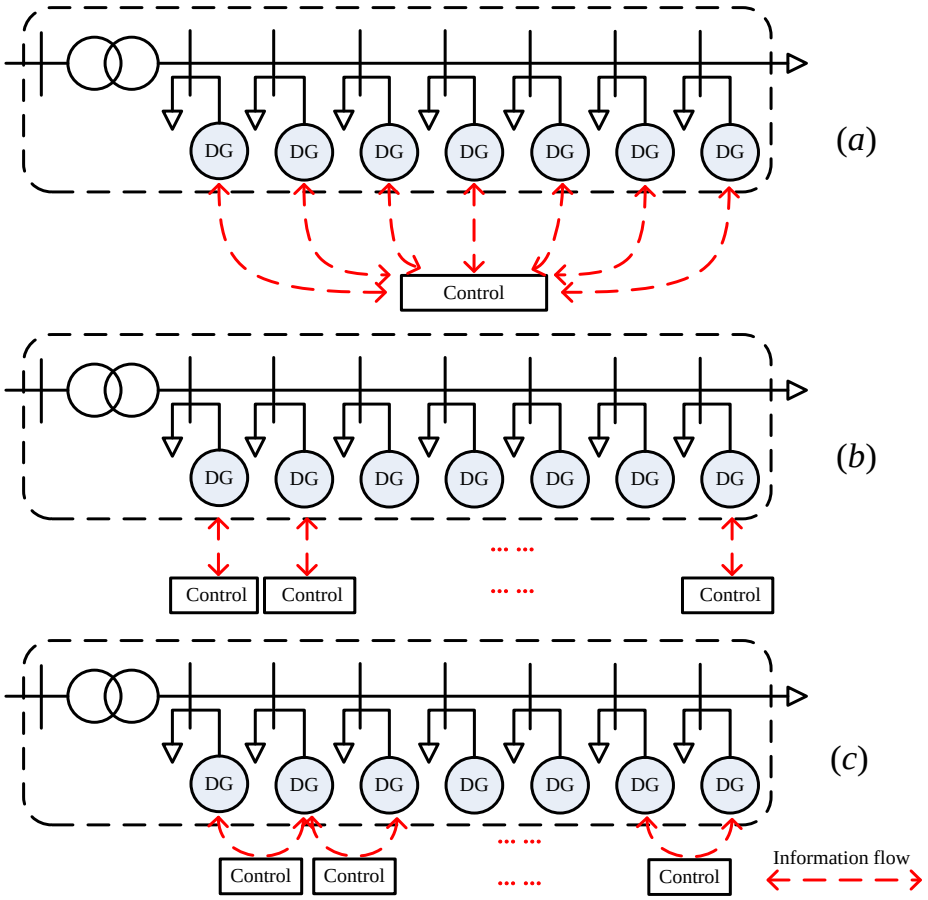

Fig. 27 Three Control Schemes in Distribution Network

(a) Centralized Control (b) Decentralized Control (c) Distributed Control

In traditional power system operation, the optimal power flow (OPF) strategy is the most widely used approach to dispatch the generators in a network. It is essentially a centralized balancing control. The control centre gathers the information from all the devices and then performs an OPF optimization. The control signals are sent back to these distributed devices again to set their power outputs. The advantage is that the highly developed algorithm can guarantee the global optimum. However, for a future distribution system that have numerous and

geographically dispersed DGs, such centralized controls have a number of weaknesses: First, it is too expensive to build all these information channels and the control centre. Secondly, the centralized control centre is also the weakest point in the system especially when huge amount of information and data congests in it, once attacked or overloaded, the system may collapse immediately. Third, In future distribution grid with a very high renewable penetration level, the amount of small scale devices is so large that the "curse of dimensionality" would overwhelm traditional centralized algorithms, resulting in the calculation speed droping significantly, or even make them unsolvable.

The second scheme is decentralized control, which is the totally different to the centralized scheme. For example, the maximum photovoltaic power tracking (known as MPPT), constant voltage and frequency (VF) with droop mode, or the feeder power flow control mode are such controls. The controls are performed within each individual device as shown in (b) of Fig. 27. Although it is simple and cheap to realize, i.e. no need to invest in communication channels at all, yet the main flaw is that it only uses the information of the target device itself so only an individual optimum can be achieved.

In contrast with them, the last scheme is called distributed control. It can be seen that a local communication network is adopted to link the distributed devices. Specifically, a device should incorporate whatever information available from its neighbouring device or critical nodes into its control law to make an optimal decision. Despite the relatively more complicated controller design process, the distributed control scheme is quite suitable for tackling numerous scattered devices. Not only can it use the information exchange in local communication network to achieve a global optimum, but also it enhance the robustness of the system with respect to intermittency and latency of its feedbacks, tolerate connection and disconnection of network

components with a suitable design. Furthermore, it helps to avoid the “curse of dimensionality” and saves fixed cost for building redundant infrastructures. Therefore, it combines the positive features of both centralized and decentralized controls while limiting their disadvantages, making it the most promising approach for future distribution networks.

4.2.2 Problem Description

In this study, we consider the specific scenario in the future that a power distribution company or an aggregator installs the infrastructure for the customers, which means that the profit of this distributor should be maximized through comprehensive optimal dispatching approach.

The concept of “multi-agents” and the consensus algorithm can be adopted because these distributed facilities can be regarded as small “agents”, i.e. they can exchange information with their neighbours through the communication channel built between them. Apart from the security of operation issues, the economic performance should be taken into account simultaneously. Through the proposed Enhanced Optimal Distributed Consensus Algorithm (EODCA) in the following sections, these “agents” can update their individual information separately during the iteration process only use limited information instead of gathering all the data from all the devices in traditional ways. Regardless of what initial value they take, they can reach the consensus optimal value in the end, i.e. collaboratively achieve a same goal: to maximize the certain profits while ensure the secure operation (avoid the voltage/transmission power over limit problem) of the distribution networks simultaneously.

4.2.3 Mathematical Modelling

The mathematical model of the problem is formulated as follows:

Define x=($P_{PV,1}$, $P_{PV,2}$,…, $P_{PV,N}$, $P_{ES,1}$, $P_{ES,2}$,…, $P_{ES,M}$);

Objective function *f* (Max net profit of the aggregator):

$$f(x)=\sum_{k=2}^{K}\rho_D P_{D,k}-\rho_b P_b+\sum_{n=1}^{N}[\rho_s P_{PV,n}-C_{PV}(P_{PV,n})]-\sum_{m=1}^{M}C_{ES}(P_{ES,m}) \tag{25}$$

Where ρ_D is the retail price selling to the customers; ρ_b is the wholesale price selling to the aggregators; $P_{D,k}$ is the load of the node k; P_b is the total power bought from external grid; ρ_s is the financial subsidies set by the external grid/government to absorb and stimulate sustainable energy generation; $P_{PV,n}$ is the power output of the nth PV; ($n \in N$); $P_{ES,m}$ is the charging/discharging power of the mth ES ($m \in M$); $C_{PV}(P_{PV,n})$ is the cost function of the nth PV, which can be written as the quadratic form[45]:

$$C_{PV}(P_{PV,n})=a_{PV}P_{PV,n}^2+b_{PV}P_{PV,n} \tag{26}$$

$C_{ES}(P_{ES,m})$ is the cost function of the mth ES, which can be written as the quadratic form[45]:

$$C_{ES}(P_{ES,m})=a_{ES}P_{ES,m}^2+b_{ES}P_{ES,m} \tag{27}$$

K denotes the set of nodes that have loads connected; N denotes the number of PV; M denotes the number of ES.

Constraints:

1) Total power balance:

$$P_b+\sum_{n=1}^{N}P_{PV,n}+\sum_{m=1}^{M}P_{ES,m}=\sum_{k=2}^{K}P_{D,k} \tag{28}$$

2) The power limitation of the PV output:

$$\underline{P_{PV,n}} \le P_{PV,n} \le \overline{P_{PV,n}}\ ; \forall n \in N \tag{29}$$

Where $\underline{P_{PV,n}}$ and $\overline{P_{PV,n}}$ are the lower and upper limits of the n*th* PV power output separately, $\underline{P_{PV,n}} = 0$;

3) The power limitation of the storage charging/discharging:

$$P_{dCH,m} \le P_{ES,m} \le P_{CH,m},\ \forall m \in M \tag{30}$$

Where $P_{CH,m}$ is the maximum charging power of *m*th storage while $P_{dCH,,m}$ is the maximum discharging power of the *m*th storage. $P_{ES,m}>0$ indicates charging whilst $P_{ES,m}<0$ denotes discharging.

4) The power flow equation of the distribution network:

$$\left.\begin{aligned} &P_i = P_{D,i} + P_{PV,i} + P_{ES,i}; \\ &Q_i = Q_{D,i} + \alpha P_{PV,i} + \beta P_{ES,i}; \\ &P_i - U_i \sum_{j=1}^{I} U_j (G_{ij} \cos\delta_{ij} + B_{ij} \sin\delta_{ij}) = 0; \\ &Q_i - U_i \sum_{j=1}^{I} U_j (G_{ij} \sin\delta_{ij} - B_{ij} \cos\delta_{ij}) = 0 \end{aligned}\right\} i = 2,3,...I \tag{31}$$

Where P_i is the algebraic sum of (generation/load) active power injected to node *i*; Q_i is the algebraic sum of (generation/load) reactive power injected to node *i*; α is the required (predetermined) power factor of PV; β is the required (predetermined) power factor of ES; *I* denotes the set of the nodes in this system; G_{ij} is the conductance between node *i* and *j*; B_{ij} is the susceptance between node *i* and *j*; δ_{ij} is the phase angle difference between node *i* and *j*;

5) The voltage limitation of the system:

$$0.95 \le U_i \le 1.05; \forall i \in I \tag{32}$$

6) The line power limitation of the distribution system:

$$\begin{gathered}[P_1^{'}\ P_2^{'} \ldots P_l^{'} \ldots P_L^{'}]^T = A[P_1\ P_2 \ldots P_i \ldots P_I]^T; \\ -P_{\max,l}^{'} \le P_l^{'} \le P_{\max,l}^{'}, \forall l \in L\end{gathered} \tag{33}$$

Where L denotes the number of lines in the system; $A \in \mathbb{R}^{L \times I}$ is the matrix that denotes the topology relation; $P_l^{'}$ is the line flow of the system; $P_{\max,l}^{'}$ is the maximum transmission limit of the *lth* line.

The traditional OPF problem has been successfully resolved by centralized approaches, such as interior point method [46]. However, as is analysed before, in future grid situations, it is better to solve the problem in a distributed way to overcome the drawbacks of centralized methods. It means that during the iteration process of each "agent", the distributed PV/battery updates their decision variables only based on information from itself and neighbours, its local objective function, local upper/lower constraints and a global constraint (power flow). Neither do they know the global objective function nor the upper/lower range information of other agents except their neighbours. In order to solve this problem, we should reformulate the above mentioned model to the standard format.

By substituting (28) into the objective function, we can get:

Max net profit f

$$\begin{aligned}f(x) = &\sum_{k=2}^{K}(\rho_D - \rho_b P_{D,k}) \\ &+ \sum_{n=1}^{N}[\rho_b P_{PV,n} + \rho_S P_{PV,n} - C_{PV}(P_{PV,n})] + \sum_{m=1}^{M}[\rho_b P_{ES,m} - C_{ES}(P_{ES,m})]\end{aligned} \tag{34}$$

Note that we can eliminate the first term, because it is a constant value without considering the demand response. It is irrelevant and indifferent to the objective function. Then the model can be expressed as:

$$\begin{aligned} Min\ f(x) &= \sum_{n=1}^{N}[C_{PV}(P_{PV,n}) - \rho_b P_{PV,n} - \rho_S P_{PV,n}] + \sum_{m=1}^{M}[C_{ES}(P_{ES,m}) - \rho_b P_{ES,m}] \\ &= \sum_{i=1}^{N'} f_i(x_i);\ N' = N + M \end{aligned} \tag{35}$$

Constraints (29) and (30) are local constraints that are only known by agent *i* itself. It can be mathematically expressed as:

$$x \in \bigcap_{i=1}^{N'} X_i \tag{36}$$

Where X_i represents the separate local constraint set of each agent *i*.

Constraint (33) is essentially a global linear inequality constraint and can be simplified easily to the following format:

$$g(x) = A'x \le 0 \tag{37}$$

Constraint (31) and (32) will be discussed later in Section 4.4.

4.3 Prototype of Sub-Gradient based Distributed Consensus Algorithm

In the latest research work [28], the authors proposed a sub-gradient based algorithm to realize distributed optimization considering inequality and equality constraints. Here in this section, we briefly introduce the prototype of the distributed method and then analyse its shortcomings when combining the algorithm with practical power system problems.

Firstly, let us analyse a network of separate agents marked by $V := \{1, 2, \ldots, N\}$. The objective of this multi-agent group is to optimize the common goal cooperatively, which in the standard form of the problem is described as:

$$\min_{x \in \mathbb{R}^n} \sum_{i=1}^{N} f_i(x), \;\; s.t.\; g(x) \leq 0; h(x) = 0; x \in \bigcap_{i=1}^{N} X_i \tag{38}$$

Here f_i is the separate objective of each agent while the final objective function is the sum of them. It is assumed that these multi-agents operate synchronously. The constraint $g(x) \leq 0$ is satisfied for all $l \in \{1, \ldots, m\}$, i.e. it is a global inequality constraint. The constraint $h(x) = Ax - b$ is known to all the agents and denotes a global equality constraint. X_i represents the separate local constraint set of each agent i.

The communication connection relations of the network is depicted by an adjacency matrix $A(k)$ and its elements represent the weight assigned between the edge i and j. The communication graph has to satisfy three assumptions: "Non-Degeneracy", "Balanced Communication" and "Periodical Strong Connectivity" which can be referred to [28].

The adjacency matrix $A(k)$ denotes the communication network connection between all the different agents. If the agent i and agent j have the communication connection and the information exchange, then the element $a_{ij} > 0$; otherwise $a_{ij} = 0$. In regards to the value of a_{ij}, it is assigned according to the average total amount of information exchanged between the agent i and agent j. Usually the diagonal element a_{ii} is larger than the other elements and the matrix is symmetrical because $a_{ij} = a_{ji}$. In addition, the matrix has to satisfy both the "Non-Degeneracy" and the "Balanced Communication" conditions, which means the sum of the all the elements in each row and each column equals 1.

In the algorithm, firstly each agent i chooses any initial state $x^i(0) \in X_i$, $\mu^i(0) \in \mathbb{R}^m_{\geq 0}$. Then at each step $k \geq 0$, each agent i generates the next value $x^i(k+1)$, $\mu^i(k+1)$ according to (39):

$$\begin{aligned} &\text{Consensus}: \begin{cases} v_x^i(k) = \sum_{j=1}^{N} a_j^i(k) x^j(k); \\ v_\mu^i(k) = \sum_{j=1}^{N} a_j^i(k) \mu^j(k); \end{cases} \\ &\text{Projection}: \begin{cases} x^i(k+1) = P_{X_i}[v_x^i(k) - \alpha(k) D_x^i(k)]; \\ \mu^i(k+1) = P_{M_i}[v_\mu^i(k) + \alpha(k) D_\mu^i(k)]; \end{cases} \end{aligned} \tag{39}$$

where $a_j^i(k)$ is the corresponding element in adjacency matrix $A(k)$ which denotes the communication connection between agents; P_{Xi} is the projection operation onto the set X_i (respectively, P_{Mi} is the projection operation onto the set M_i); the scalars $\alpha(k)>0$ are step-sizes and should satisfy: $\lim_{k\to\infty} \alpha(k) = 0; \sum_{k=0}^{+\infty} \alpha(k) = +\infty; \sum_{k=0}^{+\infty} \alpha(k)^2 < +\infty;$. The notations are: $D_x^i(k) \equiv DL_{iv_x^i(k)}(v_x^i(k))$, and $D_\mu^i(k) \equiv DL_{iv_x^i(k)}(v_\mu^i(k))$.

Although the prototype algorithm can solve the optimization problem in a distributed manner, it cannot be applied directly in the proposed model due to the highly non-linear voltage magnitude constraints (31) and (32). In the following section, a novel power system sensitivity analysis based-linearized approach is developed to enhance the algorithm, making it compatible with the revised piecewise linearized voltage constraints during the iteration process.

4.4 Linearized Enhancement based on Power System Sensitivity Analysis

4.4.1 The Limitations of the Existing Methodology

In the algorithm proposed in [28] described in the previous section, $h(x):=Ax-b$ is required, which means that the equality constraint should be the linear combination of the state variables.

Whilst in our model, the power flow constraint (31) combined with limits (32) is highly non-linear. Besides, (32) is essentially an inequality constraint that can be written as $x=h(u)$. Due to the non-convex characteristic of the h, the uniqueness of the mapping $x \rightarrow u$ cannot be guaranteed. Which means that the implicit function $u=h^{-1}(x)$ doesn't exist at all. Therefore, the combination of (31) with (32) cannot be written as $u=h^{-1}(x) \leq 0$, which indicates it impractical to use the previous algorithm directly.

Therefore, the linearization of the power flow equation (31) should be adopted. Although the DC power flow method is the most straightforward way, the inherent and insurmountable drawback is only the active power flow can be calculated whilst the voltage profile and the reactive power calculations are neglected, which is a pivotal security operation problem in this scenario.

In order to make the problem solvable, more theory of the power systems should be considered and adopted. The brand new approach we propose here is based on the power system sensitivity analysis method. We call it **Enhanced Optimal Distributed Consensus Algorithm (EODCA, for short)** to find a saddle point of the Lagrangian function L over $X \times M$ and the optimal value.

4.4.2 The Power System Sensitivity Analysis based Piecewise Linearization Modification and Enhancement

Since during two steps of the iteration processes, the updated variation of renewable power outputs injected into the nodes are quite small, so we can regard the renewable power output injected into the nodes as a certain form of disturbance, and through the Taylor Series Expansion, the sensitivity matrix can be deduced.

For a system that is working under stable operation status, the equation (31) can be written as:

$$W_0 = f(X_0, Y_0) \tag{40}$$

Where, the W_0 is the active and reactive power injected into the nodes, X_0 is the vector that consists of the node voltage and angle; Y_0 denotes the parameters of the network itself under normal operation status.

If the injected power changes ΔW, or the network changes ΔY, the state variables should also changes ΔX. Therefore, the (40) can be written as:

$$W_0 + \Delta W = f(X_0 + \Delta X, Y_0 + \Delta Y) \tag{41}$$

Perform the Taylor series expansion of (41), we can get:

$$\begin{aligned} W_0 + \Delta W &= f(X_0 + \Delta X, Y_0 + \Delta Y) \\ &= f(X_0, Y_0) + f_x^{'}(X_0, Y_0)\Delta X + f_y^{'}(X_0, Y_0)\Delta Y \\ &+ \frac{1}{2}[f_{xx}^{''}(X_0, Y_0)(\Delta X)^2 + 2 f_{xy}^{''}(X_0, Y_0)\Delta Y \Delta X + f_{yy}^{''}(X_0, Y_0)(\Delta Y)^2] + \ldots \end{aligned} \tag{42}$$

When the disturbance variables and the status variables are small, we can neglect the $(\Delta X)^2$ and the high-order terms. Besides, due to the fact that $f(X,Y)$ is the linear function of Y, so $f_{yy}^{''}(X,Y) = 0$. Therefore, the (42) can be simplified as:

$$W_0 + \Delta W = f(X_0, Y_0) + f_x^{'}(X_0, Y_0)\Delta X + f_y^{'}(X_0, Y_0)\Delta Y + f_{xy}^{''}(X_0, Y_0)\Delta Y \Delta X \tag{43}$$

By substituting (40) into the above equation, we can get:

$$\Delta W = f_x^{'}(X_0, Y_0)\Delta X + f_y^{'}(X_0, Y_0)\Delta Y + f_{xy}^{''}(X_0, Y_0)\Delta Y \Delta X \tag{44}$$

Therefore, the linear relation between the status variables with the disturbance variables and the network changing variables is:

$$\Delta X = [f_x^{'}(X_0, Y_0) + f_{xy}^{''}(X_0, Y_0)\Delta Y]^{-1}[\Delta W - f_y^{'}(X_0, Y_0)\Delta Y] \tag{45}$$

If we consider a time-invariant network, i.e. ΔY=0, (45) becomes:

$$\Delta X = [f_x^{'}(X_0, Y_0)]^{-1}\Delta W = S_0 \Delta W \tag{46}$$

where:

$$f_x^{'}(X_0, Y_0) = \left.\frac{\partial f(X,Y)}{\partial X}\right|_{\substack{X=X_0 \\ Y=Y_0}} = J_0 \tag{47}$$

J_0 is the Jacobian matrix when the load flow calculation finishes and the S_0 is called the sensitivity matrix.

In this problem, we only consider the magnitude limitation of the voltage. Through partitioning of the matrix, (46) can be written as:

$$\begin{bmatrix} \Delta\theta \\ \Delta U \end{bmatrix} = J_0^{-1}\begin{bmatrix} \Delta P \\ \Delta Q \end{bmatrix} = S_0\begin{bmatrix} \Delta P \\ \Delta Q \end{bmatrix} = \begin{bmatrix} A & B \\ C & D \end{bmatrix}\begin{bmatrix} \Delta P \\ \Delta Q \end{bmatrix} \tag{48}$$

Further, in the problem proposed, the power factor of PV and ES is predefined as a fixed value. i.e. $Q=\alpha P$, hence we can get:

$$\Delta U = (C + \alpha D)\Delta P = S^{'}\Delta P = S^{'}\Delta x \tag{49}$$

This is very important because the relation is linear now (essentially piece-wise linear). During the iteration process, (49) can guide the algorithm to find a suitable direction of changing

x. To be specifically, during the iteration step *i*, after an agent updates its information based on consensus process of (48), i.e.

$$\begin{aligned} x^i(k+1) &= [\sum_{j=1}^{N} a_j^i(k) x^j(k)] - \alpha(k) D_x^i(k) \\ \mu^i(k+1) &=]\sum_{j=1}^{N} a_j^i(k) \mu^j(k)] + \alpha(k) D_\mu^i(k) \end{aligned} \tag{50}$$

Then the (49) should be calculated. Since the ΔU is bounded by (32), i.e.:

$$\Delta U \le \min\{1.05 - U^{step\,i}, U^{step\,i} - 0.95\} \tag{51}$$

So the Δx is bounded because of (49) by simply projecting the vector onto the feasible region, which is a convex set given by linear inequalities (52).

$$S' \Delta x = \Delta U \le \min\{1.05 - U^{step\,i}, U^{step\,i} - 0.95\} \tag{52}$$

Inequality (52) should replace the simple Max-Min restrictions in the projection operator of the (39) in the prototype of the algorithm, which can be used to restrain the power outputs of the renewables in some critical period when the voltage constraints are violated even with the help of ES so as to guarantee the voltage security operation issues.

$$\begin{cases} P_{X_i}: \quad S' \Delta x^{step\,i} \le \min\{1.05 - U^{step\,i}, U^{step\,i} - 0.95\}; \\ x^i(k+1) = P_{X_i} x^i(k+1); \end{cases}$$
$$\begin{cases} P_{M_i}: \quad \mu^{step\,i} \ge 0; \\ \mu^i(k+1) = P_{M_i} \mu^i(k+1); \end{cases} \tag{53}$$

In conclusion, the flow chart of the above proposed power system sensitivity analysis based-EODCA can be described as:

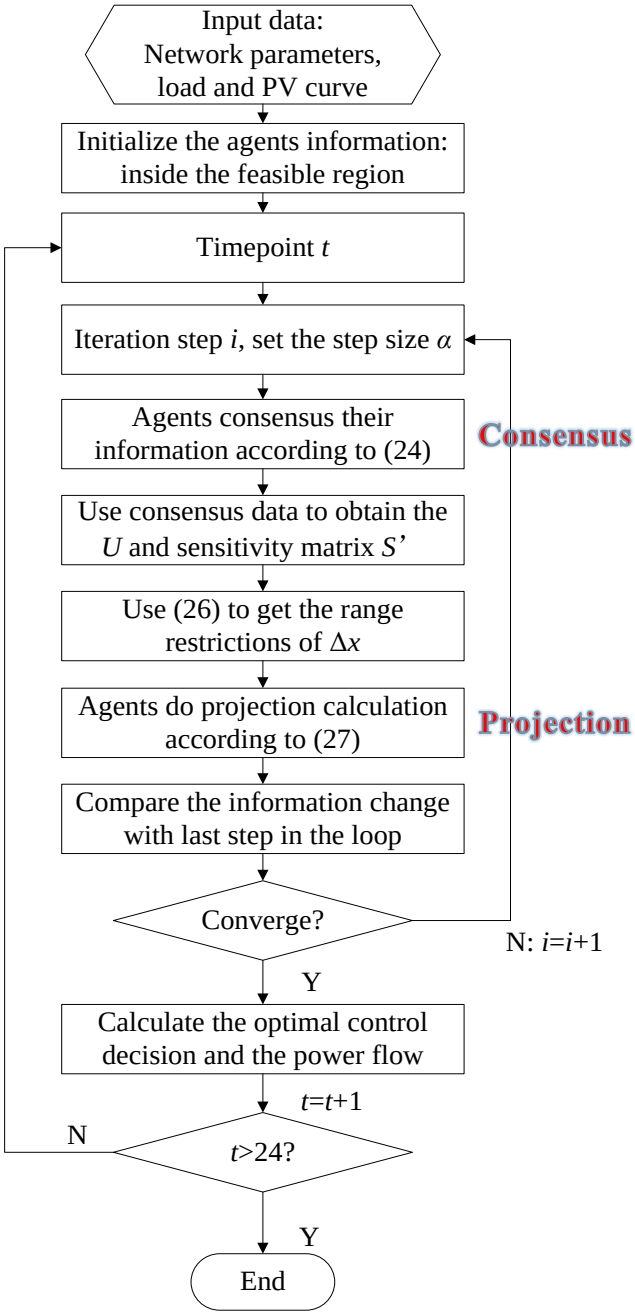

Fig. 28 The Flow Chart of the EODCA

4.5 Case Studies

4.5.1 System Description

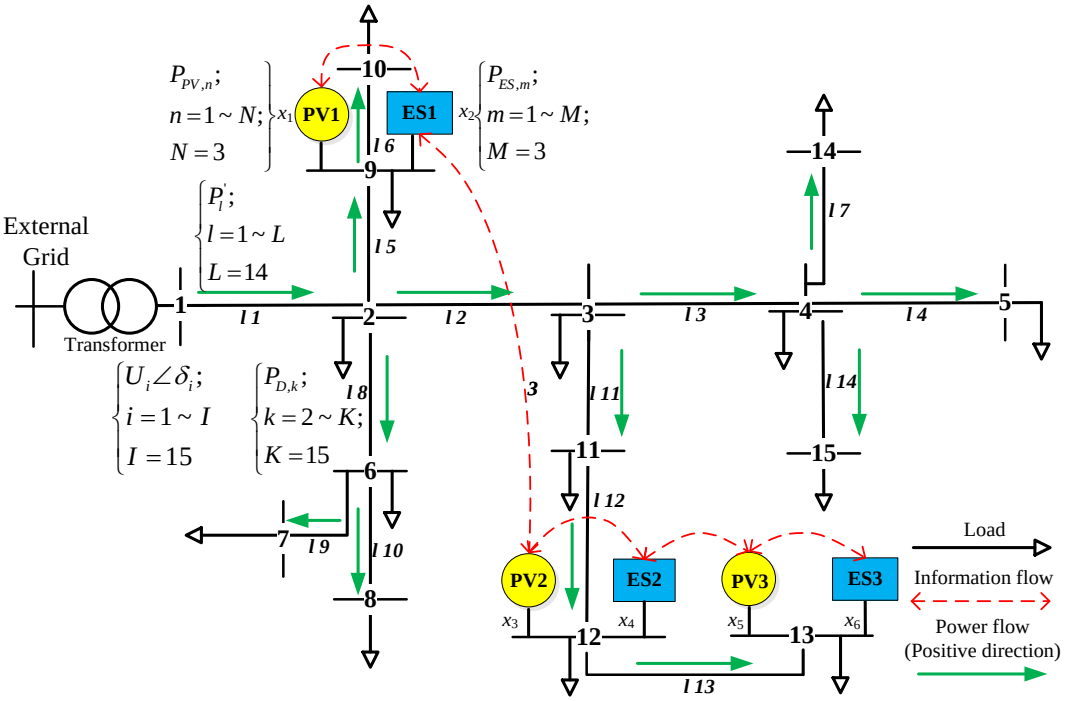

Fig. 29 The Topology of the Future Distribution Network with Renewables and Energy Storage Devices Integrated

In order to demonstrate the effectiveness and the characteristics of the proposed method, the algorithm is coded in a Matlab environment and simulations are performed with MatPower toolbox. The topology shown in Fig. 29 is a future distribution network, where at bus 9, 12 and 13, the scattered rooftop PVs and energy storages (ES) are integrated. The local distribution company has the ownership of installing and dispatching these devices and only limited information channels are built between adjacent devices for the sake of saving costs. Meanwhile, apart from the inherent incentive of obtaining more profits, another important responsibility of

the power distribution company is to guarantee the safety operation of the whole distribution network at any time point of the day, i.e.: both the transmission power in all lines and the voltage at all nodes should not exceed the maximum and the minimum boundaries.

Therefore, the enhanced optimal distributed consensus algorithm can be implemented here to help to achieve these goals from a brand new perspective.

The system parameters are summarized as follows in the Table 6:

Table 6 System Parameters

System Parameters	Values	System Parameters	Values
N	3	P_{PVmax_base} (MW)	0.9
M	3	P_{ESmax_charge} (MW)	1.2
I	15	$P_{ESmax\_discharge}$ (MW)	-1.2
L	14	$P_{max,1}{}'(MW)$	19
K	15	$P_{max,2}{}'(MW)$	15
a_{PV} $(\$/MWh^2)$	70	$P_{max,3}{}' \sim P_{max,14}{}'(MW)$	6
b_{PV} $(\$/MWh)$	65	α	0.2
a_{ES} $(\$/MWh^2)$	43	β	0.2
b_{ES} $(\$/MWh)$	82	ρ_s $(\$/MWh)$	250
ρ_b $(\$/MWh)$	180	ρ_D $(\$/MWh)$	270

As is seen from the graph, the information channels only exist between the neighbouring devices. Therefore, the “adjacency matrix” can be formulated as the following format, with the

assigned weights as the elements that satisfy both the “Non-Degeneracy” and the “Balanced Communication” conditions:

$$a = \begin{bmatrix} 5/6 & 1/6 & 0 & 0 & 0 & 0 \\ 1/6 & 4/6 & 1/6 & 0 & 0 & 0 \\ 0 & 1/6 & 4/6 & 1/6 & 0 & 0 \\ 0 & 0 & 1/6 & 4/6 & 1/6 & 0 \\ 0 & 0 & 0 & 1/6 & 4/6 & 1/6 \\ 0 & 0 & 0 & 0 & 1/6 & 5/6 \end{bmatrix}$$

In our study, we assume that the maximum value of each PV power output equals 0.9 MW from 8:00 am to 6:00 pm and it drops to zero during other periods in a day. With regards to the loads, the base load of each node is given in the following Table 7. And the load profile ratio curve in a day is varying and has peaks and valleys. So in our study, we assume the loads vary according to this trend shown in the Fig. 30.

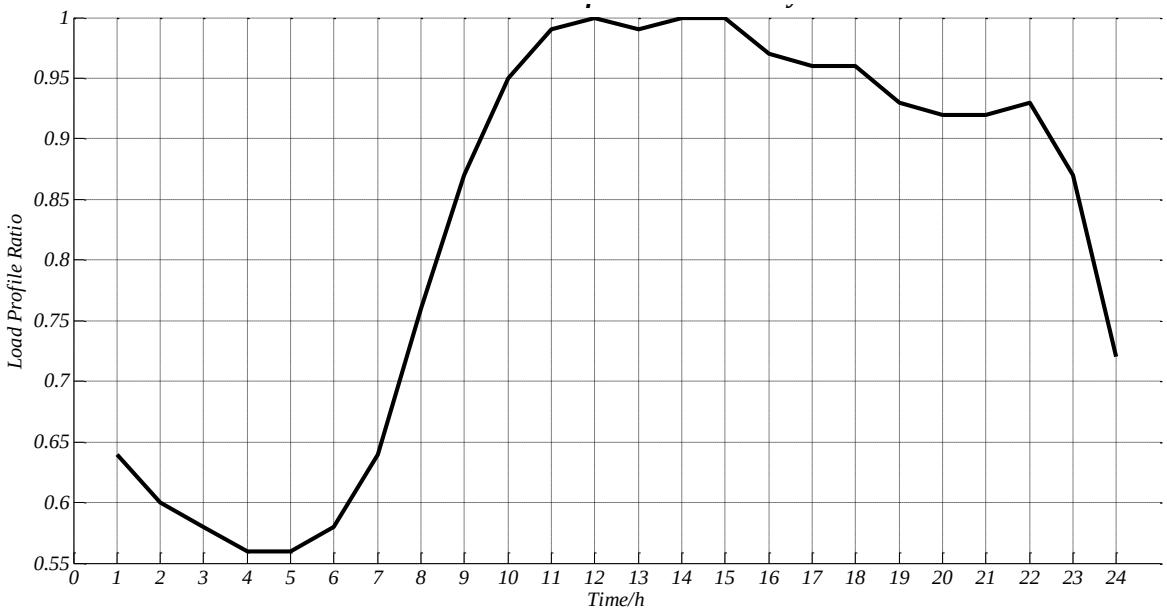

Fig. 30 The Load Profile Ratio in a Day

Table 7 The Base Load of Each Node

Node Number	2	3	4	5	6	7	8
Base Active Power/MW	1.59	1.29	1.02	1.90	0.35	1.52	1.54
Base Reactive Power/MVar	0.28	0.47	0.30	0.34	0.18	0.22	0.23
Node Number	9	10	11	12	13	14	15
Base Active Power/MW	1.47	0.69	0.81	0.44	1.90	1.60	1.11
Base Reactive Power/MVar	0.35	0.32	0.39	0.36	0.33	0.32	0.79

4.5.2 The Consensus Behaviour of the Agents during Iteration Process

First of all, we can observe the optimal consensus behaviour of the six agents during the iteration process. In each time point in a day, the algorithm is performed with randomly chosen initial values of the agents. Here we observe a specific time point: time=11.

From Fig. 31-32, we can see that during the iteration process, each agent updates its information separately regardless of the initial values they choose, until final consensus is reached. Besides, the black solid line indicates the global optimal value obtained by centralized control approach (interior-point method) while the other colourful lines show the final optimal value obtained by proposed distributed consensus control method. From the result we can see

that through limited information and data exchange between the neighbouring devices, the same global optimized value can be acquired both from centralized and distributed approaches.

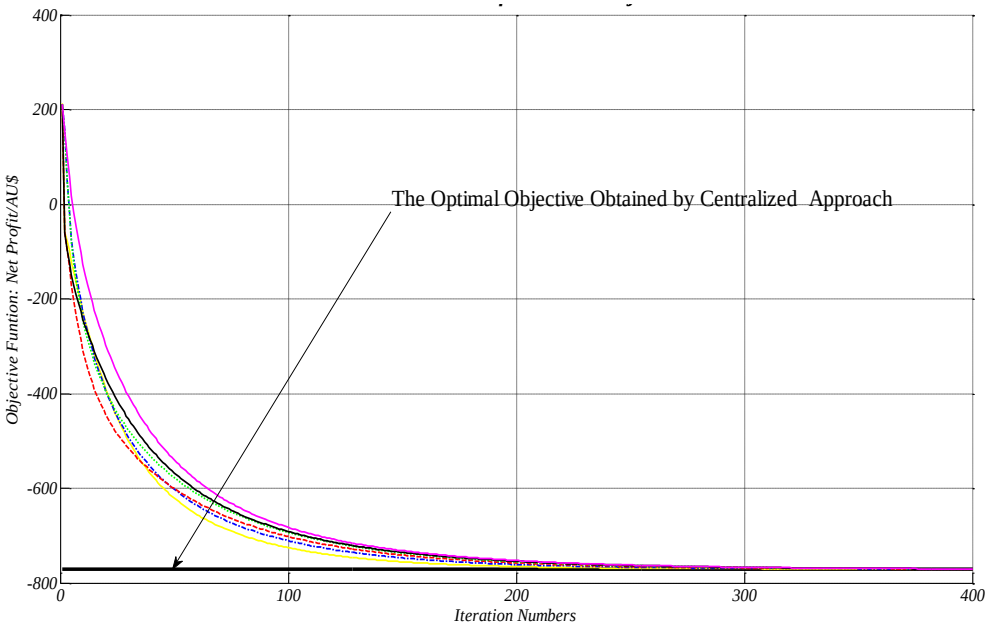

Fig. 31 The Consensus Behaviour of the Total Objective Function (time=11)

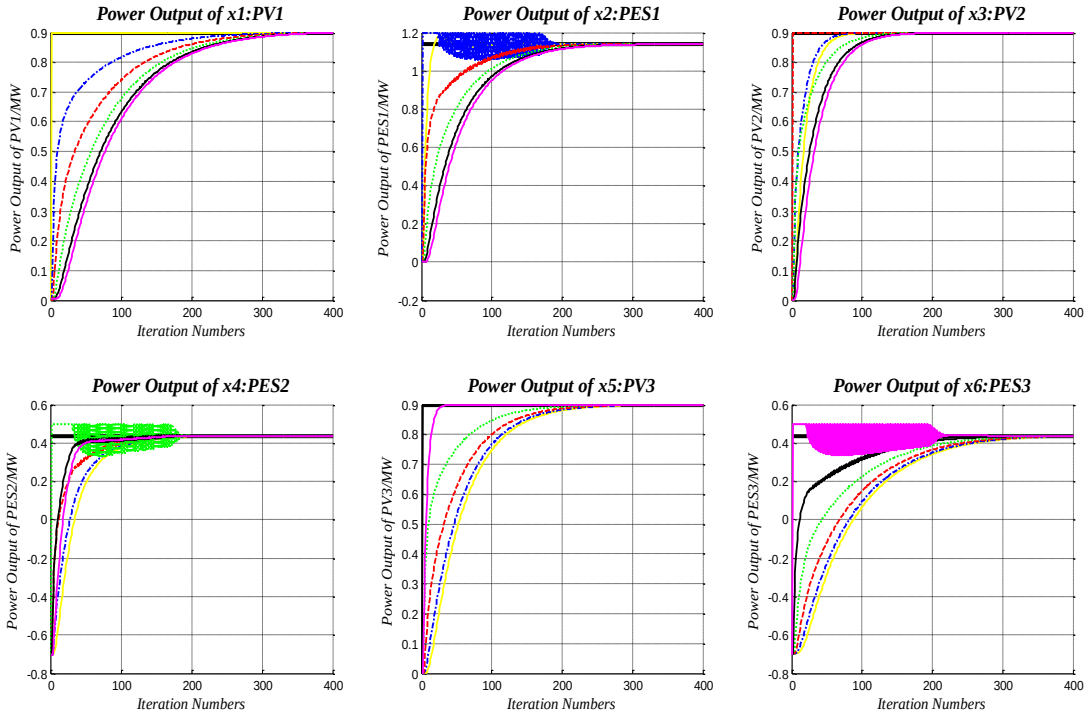

Fig. 32 The Consensus Behaviour of Different Agents (time=11) in EODCA

4.5.3 The Objective Function (Net Profit of the Company) in three Different Scenarios

In the following sections we compare the objective function (Net Profit of the Company) in a day in three different scenarios:

1) Without renewables at all;

2) With renewables behave randomly without control;

3) With renewables and they perform EODCA.

Firstly, if the devices behave randomly without control at all, the power outputs of renewables are shown in Fig. 33.

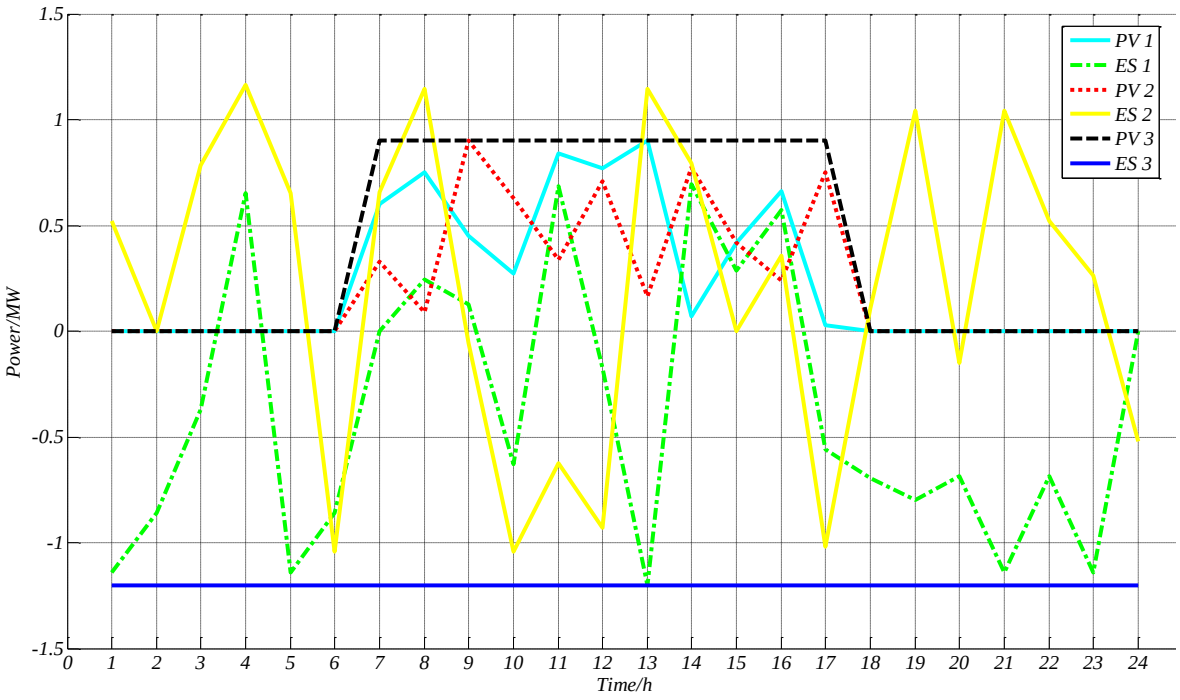

Fig. 33 The Chaotic Power Outputs of the Devices in a Day without Control

In contrast, with the EODCA, we can get the optimal power outputs of the devices, as depicted in Fig. 34.

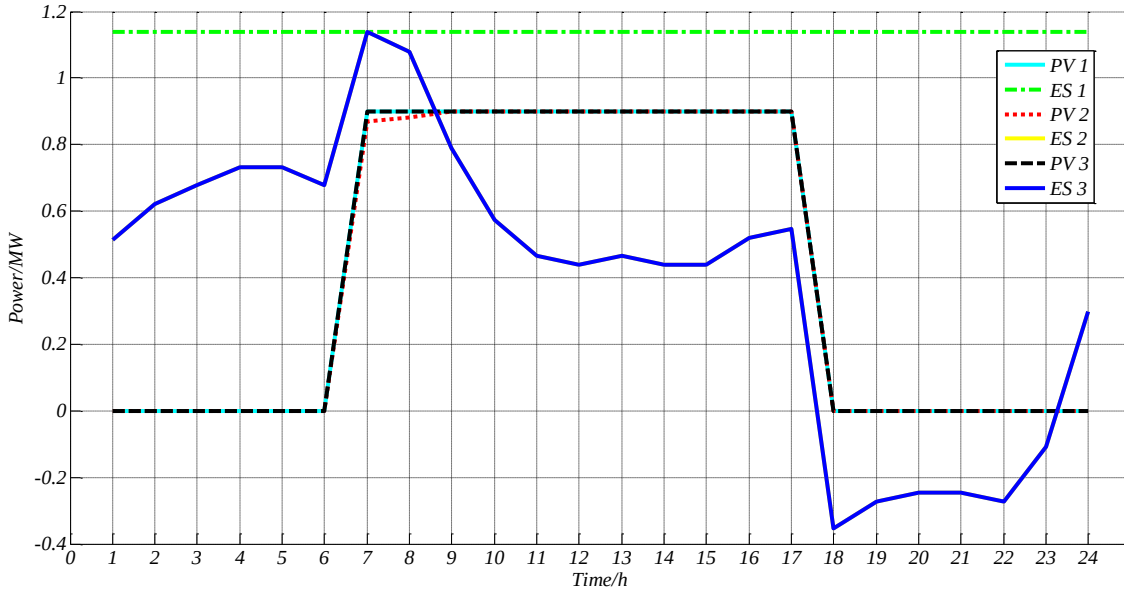

Fig. 34 The Optimal Power Outputs of the Devices in a Day with EODCA

And the Fig. 35 indicates the Net profit of the company in a day in these 3 scenarios.

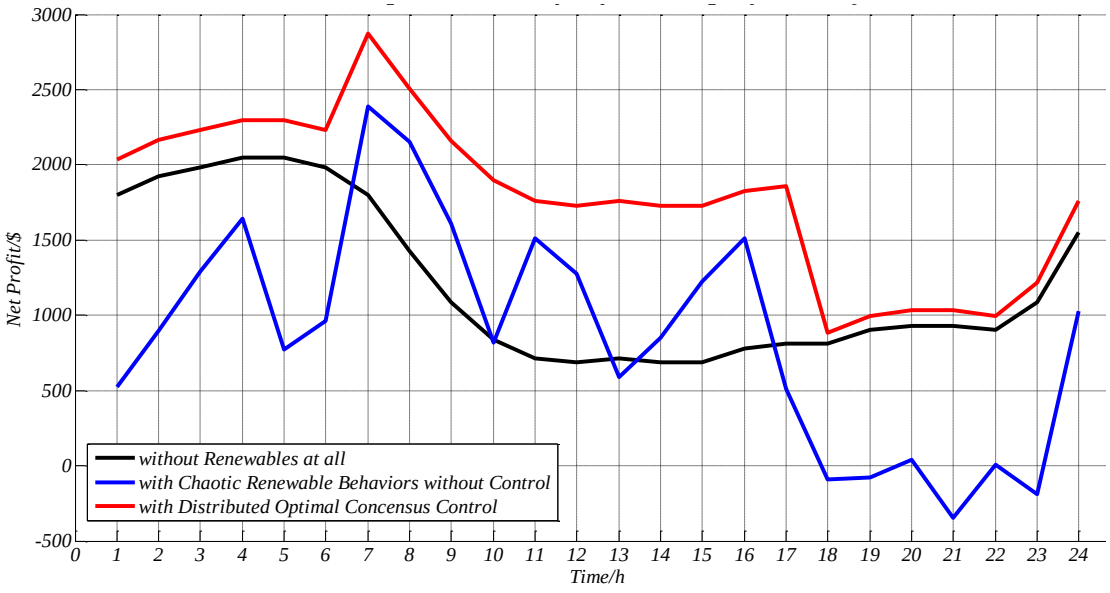

Fig. 35 The Net Profit of the Company in a Day

We can conclude that without renewables, the power distribution company can always get positive profits in current electricity markets. However, the situation changes when renewables are integrated. If we let these devices behave randomly without any regulation, sometimes the profit can be more than that without renewables but sometimes, the profit is less than zero, which means a deficit happens. In contrast, we can see the red line represents for the net profit obtained using EODCA, which is strictly larger than zero and the profit obtained without renewables. It is very useful in decision making process for companies in engineering practice.

4.5.4 The Comparison of Line Flows in three Scenarios

Here we compare the power flow in all the lines of the distribution network in above mentioned three scenarios.

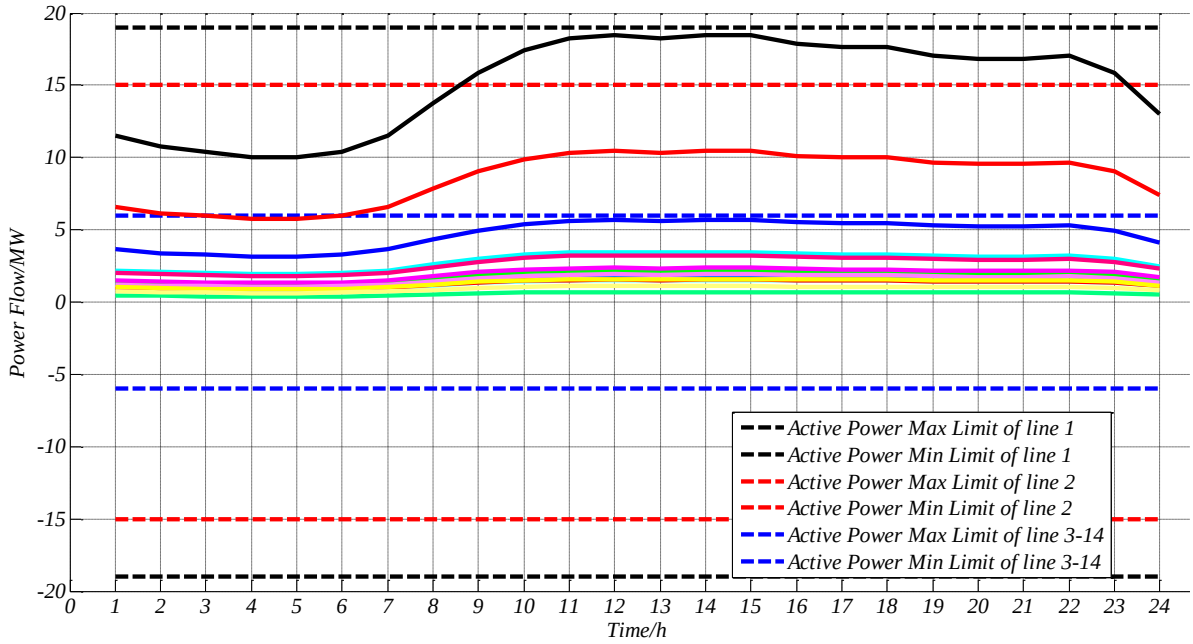

Fig. 36 The Active Power Flow Profile in a Day without Renewables at all

From the simulation results in Fig. 36-38 we can see clearly that, if there is no renewables at all, the power flows in distribution lines are all within their upper and lower limits. However, if the unregulated chaotic behaviours of the renewables happen at some time points, the reverse power flow of some distribution lines may violate the security boundaries and thus may cause system overload problems. Through the EODCA, the power flow in distribution lines remains inside the safety area and the reverse power flow problem is also alleviated.

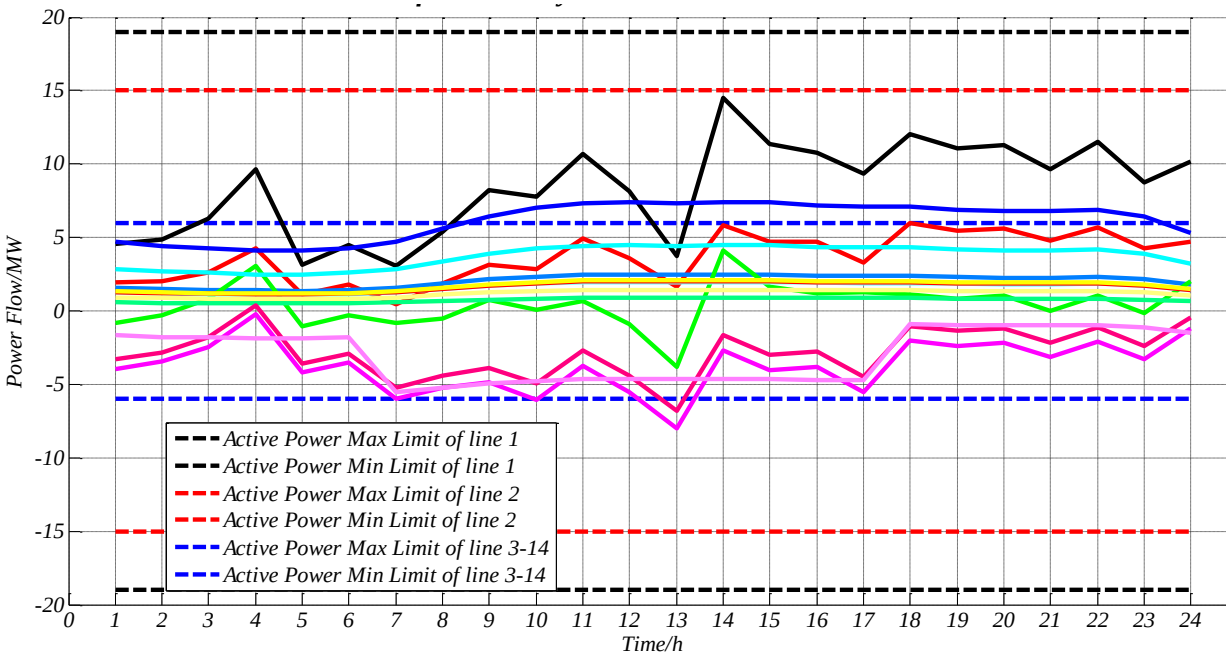

Fig. 37 The Active Power Flow Profile in a Day with Chaotic Renewable Behaviours without Control

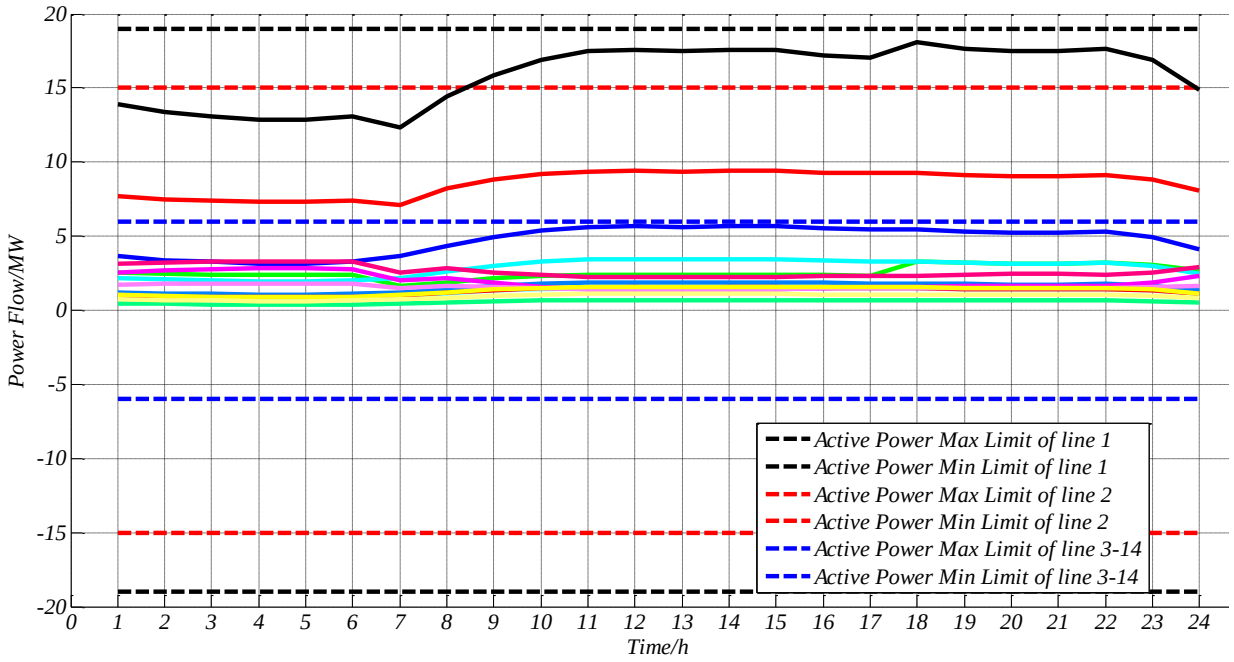

Fig. 38 The Power Flow Profile in Lines in a Day with EODCA

4.5.5 The Comparison of the Voltage Profiles in three Scenarios

Here we compare the voltage magnitude profile of all the nodes of the distribution network.

From the simulation results of Fig. 39-41, we can see that, when the renewable penetration level is 0%, the voltage in each node remains between 0.95 *p.u.* and 1.05 *p.u.* However, the chaotic behaviour of the sustainable devices would undermine the voltage profile, making it over upper limit of the safety voltage range at some time points. After using EODCA, all the voltage remains inside the safety area of the system.

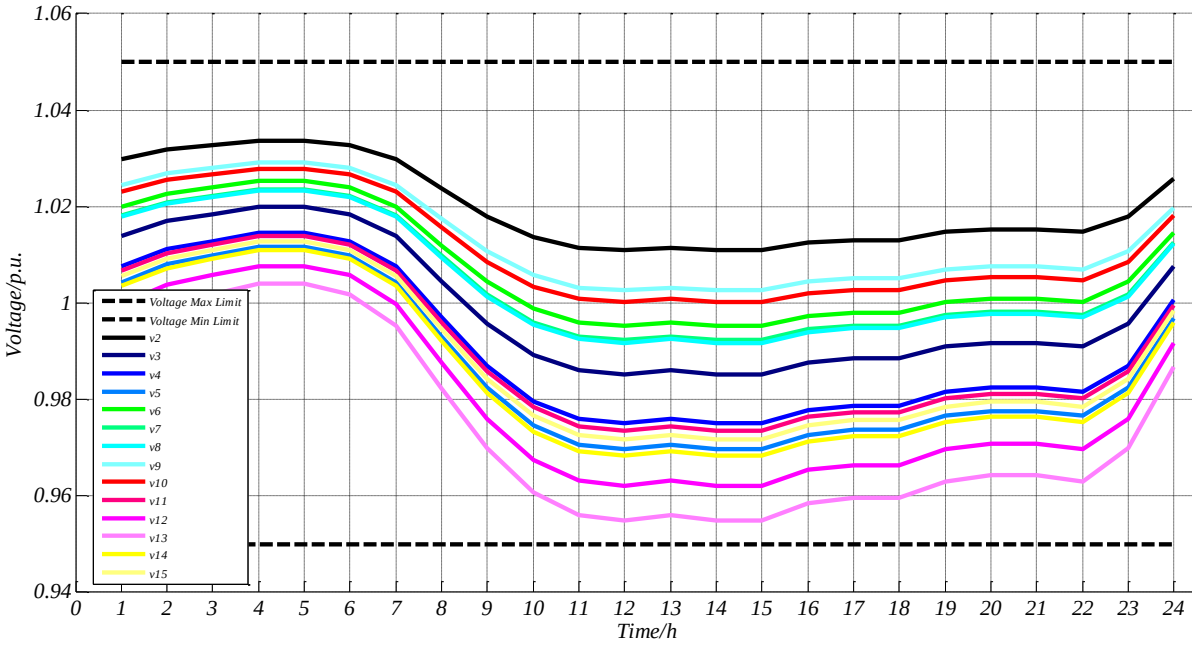

Fig. 39 The Voltage Profile of Each Node in a Day without Renewables

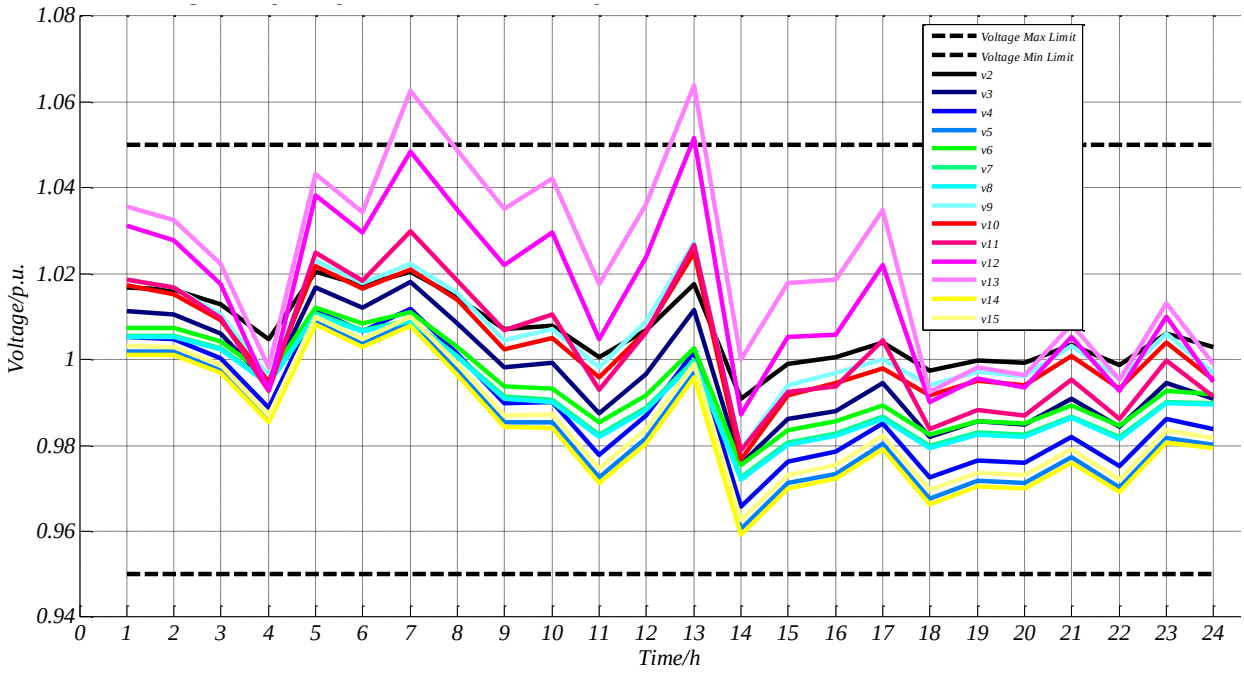

Fig. 40 The Voltage Profile of Each Node in a Day with Chaotic Renewable Behaviours without Control

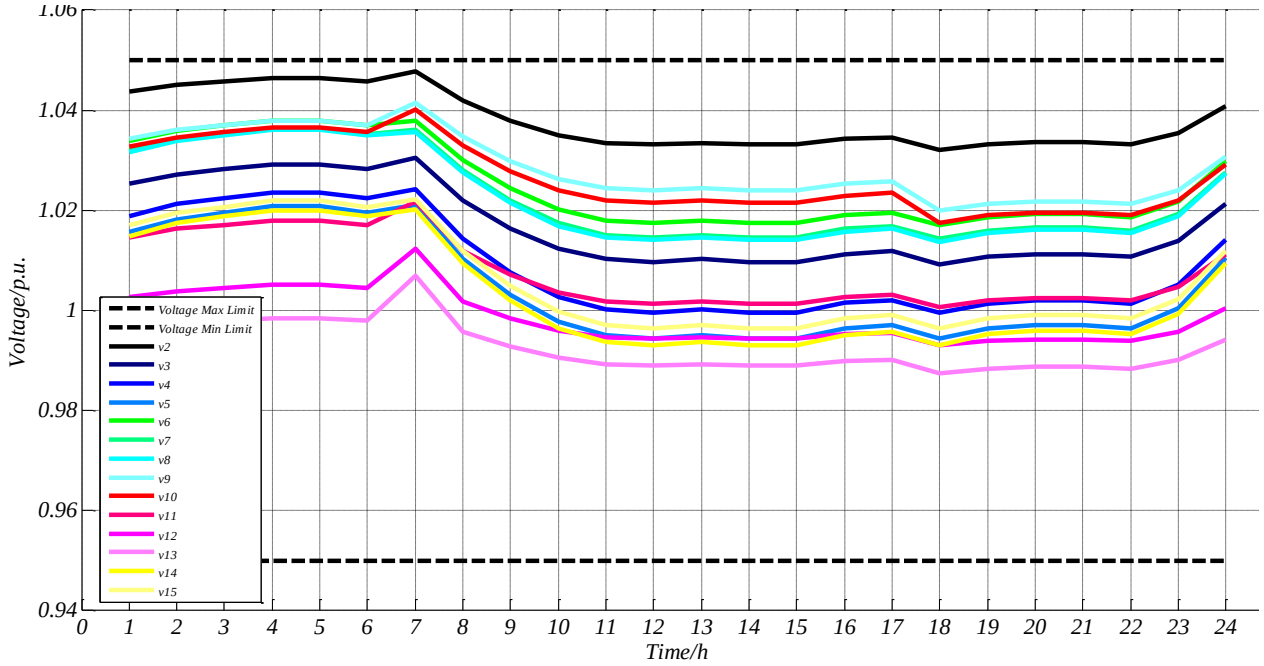

Fig. 41 The Voltage Profile of Each Node in a Day with EODCA

In the next Chapter 5, we will discuss on how to improve the calculation speed and efficiency of the proposed algorithm. Besides, the influence of the communication network topology will also be examined.

5. Modified Consensus Direction Method of Multipliers (MC-ADMM) and Communication Network Topology Analysis on Performance

As mentioned in the above chapter 4, the number of distributed photovoltaic and energy storage devices is increasing in future distribution networks. The research in chapter 4 focuses on developing a distributed consensus optimization algorithm that can optimize these devices to ensure the secure operation of the system. Units in the system exchange information through a communication network to maximize the net profit cooperatively.

In this Chapter, firstly I will focus on improving the efficiency and calculation speed of the optimization algorithms. I propose a Modified Consensus Alternating Direction Method of Multipliers (MC-ADMM) to demonstrate the effectiveness of accelerating the convergence speed. Afterwards, I also try to give some guidance on how to design a better communication network by innovatively analysing the performance in terms of network topology using graph theory. Through the simulation of several typical topologies of communication network respectively, a conjecture of the optimal topology for a communication network is given.

5.1 Modified Consensus Alternating Direction Method of Multipliers (MC-ADMM)

In this section, we develop an algorithm called Modified Consensus Alternating Direction Method of Multipliers (MC-ADMM) to solve the problem. It is based on the distributed optimization algorithm proposed in [47].

The mathematical model is quite similar with that in the previous chapter. Specifically, the same objective function is given in (25). However, here in this section, the simplified model is used, which means we only consider the power flow balance and limitation constraints (28),(29),(30) and (33) due to the requirement of the MC-ADMM.

The objective of this multi-agent group is to optimize the common goal below cooperatively, namely objective function (25) and constraints (28),(29),(30) ,(33) can be written as:

$$\min_{x\in\mathbb{R}^n} \sum_{i=1}^{2N} f_i(x_i),\ \ s.t. \sum_{i=1}^{2N} a_i x_i \le b;\ x \in \bigcap_{i=1}^{N} X_i \tag{54}$$

In this practical model, $f_i(x_i) = \alpha_i x_i^2 + \beta_i, \alpha_i > 0$, N=M. The iteration steps of MC-ADMM are as follow:

1). Given initial variables $x_i^{(0)} \in \mathbb{R}, y_i^{(0)} \in \mathbb{R}^{2M}, p_i^{(0)} = 0,$ for each agent i, $i \in V = \{1,2,...,2N\}$, set step index k=1;

2). for all $i \in V$, perform (55)-(57) in parallel:

$$p_i^{(k)} = p_i^{(k-1)} + c \cdot \sum_{j\in N_i} (y_i^{(k-1)} - y_j^{(k-1)}) \tag{55}$$

$$x_i^{(k)} = \arg\min_{x_i \in X_i} \{ f_i(x_i) + \frac{c}{4\| N_i \|} \| \frac{1}{c}(a_i x_i - \frac{b}{2N}) - \frac{1}{c} p_i^{(k)} + \sum_{j\in N_i} (y_i^{(k-1)} + y_j^{(k-1)}) \|_2^2 \} \tag{56}$$

$$y_i^{(k)} = \frac{1}{2|N_i|}[\sum_{j\in N_i} (y_i^{(k-1)} + y_j^{(k-1)}) - \frac{1}{c} p_i^{(k)} + \frac{1}{c}(a_i x_i^{(k)} - \frac{b}{2N})]_+ \tag{57}$$

3). Set k=k+1;

4). Repeat steps 2) and 3) until $\| x_i^{(k)} - x_i^{(k-1)} \| \le \varepsilon$.

In this problem, (56) can be expressed as:

$$x_i^{(k)} = \frac{1}{2\alpha_i + \frac{a_i^T a_i}{2|N_i|c}} \left[\frac{a_i^T b}{4N|N_i|c} + \frac{a_i^T p_i^{(k)}}{2|N_i|c} - \beta_i - \frac{a_i^T y_i^{(k-1)}}{2} - \frac{\sum_{j \in N_i} a_i^T y_j^{(k-1)}}{2|N_i|} \right]_{X_i} \quad (58)$$

$[*]_{Xi}$ is the projection operation onto the set X_i; $N_i = \{j \in V \mid i \neq j\}$, i.e. all agents except itself i; parameter ε is a pre-defined constant value which stands for a computational accuracy. Adaptive parameter c will be discussed later.

5.2. Case Studies & Algorithm Analysis

5.2.1 System Description

In order to demonstrate the effectiveness and the characteristics of the proposed method, the algorithm is coded in Matlab environment. The comparison algorithm is the latest proposed one called **Distributed Lagrangian Primal-Dual Sub-gradient algorithm (DLPDS)** in [28]. The dimension of the independent variable x represents the number of distributed devices, i.e. if we choose dimension=10, the topology would be demonstrated as Fig. 42. If the dimension increases, the number of devices would be increased as well, but the basic radial structure remains the same, which means the system and algorithm is easy to extend to a larger distribution network.

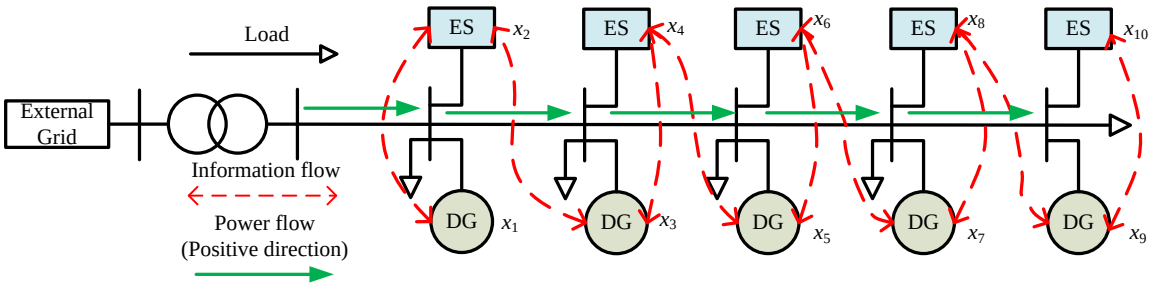

Fig. 42 Future Distribution Network with Energy Storages and Distributed Generators (Dimension=10)

5.2.2 Comparison between Algorithms

First of all, we choose dimension of independent variables: 10; ε=0.1; Maximum iteration steps: 5000. Then we implement the calculation with two algorithms. Fig. 43-44 shows the dynamic convergence performance with MC-ADMM and DLPDS, from two perspectives, namely convergence performance of the different agents and the convergence performance of the relative error.

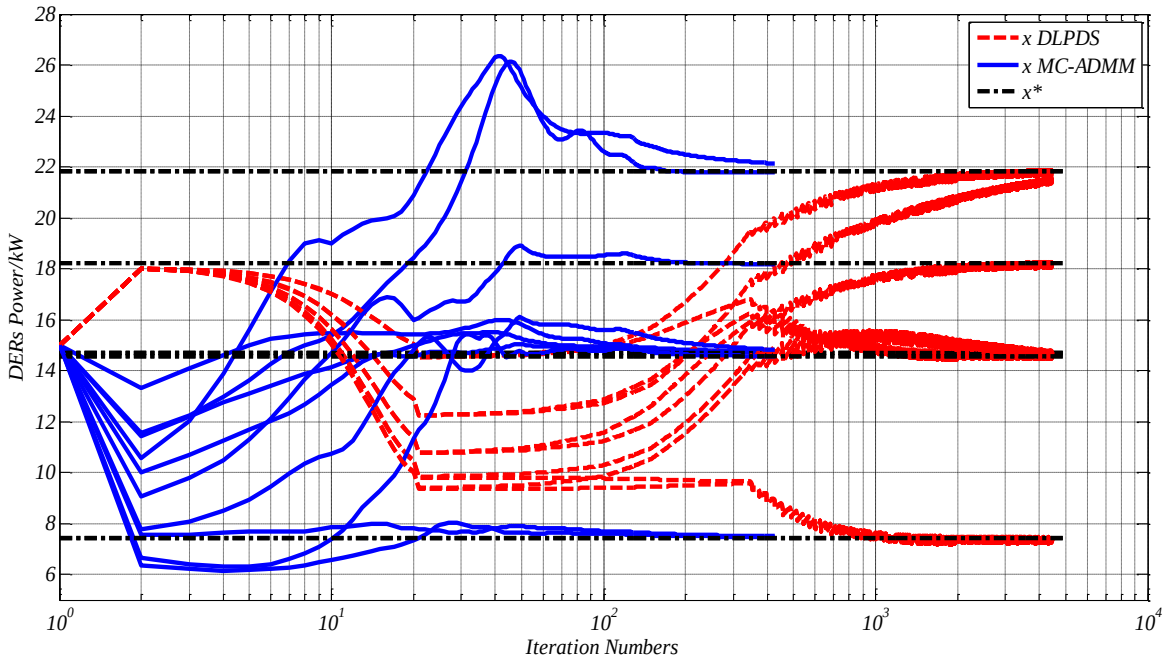

Fig. 43 The Dynamic Convergence Performance of Different Agents in MC-ADMM and DLPDS (Dimension=10)

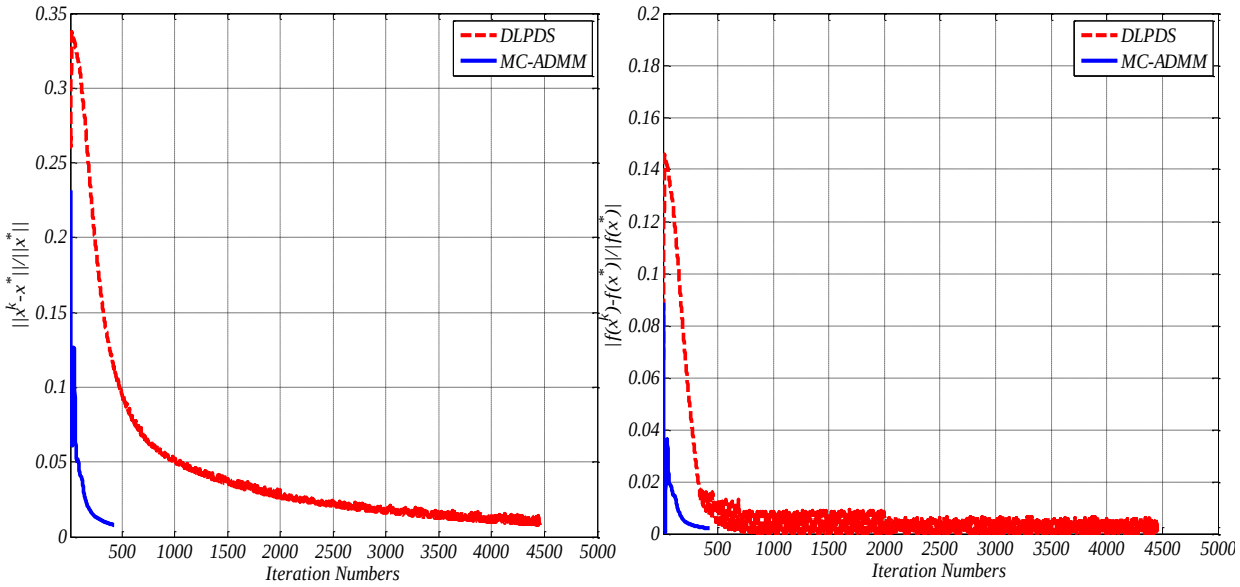

Fig. 44 The Dynamic Convergence Performance of the Relative Error (Independent Variables and Objective Function) in MC-ADMM and DLPDS (Dimension=10)

From Fig. 43-44, we can conclude that for lower dimension cases, although both of the two algorithms (MC-ADMM and DLPDS) can guarantee the convergence of the optimal value and adequate accuracy, the convergence speed of MC-ADMM is much faster than DLPDS (426 versus 4460 steps). Note that the reason for oscillation is that the DLPDS runs into the high-accuracy area (namely relative error is less than 0.02) and it is not so stable compared with MC-ADMM.

In order to compare the two algorithms especially their ability to calculate higher dimension of independent variables, we gradually increase the dimension of x. The results are shown in Fig. 45-46.

- Dimension of independent variables: 20; ε=0.1; Maximum iteration steps: 10000.

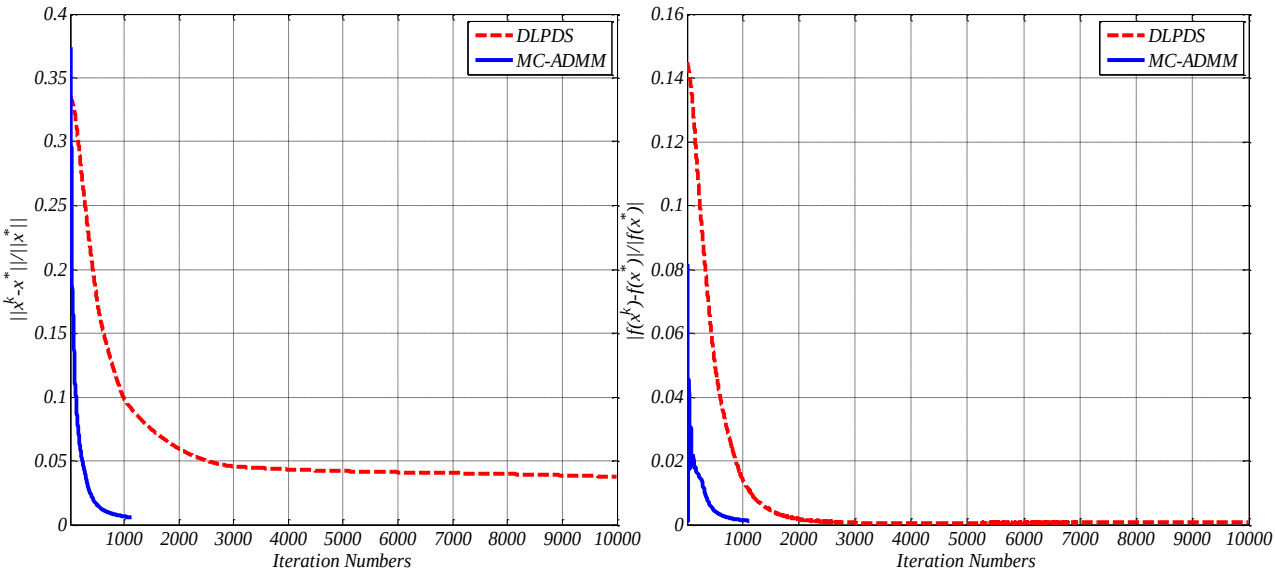

Fig. 45 The Dynamic Convergence Performance of the Relative Error (Independent Variables and Objective Function) in MC-ADMM and DLPDS (dimension=20)

- Dimension of independent variables: 40; ε=0.1; Maximum iteration steps: 20000

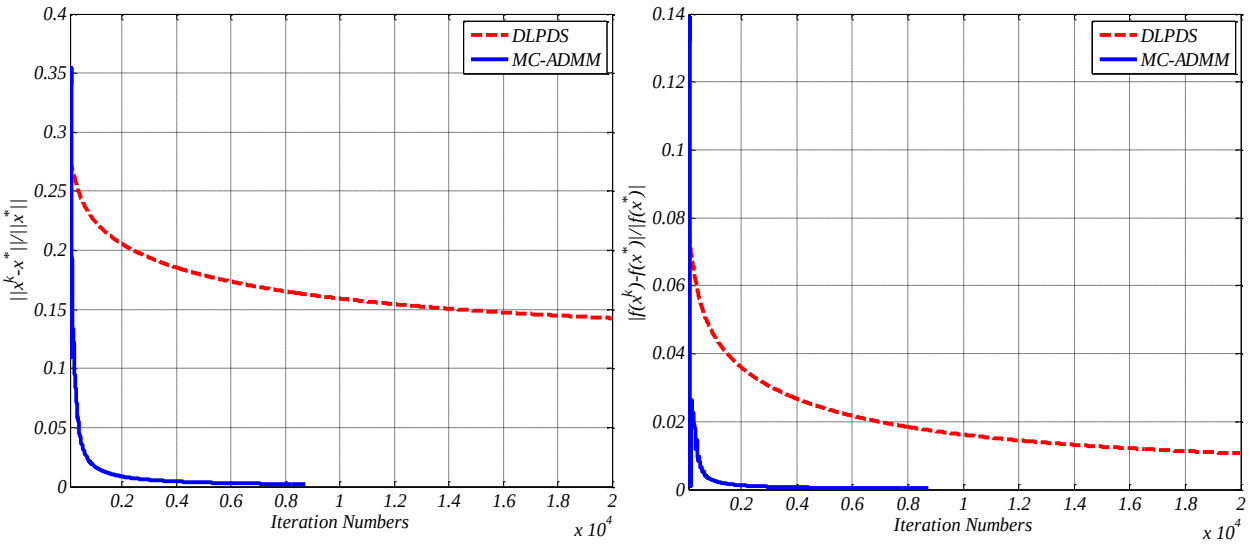

Fig. 46 The dynamic convergence performance of the relative error (independent variables and objective function) in MC-ADMM and DLPDS (dimension=40)

From the above figures, we can see that when the dimension of independent variables increases, both the speed of the two Algorithms (MC-ADMM and DLPDS) slows down. However, only MC-ADMM are much faster than the DLPDS and it can guarantee adequate accuracy (pre-defined ε=0.1) whilst DLPDS cannot. It can be noticed that the reason for smooth DLPDS curve is that the iteration stops at the maximum iteration number and it is far from the high-accuracy area. Table 8 lists the detailed calculation indexes of these two algorithms.

Table 8 Calculation Performances of two Algorithms

Dimension of *x*	**Max Iteration steps**	**DLPDS**		**MC-ADMM**	
		Steps to reach *ε*	**Computation time/*s***	**Steps to reach *ε***	**Computation time/*s***
10	5000	4460	16.0	426	0.3
20	10000	Max	261.2	2168	11.7
40	20000	Max	3844.3	8742	362.9
80	40000	Max	19249.5	12035	956.1

From the Table 8, we can draw the following conclusions:

Calculation time: when the dimension of independent variables multiples, both the calculation time of the two Algorithms (MC-ADMM and DLPDS) increases. However, the MC-ADMM maintains to be much faster than the DLPDS.

Iteration numbers used to reach the same accuracy (pre-defined ε=0.1): when the dimension of independent variables multiples, both the iteration numbers used of the two Algorithms (MC-ADMM and DLPDS) increases. However, the MC-ADMM can guarantee the high accuracy within limited iteration numbers whilst DLPDS doesn't guarantee high enough accuracy within acceptable iteration steps.

The reason why MC-ADMM performs much faster than DLPDS, especially in a large system, can be explained from a calculation perspective.

First of all, the most time-consuming process is the information updating process in each iteration step. In MC-ADMM, we can see from the (56) that in each iteration step *k*, MC-ADMM only requires the $x_i^{(k)}$ of agent *i* (*i*=1…*N*) to update. This means for a system with *N* agents, each iteration step we only need *N* agents to update their status: the calculation is a simple scalar operation and the dimension is only *N*.

By contrast, in DLPDS, during each iteration step *k*, we can see from the (39) that actually it requires each agent *i* (*i*=1…*N*) to generate a vector that has *N* elements, i.e. *N*-dimensional. Then, each agent updates their information according to the control law, which means that the complex matrix operation requires *N* vectors (each one is *N*-dimensional) calculating simultaneously. Therefore, the memory usage of the computer is high-demanding and the calculation speed is slowed down significantly. The situation gets worse at an exponential

rate when *N* increases so that the superiority of MC-ADMM is even more obvious when dealing with larger systems.

5.2.3 Comparison between Different Communication Network Topologies

In this section, we will analyse the different types of communication network topologies on calculation performance, under intact and fault conditions. We consider three typical connecting strategies for communication network, i.e. Radial, Circular and Random, as shown in Fig. 47:

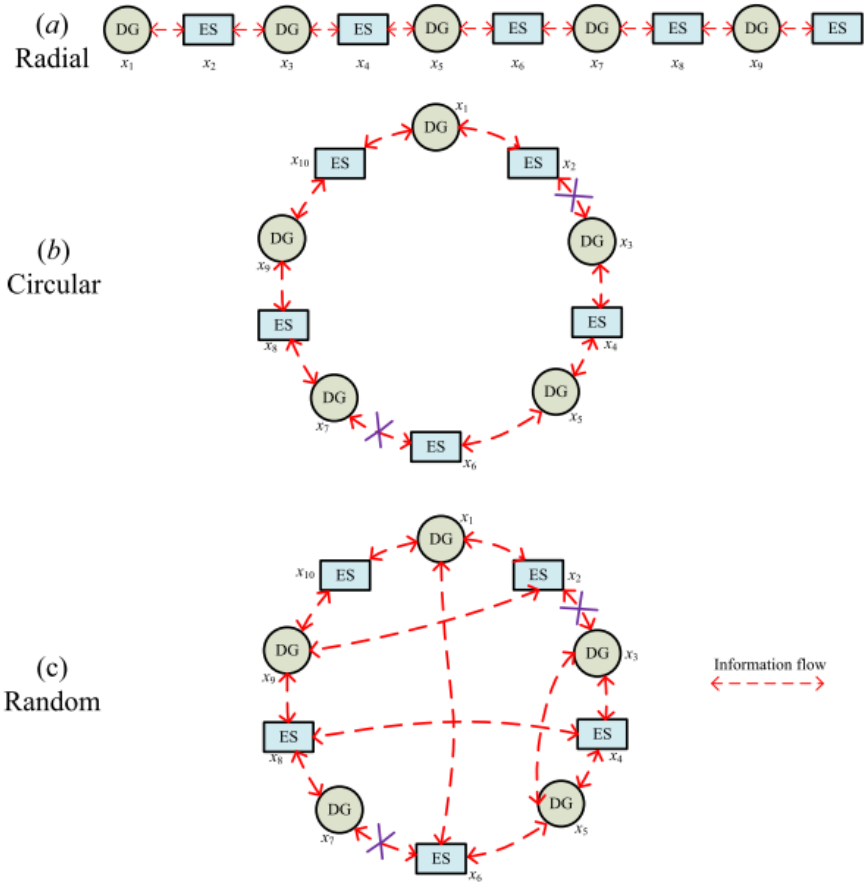

Fig. 47 Three Different Types of Communication Network Topology (dimension=10)

➢ Under intact condition:

When the network is intact and everything runs normally, we can see the dynamic convergence performance of the relative error (objective function) in three different communication network topologies (Dimension of independent variables: 10; ε=0.1; Maximum iteration steps: 1000) as shown in Fig. 48.

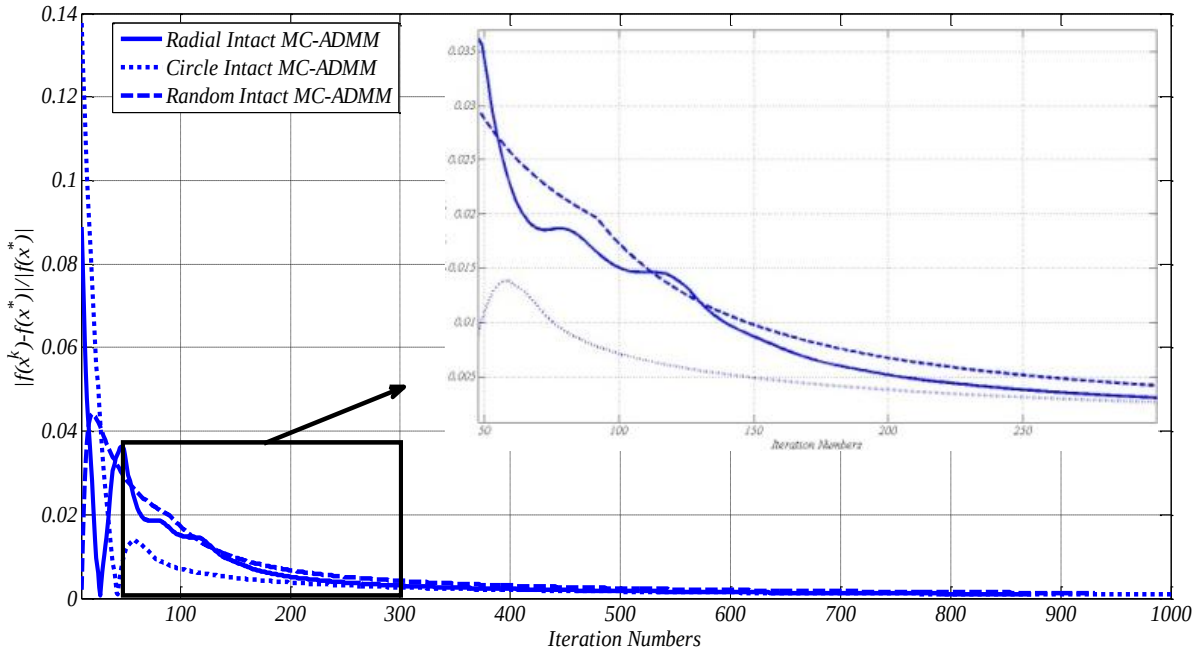

Fig. 48 The Dynamic Convergence Performance of the Relative Error (Objective Function) in Three Different Communication Network Topologies (dimension=10)

From the Fig. 48, we can conclude that the topology of the communication network has a profound influence on convergence speed of the algorithm.

Compared with the radial structure, the circular topology accelerates the convergence because some of the paths will be shortened due to the end-to-end characteristic.

However, the speed of random structure does not necessarily accelerate the algorithm, which will be discussed later in section 5.3-5.4 this Chapter.

➢ Under fault condition:

In Fig. 49, we can observe what will happen if the communication network link breaks down due to hacker attack or natural disasters.

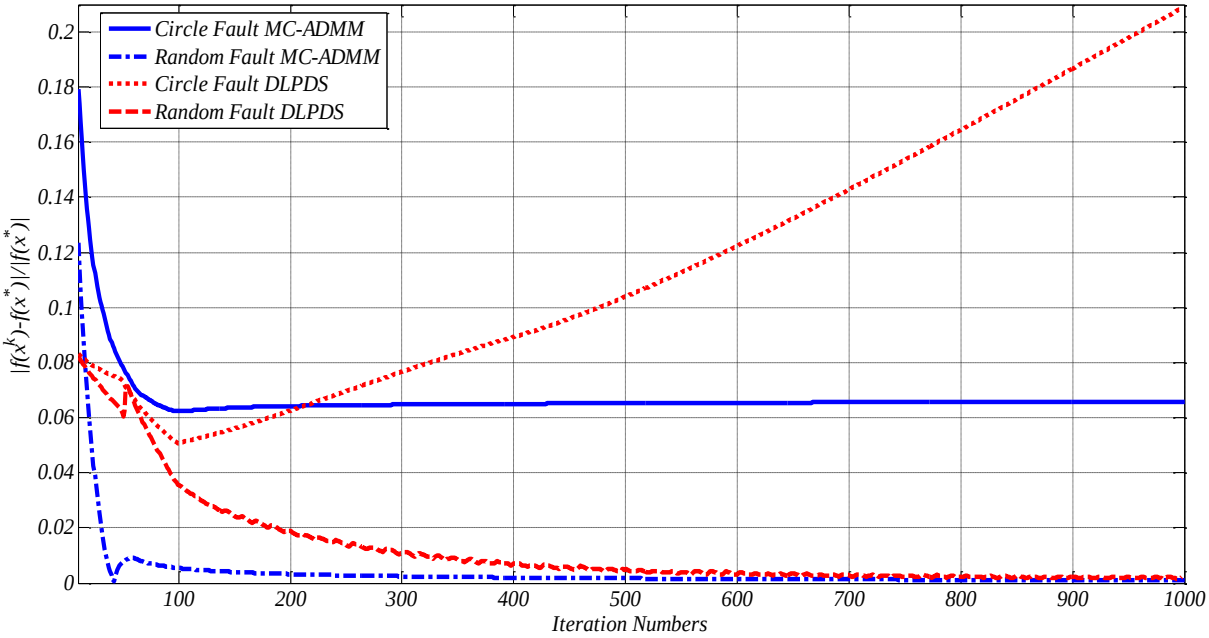

Fig. 49 The Dynamic Convergence Performance of the Relative Error (Objective Function) under Fault Condition with two Communication Network Topologies and two Algorithms

From the Fig. 49, we can conclude that the connectivity is quite crucial, if the fault happens to make the communication network into two separate parts, then both of the DLPDS and the MC-ADMM cannot guarantee the convergence and the optimal value to be reached, because some of the crucial information cannot reach some agents during iteration process. However, when the network is connected, both the DLPDS and the MC-ADMM can help the

convergence to optimal value. Hence, the random topology is more robust than the circular network.

5.2.4 The Parametric Sensitivity Analysis of MC-ADMM

The last question is to determine how to choose parameter *c* in MC-ADMM. Fig. 50 shows the calculation performance with regard to the value of *c*. (Dimension of independent variables: 10; ε=0.1; Maximum iteration steps: 1000; Radial Topology)

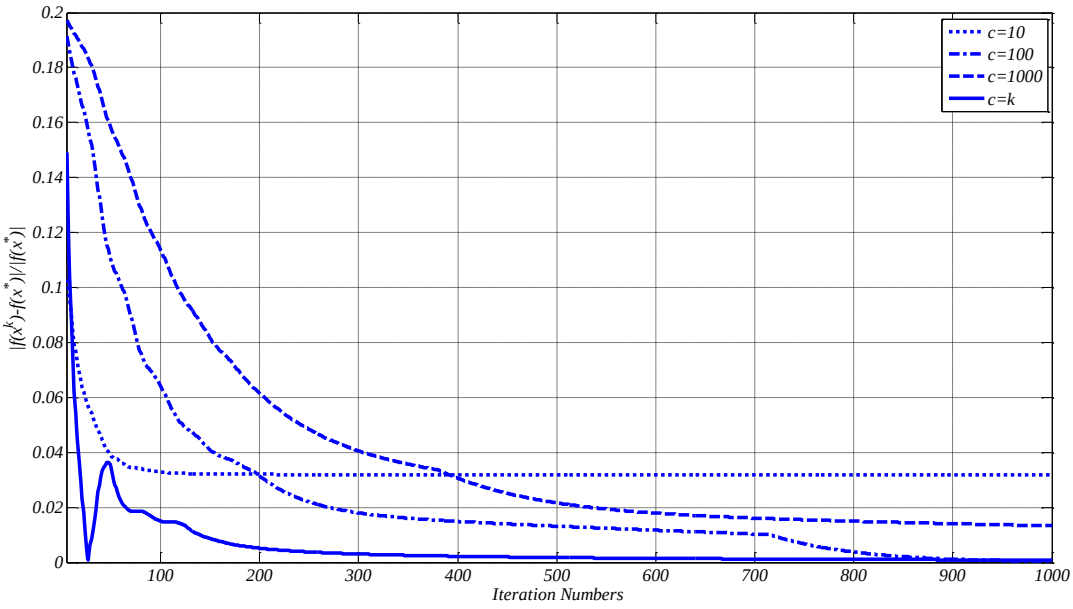

Fig. 50 The dynamic convergence performance of the relative error (objective function) with different parameter *c*

From the Fig. 50, we can see that the parameter c has a profound influence on convergence rate of the algorithm. If c is constant, it is neither appropriate to choose c too large nor too small. It's very important to choose the proper parameter c. Besides, we can see that if

we choose c increases gradually with the iteration process, the result is better than maintaining it the constant value all the time.

5.3 Topology Types of the Communication Network

In section 5.2.3, we conclude that the type of communication network plays a pivotal role in influencing the calculation performance. In this section, we are going to discuss this topic thoroughly based on graph theory and give some useful conclusions on designing a better network.

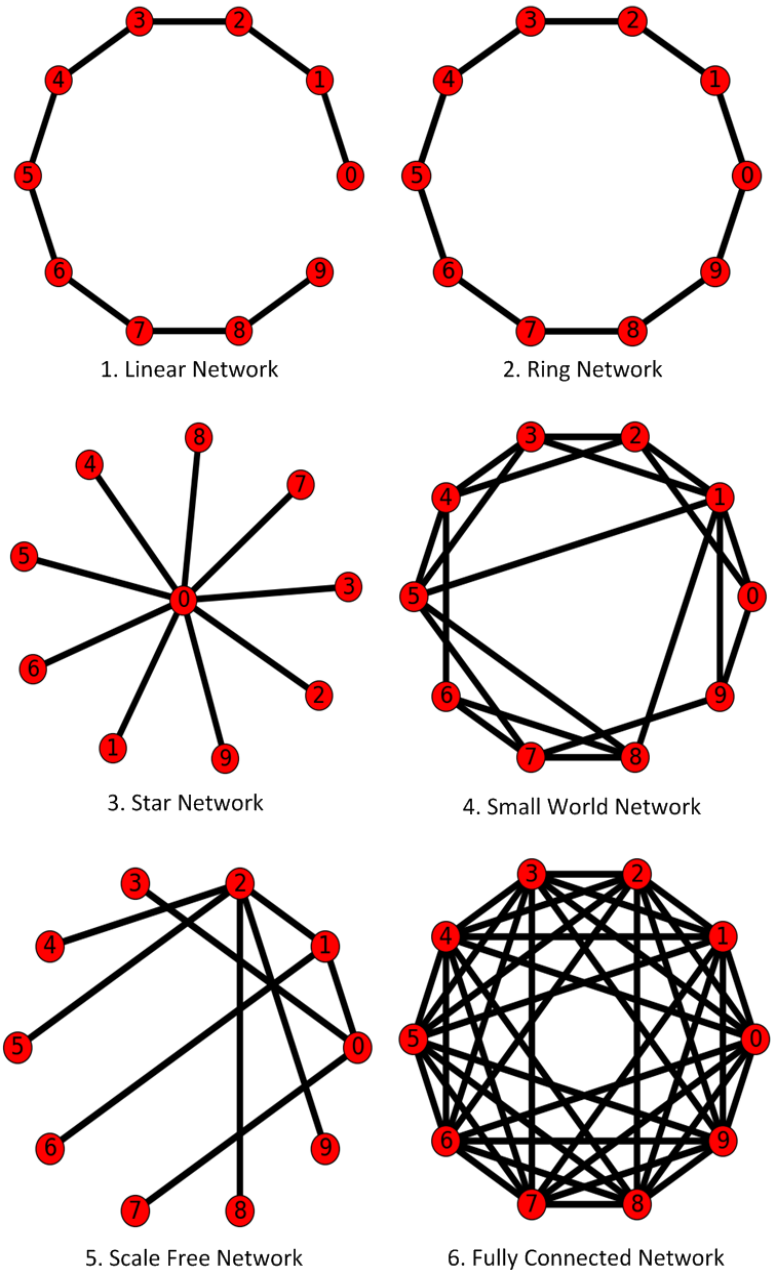

Fig. 51 Examples of Typical Topologies of Communication Networks

In the distribution power grid, the users are usually connected to the feeder line in sequence. However, the communication network can be designed to have different physical topology compared with power network. The result of MC-ADMM algorithm shows the convergence speed of optimization highly relies on the structure of the communication network.

To analyse the impact of communication network topology on the calculation speed of MC-ADMM, a series of numerical simulation have been designed. Six scenarios with different typical network connections demonstrated in Fig. 51 are proposed in this study [48, 49].

- **Linear network**

The simplest topology, all "agents" are connected one by one. Most of the feeder systems are formed as this kind of topology. A linear network has high expandability. To add a new "agent" into the network, the operator only needs to connect this new "agent" to the edge of the network and it is not necessary to change the network topology. On the contrary, an "agent" is only able to communicate with another "agent" via the neighbours between them.

- **Ring network**

A ring network is a network with circular topology. Each "agent" incorporates a receiver and a transmitter to send the information to the next "agent" in the ring. Compared with the linear network, the ring network increases the transmission speed because some of the paths will be shortened due to the end-to-end characteristic. However, in ring network it's difficult to add a new "agent" into the original system. Also as a disadvantage, it's hard to identify the fault location when accident happens.

- **Star network**

In a network with star topology, each "agent" is connected to a central "agent" called hub with a point-to-point connection. The star topology is considered the easiest topology to design and implement. The central "agent" is playing a very important role during the information exchanges. Thus, there is high risk for the whole network to collapse when a failure destroy this

hub “agent”. An advantage of the star topology is the simplicity of adding additional nodes to the existing network.

- **Small World network**

Small world network is a special network topology that arose in social science and was modelled analytically by Duncan Watts and Steven Strogatz in 1998[50]. In a network with the characteristic of small world topology, most of the “agents” are not neighbours of one another, but can be reached from most of other “agents” by a small number of steps. That is to say, in a small world network the average distance between two “agents” is far smaller than the number of “agents” that exists in the network.

- **Scale Free network**

The most notable characteristic in a scale-free network is the relative commonness of “agents” with a degree that greatly exceeds the average[51]. Differently with the Poisson distribution degree in most random networks, the degree distribution of scale free network obey the power law. Namely, most of the “agents” in a scale free network have only small number of connections but several “agents” have extremely high degree. The ascendancy of these critical “agents” makes this kind of network robust to random failures, but can be very vulnerable to targeted attacks.

- **Fully connected network**

A fully connected network is also known as a complete graph. It’s a network in which each of the nodes is connected to each other. This kind of network provides a high degree of reliability due to the multiple paths for data transportation between nodes. On the contrary, it's

very expensive to set up a network with this topology, since it requires extremely large numbers of direct links.

5.4 Influence of the Different Communication Network Topology on Calculation Performance

To illustrate the difference of calculation speed among typical communication networks mentioned above, a numerical simulation is performed. The topology of the network is the same with Fig. 42 and MC-ADMM is utilized to solve this problem. The simulation results are elucidated in Fig. 52.

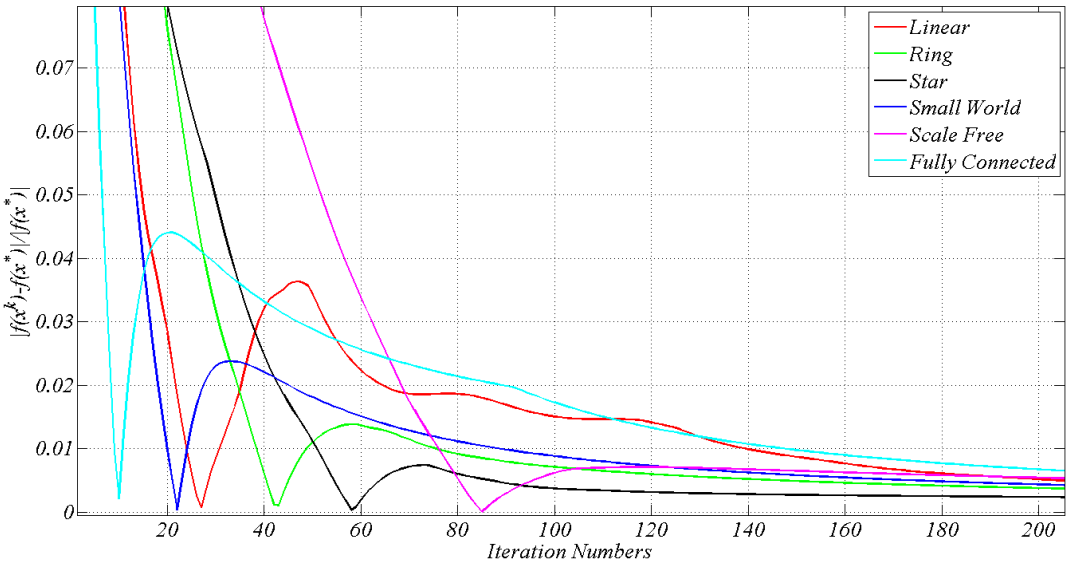

Fig. 52 Iteration Performance of MC-ADMM under Different Communication Network Topologies

From the Fig. 52 it can be seen that there are two phases during the convergence process, descent phase and fluctuation phase. In the descent phase, all curves experience the decreasing to

the optimal solution with different velocities. Then after several fluctuations, they converge to the optimal value. However, it can be clearly seen that the iteration steps and converge speed are totally different. In some of the topologies, the curve decrease very fast and draw a severe tails, and others draw very long tails. On the other hand, several curves fluctuate dramatically and take further steps to converge.

To identify the reasons of disparity in convergence performance, several basic characteristics of network topology in graph theory are introduced.

- Degree

In graph theory, the degree of a node is the number of edges incident to the node[52]. The degree of a node v denoted $deg(v)$. The degree expresses the adjacency relationship between v and other nodes, which shows the significance of it in the network. The degrees of each node in the network topologies used in simulation were calculated.

- Laplacian eigenvalue

A Laplacian eigenvalue is the eigenvalue of a Laplacian matrix[53]. For a graph G with n nodes, its Laplacian matrix L is defined as:

$$L=D-A \tag{59}$$

where D is the degree matrix and A is the adjacency matrix of the graph. In terms of node degrees, it can be written as:

$$L_{i,j} := \begin{cases} \deg(v_i) & i = j \\ -1 & i \neq j \text{ and } v_i \text{ is adjacent to } v_j \\ 0 & \text{otherwise} \end{cases} \tag{60}$$

The Laplacian eigenvalues can be used to find many properties of the graph. One of the most important theorem and applications in spectral graph theory is to calculate the approximate sparsest cut of a graph through the second-largest Laplacian eigenvalue[52].

It can be approved that the second-smallest Laplacian eigenvalues, namely λ_{n-1}, can reflect connectivity of a network[52]. Connectivity is one of the basic concepts of graph. It represents the minimum number of nodes or edges that need to be removed to disconnect the remaining nodes from each other. If a graph has a large λ_{n-1} this means nodes in this graph are highly connected. The distributions of λ_{n-1} in the typical network topologies are demonstrated in Fig. 53.

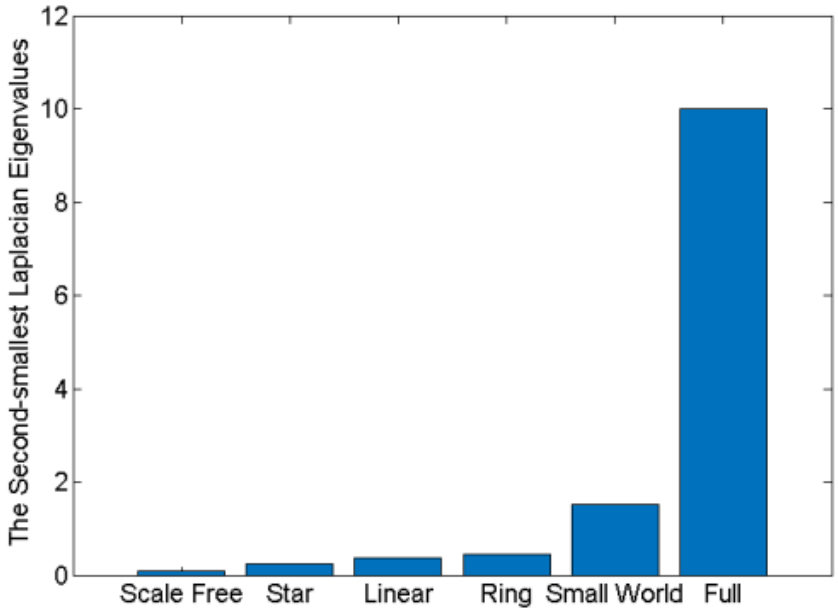

Fig. 53 Distribution of λ_{n-1} in Typical Topologies

From the introductions above, it can be known that, MC-ADMM algorithm requires "agents" share the information with their neighbours during the calculation. Thus, in a graph with higher connectivity, "agents" can finish information exchange in fewer steps. This can explain the

difference of descent velocity in simulation result. From Fig. 53 it can be seen that fully connected graph has the biggest λ_{n-1}, that's why it takes the least iteration numbers in descent phase. On the contrary, the scale free network topology used in this simulation has the lowest connectivity. So the iteration curve decreases very slow and takes almost five times iteration steps more than that in fully connected topology.

The distribution of degree in a topology is also found to affect the calculation speed. In [54] Li and Pan have proved a lemma:

$$\lambda_2 \geq D_2 \tag{61}$$

Where D_2 is the second-largest degree in the graph. They also pointed out that it is difficult to find a graph with $\lambda_2=D_2$, most of the graph has a difference between λ_2 and D_2. This can be classified as an extremal graph[55] problem in graph theory, which means to search for a graph with largest number of edges with certain property. A graph with $\lambda_2=D_2$ can be called an extremal graph here. Then the smaller difference between λ_2 and D_2, the closer a graph is to an extremal graph.

The reason of long term fluctuation is analysed as follows. It may be caused by the redundancy information between “agents” communication during the distributed optimization. But from the simulation result, it can be deduced that the difference between λ_2 and D_2 affecting to the fluctuation level during iteration. The distribution of difference between λ_2 and D_2 in each topology is shown in Fig. 54. It is not hard to find, the larger difference there is, the more intense fluctuation it has. In other words, if a graph is closer to an extremal graph, it can reduce the level of fluctuation during iteration.

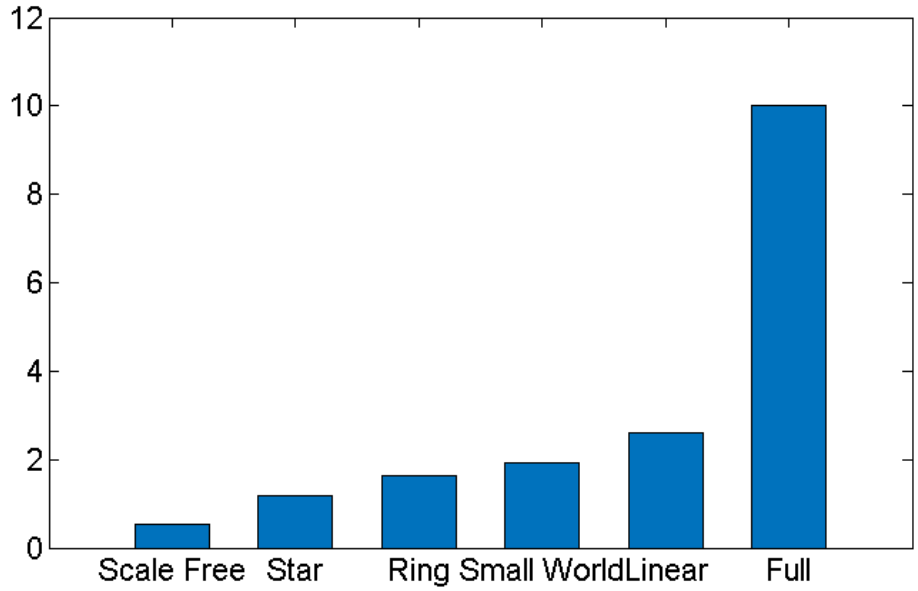

Fig. 54 Distribution of Difference between λ_2 and D_2

From the discussions above, it is known that connectivity of a communication network will influence the calculation speed. But it doesn't mean a network with a higher connectivity will gain the faster converge speed, it also has the risk to get into a long term fluctuation. Therefore, there might exist an optimum topology for communication network in distributed PV-ES combined system. Such topology can help to improve the calculation speed of distributed algorithms. In this case, the ideal topology should have maximum λ_{n-1} and minimum difference between λ_2 and D_2. With such a communication network, an optimum iteration curve with the highest descent velocity and the smallest fluctuation level can be gained. Also this means the fastest calculation speed of distributed algorithm can be achieved.

6. Conclusions

In this Master thesis, I investigated several problems in the future smart grid environment related to higher renewable generation. In particular I have emphasised the impact of the renewable power on balancing and stability, use of storage and some control problems arising. Specifically, I proposed several practical and promising methods using energy storage devices to better control and dispatch these intermittent resources to mitigate the adverse impact. The summary and conclusions are listed as follows on a chapter by chapter basis:

In **Chapter 2,** A comprehensive simulation test platform for the Australian future grid with high penetration level of RE and ES is built in DIgSILENT. The platform includes steady state power flow calculation scanning, dynamic stability analysis considering different penetration levels as well as DSM uptakes.

The simulation results show that in steady state the penetration level of RE and the locations of ES play a very important role. These two factors will impact the result of power flow distribution greatly. In the aspect of voltage stability, the performance deteriorates significantly due the lack of reactive power. Result shows rotor angle stability is insensitive with regard to the RE penetration level. In terms of frequency stability, during disturbance the frequency dynamic speed becomes faster because of the increasing inverter based RE.

In **Chapter 3,** A novel block diagram of the closed-loop LFC system with ES and wind power module has been proposed. Two important factors that exist in future power network, i.e. parametric uncertainty as well as ubiquitous time delay in control channel, are considered simultaneously. Based on rigorous mathematical LMI theory, a Robust H_∞ controller is designed

to deal with the above mentioned problems and meanwhile it maintains the frequency stability of the system.

Through a comprehensive case study of the two-area practical system, we can verify that the proposed controller outperforms the conventional PI one: it can guarantee the robustness of the system as long as the parametric uncertainty and the time delay are bounded, without changing the coefficients of the controller itself all the time. The case studies have also demonstrated that with the appropriate controller, ES can be quite effective to the overall power system frequency regulation when the system contains intermittent renewable power generation sources.

In **Chapter 4,** we develop a sensitivity analysis based-enhanced optimal distributed consensus algorithm (EODCA) that combines the theory of power system itself and the concept of multi-agents together.

The effectiveness of the proposed algorithm is verified: Firstly, it can help the power distribution company to maximize its net profits with very limited information channel built among devices instead of setting up a control centre, and the optimal value is the same with that of the centralized approach. This scheme can help the power distribution company save the costs and achieve a better economic goal. Furthermore, the optimal solutions can also guarantee the safety operation of the distribution network simultaneously, i.e. to alleviate the reverse power flow problem and ensure the transmission power in all lines and the voltages of all nodes are restrained within the engineering required envelopes. Therefore, the EODCA can be utilized to improve the penetration level of the sustainable energy integration in the future. The more numbers of renewables connected into the distribution network, the more cost can be reduced.

In **Chapter 5,** we propose and utilize a Modified Consensus Alternating Direction Method of Multipliers (MC-ADMM) to solve a practical problem in future power distribution networks. Besides, we also analysed the influence of the communication network topology on the calculation performance.

Compared with a latest version of the distributed optimization algorithm called DLPDS, we can see that MC-ADMM performs better in terms of the speed, the accuracy and the ability to handle larger systems with more devices. Simulation result shows the distributed optimization algorithm speed in this model is highly sensitive to the topology of communication networks. By analysing the degrees and Laplacian eigenvalues of these networks, a conjecture is made. The descent velocity during the iteration is determined by the second-largest Laplacian eigenvalue, and the level of fluctuation is related to the difference between the second-largest Laplacian eigenvalue and second-largest degree. Therefore, we can give the hypothesis that there might be an optimum topology for communication network connections.

General Conclusion and Future Work:

As we can see from the above discussions, the integration of highly intermittent RE will pose potential adverse impacts on future grid operation and stability. Therefore, with the smart grid technologies such as the advanced control approach and distributed optimization methods proposed in this thesis, we can have a promising way to tackle this problem with energy storage devices.

I present these findings, conclusions and algorithms as fundamental contributions in helping us to face the upcoming challenges for future power grids.

There are quite a few interesting topics for further work with regard to the topic of integrating renewables and applying storages. For example, how to mathematically design and verify an optimum communication network topology that can minimize the distributed calculation time; how to design an output feedback frequency controller instead of the full-state feedback one, that can not only tackle time delay and parametric uncertainty but can also deal with the data disorder and loss problems in the future situation? These topics are all challenging and require a further research.

References

[1] P. Hearps, M. Wright and B.Z. Emissions, "Australian sustainable energy zero carbon Australia stationary energy plan," *The University of Melbourne Energy Research Institute*, 2010.

[2] L. Zieland, S. Rajakaruna and D. Liyanage, "Modelling and performance assessment of large scale solar photovoltaic plants in rural Australia", in *Australasian Universities Power Engineering Conference*(*AUPEC*), pp. 1-6, 2013.

[3] L. Meegahapola and D. Flynn, "Impact on transient and frequency stability for a power system at very high wind penetration," in *Power and Energy Society General Meeting*, pp. 1-8, 2010.

[4] H. Ibrahim, A. Ilinca and J. Perron, "Energy storage systems-characteristics and comparisons," *Renewable and Sustainable Energy Reviews*, vol. 12, no. 5, pp. 1221-1250, Jun. 2008.

[5] R.A. Walling, R. Saint, R.C. Dugan, J. Burke and L.A. Kojovic, "Summary of distributed resources impact on power delivery systems," *IEEE Trans. Power Delivery*, vol. 23, no. 3, pp. 1636-1644, Jul. 2008.

[6] L. Li, Z. Yi, T. Zhang and W. Sun, "Study on influence of inserted photovoltaic power station to voltage distributing of distribution network," in *Innovative Smart Grid Technologies - Asia* (*ISGT Asia*), pp. 1-5, 2012.

[7] A.M. Azmy and I. Erlich, "Impact of distributed generation on the stability of electrical power system," in *Power Engineering Society General Meeting*, pp. 1056-1063, 2005.

[8] L.F. Ochoa, A. Padilha-Feltrin and G.P. Harrison, “Evaluating distributed generation impacts with a multi-objective index,” *IEEE Trans. Power Delivery*, vol. 21, no. 3, pp. 1452–1458, Jul. 2006.

[9] T. Masuta and A. Yokoyama, “Supplementary load frequency control by use of a number of both electric vehicles and heat pump water heaters,” *IEEE Trans. Smart Grid*, vol. 3, no. 3, pp. 1253-1262, Sept. 2012.

[10] Z. Jiang and X. Yu, “Modelling and control of an integrated wind power generation and energy storage system,” in *Power & Energy Society General Meeting*, pp.1-8, 2009.

[11] I. Serban, R. Teodorescu and C. Marinescu, “Energy storage system impact on the short-term frequency stability of distributed autonomous micro grids, an analysis using aggregate models,” *IET Renewable Power Generation*, vol. 7, no. 5, pp. 531-539, Sept. 2013.

[12] X. Yu and K. Tomsovic, “Application of linear matrix inequalities for load frequency control with communication delays,” *IEEE Trans. Power Systems*, vol. 19, no. 3, pp. 1508-1515, Aug. 2004.

[13] K. J. Arrow, L. Hurwicz and H. Uzawa, “Studies in linear and nonlinear programming,” *Stanford Univ. Press*, 1958.

[14] R. Olfati-Saber, J. A. Fax and R. M. Murray, “Consensus and cooperation in networked multi-agent systems,” *Proc. IEEE*, vol. 95, no. 1, pp. 215–233, Jan. 2007.

[15] A. Jadbabaie, J. Lin and A. S. Morse, “Coordination of groups of mobile autonomous agents using nearest neighbour rules,” *IEEE Trans. Autom. Control*, vol. 48, no. 6, pp. 988-1001, Jun. 2003.

[16] L. Moreau, “Stability of multi-agent systems with time-dependent communication links,” *IEEE Trans. Autom. Control*, vol. 50, no. 2, pp.169 – 182, Feb. 2005.

[17] M. Mehyar, D. Spanos, J. Pongsajapan, S.H. Low and R.M. Murray, “Asynchronous distributed averaging on communication networks,” *IEEE/ACM Trans. Netw.*, vol. 15, no. 3, pp. 512 – 520, Jun. 2007.

[18] S. Boyd, A. Ghosh, B. Prabhakar and D. Shah, “Randomized gossip algorithms,” *IEEE Trans. Inform. Theory*, vol. 52, no. 6, pp. 2508-2530, Sep. 2006.

[19] R. Carli, G. Como, P. Frasca and F. Garin, “Distributed averaging on digital erasure networks,” *Automatica*, vol. 47, no. 1, pp. 115-121, Jan. 2011.

[20] A. Kashyap, T. Basar and R. Srikant, “Quantized consensus,” *Automatica*, vol. 43, no. 7, pp. 1192-1203, Jul. 2007.

[21] A. Nedic and A. Ozdaglar, “Distributed sub-gradient methods for multi-agent optimization,” *IEEE Trans. Autom. Control*, vol. 54, no. 1, pp.48-61, Jan. 2009.

[22] A. Nedic, A. Ozdaglar and P.A. Parrilo, “Constrained consensus and optimization in multi-agent networks,” *IEEE Trans. Autom. Control*, vol. 55, no. 4, pp. 922-938, Apr. 2010.

[23] P.N. Vovos, A.E. Kiprakis, A.R. Wallace and G.P. Harrison, “Centralized and distributed voltage control: impact on distributed generation penetration,” *IEEE Trans. Power Systems*, vol. 22, no. 1, pp. 476-483, Feb. 2007.

[24] G. Mokhtari, G. Nourbakhsh, F. Zare and A. Ghosh, "Overvoltage prevention in LV smart grid using customer resources coordination," *Energy and Buildings*, vol. 61, pp. 387-395, Jun. 2013.

[25] G. Mokhtari, G. Nourbakhsh and A. Ghosh, "Smart coordination of energy storage units (ESUs) for voltage and loading management in distribution networks," *IEEE Trans. Power Systems*, vol. 28, no. 4, pp. 4812-4820, Nov. 2013.

[26] H. Xin, Z. Qu, J. Seuss and A. Maknouninejad, "A self-organizing strategy for power flow control of photovoltaic generators in a distribution network," *IEEE Trans. Power Systems*, vol. 26, no. 3, pp. 1462-1473, Aug. 2011.

[27] M.E. Baran and I.M. El-Markabi, "A multiagent-based dispatching scheme for distributed generators for voltage support on distribution feeders," *IEEE Trans. Power Systems*, vol. 22, no. 1, pp. 52-59, Feb. 2007.

[28] M. Zhu and S. Martinez, "On distributed convex optimization under inequality and equality constraints," *IEEE Trans. Automatic Control*, vol. 57, no. 1, pp. 151-164, Jan. 2012.

[29] M. Gibbard and D. Vowles, "Simplified 14-genrator model of the SE Australian power system," *The University of Adelaide*, 30 June 2010.

[30] D. Vowles and M. Gibbard, "Mudpack-a software package for the analysis of the small-signal dynamic performance and control of large electric power systems," *The University of Adelaide*.

[31] Online Resource: www.uq.edu.au/solarenergy/pv-array/sunlight

[32] S. Agnew, G. Andrews, B. Archer, et.al, "Change and choice: the future grid forum's analysis of Australia's potential electricity pathways to 2050," *CSIRO*, 2014.

[33] Australian Energy Market Operator (AEMO), "100 percent renewables study - modelling outcomes," 2013.

[34] P. Kundur, J. Paserba, V. Ajjarapu, G. Andersson, A. Bose, C. Canizares, N. Hatziargyiou, D. Hill, A. Stankovic, C. Taylor, T. V. Cutsem and V. Vittal, "Definition and classification of power system stability," *IEEE Trans. on Power Systems*, vol. 19, no. 2, pp. 1387-1402, May 2004.

[35] R. Tonkoski, L.A.C. Lopes and T. H. M. El-Fouly, "Coordinated active power curtailment of grid connected PV inverters for overvoltage prevention," *IEEE Trans. Sustainable Energy*, vol. 2, no. 2, pp 139-147, Apr. 2011.

[36] Online Resource: http://investor.aes.com

[37] C.-F. Lu, C.-C. Liu and C.-J. Wu, "Dynamic modelling of battery energy storage system and application to power system stability," *Proc. Inst. Elect. Eng., Gen., Transm., Distrib.*, vol. 142, no. 4, pp. 429-435, Jul. 1995.

[38] P. A. Pegoraro and S. Sulis, "Robustness-oriented meter placement for distribution system state estimation in presence of network parameter uncertainty," *IEEE Tran. Instrumentation and Measurement*, vol. 62, no. 5, pp. 954-962, May. 2013.

[39] L. Yu, "Method of linear matrix inequality," *Tsinghua University Press*, Beijing, 2002.

[40] T. Amemiya and G. Leitmann, "A method for designing a stabilizing control for a class of uncertain linear delay systems," *Dyn Control*, vol. 4, no. 2, pp. 147-167, Apr. 1994.

[41] G. Liu and S. Jia, "Robust H∞ controller for systems with time varying delays and parameter uncertainty," *Journal of Southeast University*, vol. 36, pp. 53-57, Jul. 2006.

[42] M. Takagi, K. Yamaji and H. Yamamoto, "Power system stabilization by charging power management of plug-in hybrid electric vehicles with LFC signal," in *Proceedings of Vehicle Power and Propulsion Conf.*, pp. 822-826, Sep. 2009.

[43] Z. Haiwang, X. Le and X. Qing, "Coupon incentive-based demand response: theory and case study," *IEEE Trans. on Power Systems*, vol. 28, no. 2, pp. 1266-1276, May. 2013.

[44] A. ‐H. Mohsenian-Rad, V. W. S. Wong J. Jatskevich, R. Schober and A. Leon-Garcia, "Autonomous demand-side management based on game-theoretic energy consumption scheduling for the future grid," *IEEE Trans. on Smart Grid*, vol. 1, no. 3, pp. 320-331, Dec. 2010.

[45] H. Yang, D. Y, J. Zhao, F. Luo and Z. Dong, "Distributed optimal dispatch of virtual power plant based on ELM transformation," *Journal of Industrial and Management Optimization*, vol. 10, no. 4, pp. 1297-1318, Oct. 2014.

[46] J.A. Momoh and J.Z. Zhu, "Improved interior point method for OPF problems," *IEEE Trans. Power Systems*, vol. 14, no. 3, pp. 1114-1120, Aug. 1999.

[47] T.-H. Chang, M. Hong and X. Wang, "Multi-agent distributed optimization via inexact consensus ADMM," *IEEE Trans. on Signal Processing*, vol. 63, no. 2, pp. 482-497, Jan. 2015.

[48] M. Xin and C. Xi, "Research on optical fibre transport network topology optimization supporting smart grid core services," in *International Conference on Intelligent System Design and Engineering Application* (*ISDEA*), pp. 232-235, Oct. 2010.

[49] G. Chen, X. Wang and X. Li, "Introduction to complex networks," *Higher Education Press*, 2012.

[50] D.J. Watts and S. H. Strogatz, "Collective dynamics of small-world networks," *Nature*, vol. 393, no. 6684, pp. 440-442, Jun. 1998.

[51] R. Albert and A.L. Barabasi, "Emergence of scaling in random networks," *Science*, vol. 286, no. 5439, pp. 509-512, Oct. 1999.

[52] R. Diestel, "Graph theory," *New York: Springer-Verlag*, 2005.

[53] M. Nica, "Eigenvalues and eigenfunctions of the laplacian," *The Waterloo Mathematics Review*, vol. 1, no. 2, pp. 23-34.

[54] J.-S. Li and Y.-L. Pan, "A note on the second largest eigenvalue of the laplacian matrix of a graph," *Linear and Multilinear Algebra*, vol. 48, no. 2, pp. 117-121, Dec. 2000.

[55] B. Bollobás, "Extremal graph theory," *New York: Dover Publications*, 2004.